University of Reading

PHD DISSERTATION

on

Comparative Evaluation of Ising Couplings, Kinetic Ising Couplings, and Partial Correlations in Inferring Structural Connectivity

Submitted by

Balasundaram KADIRVELU

b.kadirvelu@pgr.reading.ac.uk

Thesis Advisors

Prof. Slawomir J. Nasuto

&

Dr. Yoshikatsu Hayashi

Prepared at

The School of Biological Sciences

University Of Reading

July 2017

Declaration of Authorship

I confirm that this is my own work and the use of all material from other sources has been properly and fully acknowledged.

Signed:

_____

Date:

_____

Comparative evaluation of Ising couplings, kinetic Ising couplings and partial correlations in inferring structural connectivity

Abstract: The problem of inferring the structural connections from the functional connections obtained from the activity of the neuronal networks is one of the major challenges in neuroscience. Studies suggest that maximum entropy based Ising models can discount the effect of indirect interactions and provide good results in inferring the underlying structural connections in neuronal networks. Parameters of the kinetic formulation of the Ising models, kinetic Ising models, have been found to agree well with anatomical connectivity in *in silico* models of neuronal networks. Following this, Ising and kinetic Ising models have attracted attention in the area of connectivity studies. However, the performance of the Ising couplings and kinetic Ising couplings have not been evaluated in comparison with other functional connectivity metrics in the microscopic scale of neuronal networks for a varied set of network conditions and network structures. This thesis sets out to resolve this through a comparative evaluation of the ability of Ising couplings and kinetic Ising couplings to unravel the structural connections when compared to the widely used functional connectivity metrics of partial and cross-correlations in *in silico* networks.

The thesis presents the finding that the network correlation level determines the relative performance of the functional connectivity metrics in detecting the synaptic connections. At weak levels of network correlation, Ising couplings and kinetic Ising couplings yielded better performance when compared to partial and cross-correlations. Whereas at strong levels of network correlation, partial correlations detected more structural links when compared to other functional connectivity metrics in this study. This result was consistent across varying firing rates, network sizes, densities and topologies. Along with being directional and applicable in nonstationary cases, kinetic Ising couplings also displayed better performance when compared to Ising couplings. The findings of this thesis serve as a guide in selecting the right functional connectivity tool to reconstruct the structural connectivity.

Keywords: - Functional connectivity, Structural connectivity, Ising models, Kinetic Ising models, Partial correlations

Acknowledgements

I would like to take this opportunity to thank a number of people who welcomed me, encouraged me, and supported me throughout my research.

First, I would like to thank my supervisors, Prof. Slawomir Nasuto and Dr. Yoshikatsu Hayashi, for their support, direction, and insight that guided me along my path. In particular, I would like to thank Slawek for giving me the chance to pursue my lifetime ambition of a career in academic research. My deepest gratitude to Slawek and Yoshi for the late Friday evening meetings, weekends and holidays spent reviewing my work, for the extended hours of discussions that have ultimately become this thesis, and for the countless opportunities to challenge myself.

During my time at the University of Reading, I have worked closely with a number of people. I would like to thank my friends and colleagues at BEL for their enthusiasm and help over the years.

Last, but not least, I would like to thank my mum Ayyammal and my dad Kadirvelu for their constant encouragement and support, my best friend and wife, Shobana and my children Siva and Akhil for their never ending love and motivation during these intense years of my life.

Contents

List of Figures

Chapter 1

Introduction

Contents

1.1 Overview

The human brain, with its astounding capacity for learning, memory, calculation, thoughts, coordination, and control is the most complex human organ. The brain is made up of a complex network of billions of cells forming two main cell classes - neurons and glia [Aze+09]. Over the last few decades, we have made considerable progress in understanding how the individual neuronal cell works. In this light, scientists have understood

the mechanisms behind the excitatory postsynaptic potentials (EPSP), inhibitory postsynaptic potentials (IPSP), action potentials and synaptic transmissions. However, we still know little about how neurons interact in a network and how networks of neurons perform complex computations [Yus15].

It is through these networks that the brain is able to perform complicated activities such as thought and speech. Understanding individual neurons is not sufficient to understand how the brain achieves these complex feats; we must understand the connectivity and the interactions between the neurons. A great scientific challenge is to explain the principles governing the connections and interaction between groups of brain cells [Yeh+10].

While we have a long way to understanding interactions in networks of thousands and millions of neurons, recent advances have drawn us much nearer to explaining interactions amongst tens of neurons. Improvements in technology have enabled long-duration recordings from closely-spaced neurons with excellent temporal resolution [Nic07; SK11]. At the same time, technological advances in modern immunostaining and optogenetic methods [Dei11] are making available the synaptic connectivity of networks of neurons. Due to the possibility of having data about both the connectivity and the activity of many neurons at the same time, we have a chance to begin understanding how networks of neurons work. An important step in deciphering the spike train data recorded from the neuronal networks in a functional context is to understand the relationship between the synaptic connectivity among neurons and the observed neuronal activity. The inverse problem of inferring the underlying anatomical connections from the observed neuronal activity is an active area of research [PR13].

1.2 Research problem

Functional connectivity is a statistical description of the mutual dependencies observed in multi-neuronal spiking activity [Ste+08]. Functional connectivity has a non-trivial relationship with the underlying anatomical architecture of the neuronal circuits [FBC11]. The ability to reconstruct the underlying structural connectivity from the functional connectivity remains an important open question [Ste+12; Orl+14].

The most common functional connectivity measure used in the study of neuronal activity is cross-correlation [AG85]. However, the usefulness of cross-correlation in inferring the structural connectivity in a neuronal network is limited. Due to the fact that each pair of nodes is considered independently in calculating the cross-correlations, it is not possible to determine if the correlated activity of a neuron pair is the result of a direct or indirect connection between them, or the result of a common input [EDS03; Ada+12].

A second type of approach in obtaining the functional connectivity of a neuronal network is to tune the parameters of a statistical model so that the probability distribution of the spike data generated by that model agrees with the probability distribution of the spike data recorded from the neuronal network [HRT13]. Then the parameters of the model can be considered to represent the functional connections between the neurons in the network. Shlens & co-workers [Shl+06] and Schneidman & co-workers [Sch+06] observed that the computed probability distribution of the binary second-order maximum entropy model was hardly distinguishable when compared to the measured response distribution from groups of retinal

neurons. This conclusion has also been later reported by other research groups for both *in vivo* [Yu+08] and *in vitro* [Tan+08] recordings. The probability distribution of a second-order maximum entropy model is identical to the Gibbs equilibrium distribution of the Ising model, widely used in statistical physics [Sch+06; HRT13]. Thus, the coupling parameter of the Ising model lends itself as an alternative measure of functional connectivity describing the interaction between the neurons.

Studies [Sch+06; GSS11; BC13; Yu+08] suggest that the Ising coupling parameters can remove the effects of the indirect interactions and account only for the direct interactions rendering Ising coupling parameter as a robust indicator of the underlying structural connectivity in the network. Hertz et al [HRT13] observed that the coupling parameters of a kinetic formulation of the Ising model were able to reconstruct the structural connections of a model cortical network very reliably. Following this observation, there has been a growing interest [RDH15] in applying and extending kinetic Ising models to infer connectivity in simulated models of neuronal networks [Cap+15; RH11], and also to understand functional connectivity in living neuronal networks [DMR15]. Compared to other statistical models, Ising models claim a better chance to reconstruct the true underlying anatomical connectivity [HRT13].

Meanwhile, a recent study [Pol+16] has confirmed that partial correlation based on scaled partial covariance density [EDS03] outperformed two widely used functional connectivity methods, cross-correlations and one-delay transfer entropy, in inferring the structural connectivity in simulated networks.

To the best of our knowledge, no comparison has been carried out between

Ising couplings and kinetic Ising couplings against partial correlations in the microscopic scale of neuronal networks, testing through a wide set of network conditions and network topologies. Which of the functional connectivity approaches provides the best measure of the underlying structural connectivity remains an open question, which has been addressed in this dissertation.

1.3 Objectives

This thesis systematically studied the inference of the underlying structural connections by Ising couplings and kinetic Ising couplings, in comparison to partial and cross-correlations, in *in silico* neuronal networks. As it is possible to fully control the underlying topology and the different network conditions in the case of *in silico* networks, *in silico* networks of Izhikevich neurons [Izh03] were used in the study. In this thesis, Ising couplings and kinetic Ising couplings were evaluated against partial and cross-correlations in scale-free, modular small-world and random network topologies of *in silico* networks, as studies [MPM15; EM06a; Dow+12] suggest that the structural connectivity in neuronal networks exhibits features of such complex networks. The functional connectivity measures were also evaluated for different firing rates and correlation levels in networks of various sizes and network densities, as literature [Cha+15; IS10] indicates that the activity of neuronal networks is characterised by such factors.

1.4 Roadmap

The thesis is structured as follows. Chapter 2 reviews the scientific literature pertaining to structural and functional connectivity, Ising models, kinetic Ising models, partial and cross-correlations. Then, Chapter 3 describes the general methods that are used throughout this dissertation. This includes a description of the simulation network of Izhikevich neurons, methods to compute Ising and kinetic Ising model parameters along with the techniques to calculate partial and cross-correlations. Next, Chapter 4 presents the results of a detailed comparative study of the performance of Ising couplings against partial and cross-correlations in inferring the structural connections. Analogous to the previous chapter, Chapter 5 presents the comparative study of the performance of kinetic Ising couplings against partial and cross-correlations. Finally, the results are summarised and the general conclusions are discussed in Chapter 6.

Chapter 2

Literature Review

Contents

This thesis does a systematic study of the inference of the underlying structural connectivity by Ising couplings and kinetic Ising couplings, in comparison to partial and cross-correlations, in *in silico* neuronal networks. As different forms of connectivity in neuronal networks exhibit features of complex networks, the chapter first presents the basic concepts of complex networks. This chapter then introduces the necessary background concepts related to structural and functional connectivity and discusses the relation between structural and functional connectivity. Then, the chapter discusses the conventional functional connectivity metric of cross-correlation followed by the relatively newer functional connectivity metric of partial correlation which is based on scaled partial covariance density. Then the statistical models of interest in this research namely Ising models and kinetic Ising models are discussed. Inference methods of the parameters of the models are also presented. The chapter finally highlights the gap in existing literature that calls for a comparative study between the functional connectivity metrics to recover the structural connectivity.

2.1 Complex networks

Graph theory provides the mathematical framework to study the connectivity in neuronal networks at all levels [RS10]. Graph theory aims to describe complex networks of interacting entities with an abstraction called a graph. Graphs represent the entities of the system as nodes (or vertices) and interaction or relationship between the nodes as edges. In a neuronal network, the nodes correspond to either neurons or brain regions and the edges correspond to synapses or white matter tracts or statistical dependencies between the nodes. Sometimes, the term network is used to denote a graph when attributes are associated with nodes/edges. The terms networks and graphs are used interchangeably in this thesis. Graphs are described by an adjacency matrix (also called a connectivity matrix), which is a square matrix of size equal to the number of nodes. The elements of the adjacency matrix represent the strength of the edge between the pair of nodes.

The simplest type of graph is a binary undirected graph. In this graph, all the edges are unweighted (the edges have only one weight if present) and undirected (the edges do not define a direction for the relation between the nodes). All the elements of the adjacency matrix of a binary undirected matrix are either 0 or 1 and the matrix is a symmetric matrix. Weighted graphs assign weight to the edges so that the edges represent the strength of the relationship between the nodes. Directed graphs assign directions to the edges so that the edges can point the direction of the relationship between the nodes. The adjacency matrix of a directed graph is asymmetric. Weighted graphs can be converted to unweighted binary graphs by

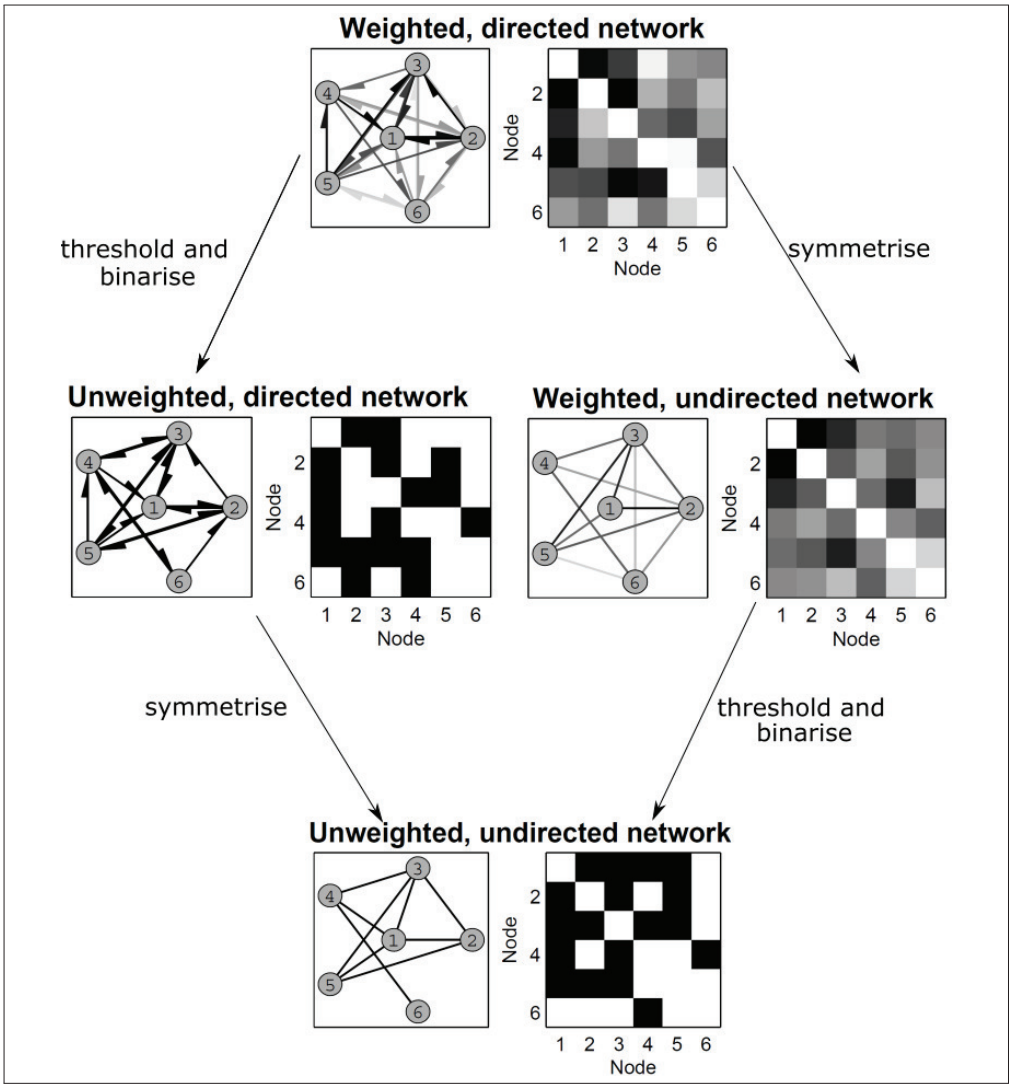

Figure 2.1: Illustration of different kinds of graphs. Weighted networks can be converted to unweighted binary networks by thresholding and binarising. Directional graphs can be converted to undirectional graphs by symmetrising.

thresholding (which omits edges whose weights are below the threshold) followed by binarising (which sets the remaining edges to unit strength). Directional graphs can be converted to undirectional graphs by symmetrising. The different types of graphs are illustrated in Figure 2.1.

A network is characterized by a number of parameters. A few key parameters used in the analysis of neuronal networks are the node degree, cluster coefficient, and the average path length.

Node degree: A key property of a node is its degree which represents the number of edges it has to other nodes (in the case of undirected networks). In directed networks, incoming degree (k_i^{in}) of a node i refers to the number of afferent (incoming) edges and outgoing degree (k_i^{out}) refers to the number of efferent (outgoing) edges. The total degree (k_i) of a node i is given by the sum of incoming degree and outgoing degree.

$$k_i = k_i^{in} + k_i^{out} \tag{2.1}$$

Some networks exhibit few nodes with a high degree and many nodes with a low degree. Nodes with high degree (at least one standard deviation above the network mean degree) are called hubs. Nodes with degree one are called leafs. The degree distribution $P(k)$ of a network is defined as the probability that a randomly selected node in the network has a degree k and is given by the fraction of nodes in the network with degree k

$$P(k) = \frac{N_k}{N}\,, \tag{2.2}$$

where N_k gives the number of nodes in the network with the degree k and N is the total number of nodes in the network.

Clustering coefficient: The local clustering coefficient of a node is a measure of how much the neighbours of a node are linked to each other. A node i with degree k_i has k_i neighbours. The maximum number of possible links amongst the neighbours is $\frac{k_i(k_i-1)}{2}$. If L_i is the number of links between the k_i neighbours of node i, then the local clustering coefficient of the node i is given by:

$$C_i = \frac{2L_i}{k_i(k_i-1)}\,. \tag{2.3}$$

The local clustering coefficient C_i can vary between 0 and 1. When $C_i = 0$, none of the neighbours of node i are connected to each other. When $C_i = 1$, all the neighbours of node i connect to each other and they form a complete graph. C_i indicates the probability that two neighbours of a node i are also neighbours with each other.

The average clustering coefficient $\langle C \rangle$ of a network is defined as the average of the local clustering coefficient of all the nodes of the network.

$$\langle C \rangle = \frac{1}{N}\sum_{i=1}^{N} C_i\,. \tag{2.4}$$

In line with the earlier probabilistic interpretation, the average clustering coefficient $\langle C \rangle$ gives the probability that two neighbours of a randomly selected node are linked to each other [Bar14]. Equation 2.4 is defined for undirected networks. The same concept can be generalized for directed and weighted networks as well.

Average path length: The average path length $\langle d \rangle$ of a network is the mean distance between the all pairs of nodes in the network. The average path length $\langle d \rangle$ is calculated as follows:

$$\langle d \rangle = \frac{1}{N(N-1)} \sum_{i \neq j} d(i,j)\,, \tag{2.5}$$

where $d(i,j)$ is the shortest path distance between the nodes i and j. Average path length is a topological measure used to measure network's level of integration.

The degree distribution discussed earlier is one of the most studied characteristics of a network. The shape of the distribution is used to classify the networks into the following classes: scale-free, regular, and random networks. Regular and random networks represent extreme cases of order and randomness, respectively. Scale-free networks, along with another class of networks called small-world networks, represent two types of real-world networks. Both structural and functional connections in the brain (reviewed in section 2.2) exhibit characteristics of scale-free and small-world networks both at the cellular scale and the whole-brain scale [BS09]. An illustration of the different classes of networks is presented in Figure 2.2.

The brain's structural and functional systems have features of complex networks — such as small-world topology, highly connected hubs and modularity — both at the whole-brain scale of human neuroimaging and at a cellular scale in non-human animals.

Random networks: Paul Erdős and Albért Rényi introduced a simple model for generating random networks in 1959. In Erdős-Rényi random networks,

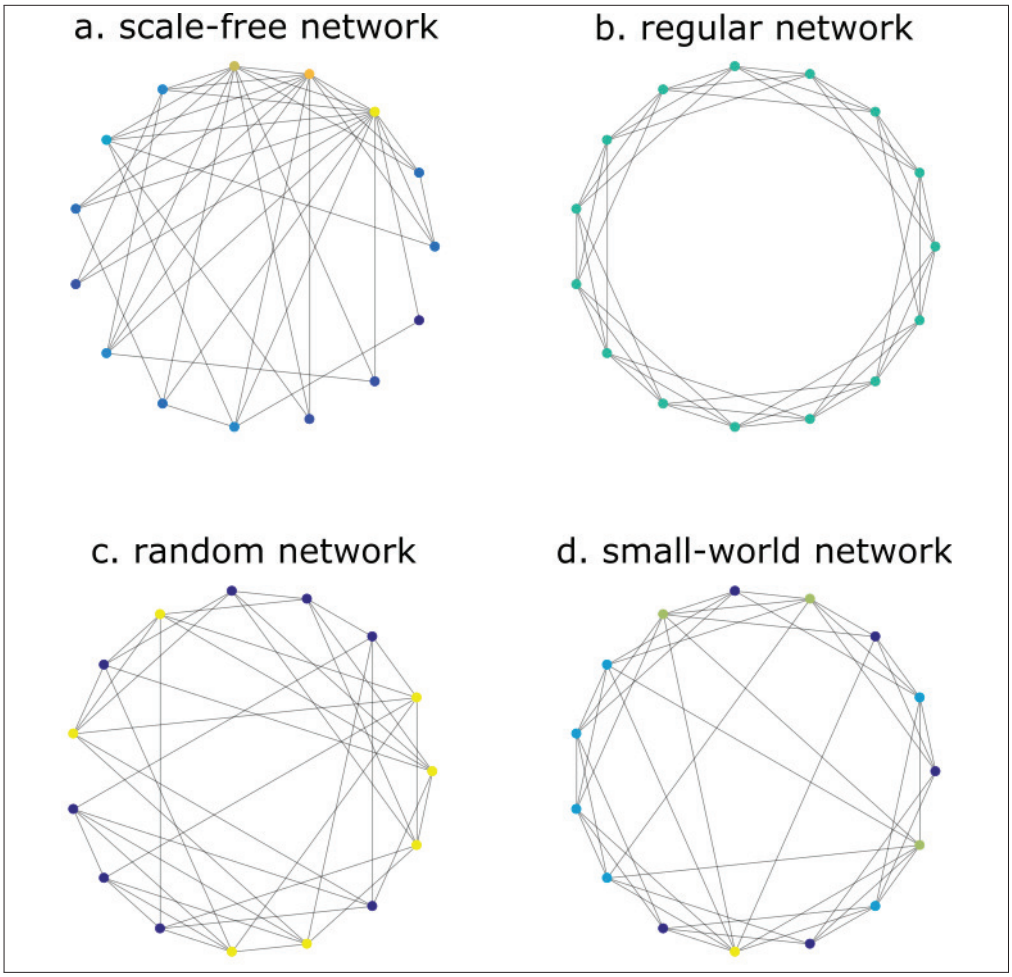

Figure 2.2: Illustration of the different classes of networks. All networks were created with similar number of links. a. Scale-free networks form a few highly connected hub nodes. b. Regular networks has localised clustering but no long range links. c. Random networks - Most nodes in random networks have a degree in the vicinity of the average degree of the network. d. Small-world networks present a balance of segregation and integration through dense local links and long-range links.

each pair of nodes is connected with a fixed probability p. As the probability p increases from 0 to 1, the network density (the number of edges in the network) is more likely to increase. In general, random networks are an extension of the concept of random variables. Each random network represents a sample network selected from a space of possible networks with the same number of nodes and edges. The exact form of the degree distribution of a random network is the binomial distribution

$$P(k) = \binom{N-1}{k} p^k (1-p)^{N-1-k} \,. \tag{2.6}$$

Most real networks are sparse, meaning the average degree <k> $<<$ N. In this limit, the degree distribution of a random network given by 2.6 is well approximated by the Poisson distribution [Bar14]:

$$P(k) = e^{-\langle k \rangle} \frac{\langle k \rangle^k}{k!} \,. \tag{2.7}$$

A random network has few local links and hence is characterised by low values of clustering coefficient.

Regular networks: Also called lattice networks, regular networks are completely non-random. They are constructed on a set of nodes where each node is connected to k nearest neighbours. The probability that a node i has a degree k is given by

$$P(k) = c \,, \tag{2.8}$$

where c is a constant. Regular networks are highly ordered and show high values of clustering coefficient.

Scale-free networks: Most real-world networks are neither completely ordered like the lattice networks nor completely random like the random networks. The degree distribution of many real-world networks are not Poisson but characterised by a power-law degree distribution given by

$$P(k) \propto k^{-\gamma}\,, \tag{2.9}$$

where γ is the degree exponent. When logarithm is taken on both sides of Equation 2.9, it becomes

$$\log P(k) = -\gamma \log k\,. \tag{2.10}$$

When the degree distribution follows a power law distribution, the plot of the degree distribution in a log-log plot will be a straight line with the degree exponent γ giving the slope of the line.

A network whose degree distribution follows a power law is called a scale-free network. Highly connected hub nodes are a characteristic feature of scale-free networks. The presence of hub nodes decreases the number of hops between the nodes in a network. As a result, the average path length in a scale-free network is smaller than that in random networks [Bar14]. Both structural and functional connectivity networks in the human brain are characterised by the presence of hub nodes [SHK07]. An analysis suggests that hub nodes promote functional integration and efficient communication across the brain [HS13]. Scale-free networks are formed based on

two principles of growth (new nodes join the network over time) and preferential attachment (new nodes prefer to get connected to the more connected nodes) [BA99].

Small-world networks: Small-world networks are a class of networks that interpolates between a regular lattice network and a random network. A lattice network has a high clustering coefficient and a high average path length. A random network has a low clustering coefficient and a low average path length. Small-world networks are characterised by high clustering coefficient and low average path length. Watts and Strogatz [WS98] demonstrated that a random rewiring of a small percentage of edges in a regular lattice results in a sharp decrease in the path length but only a small decrease in the clustering coefficient. The Watts-Strogatz model of small-world networks is illustrated in Figure 2.2d.

The small-world coefficient SW of a network is calculated by comparing both clustering and path length of the network against the same metrics from an equivalent random network having the same number of nodes and edges [HG08]. The small-world coefficient is calculated as

$$SW = \frac{\langle C \rangle / \langle C \rangle_r}{\langle d \rangle / \langle d \rangle_r}, \tag{2.11}$$

where $\langle C \rangle$ and $\langle d \rangle$ correspond to the network and $\langle C \rangle_r$ and $\langle d \rangle_r$ correspond to an equivalent random network. If the small-world coefficient is greater than one, then the network is considered to exhibit small-world

property. Small-world networks present a balance of functional integration via long-range links and functional segregation via dense local clustering. Modular networks (which are characterized by dense local connections within the module and sparse inter-modular connections) exhibit small-world property [MLB10] as they posses high clustering coefficient and low path lengths. It should be noted that all modular networks are small-world although the converse is not true. Small-world networks such as Watts-Strogatz models do not exhibit modularity [MLB10]. An example of modular small-world networks is presented in Figure 4.5b. Small-world networks have been observed in the anatomical and functional connection networks of the brain [Spo13].

2.2 Brain connectivity

Connectivity is described as one of the intrinsic characteristics of a neuronal circuit as the neuronal activity cannot be attributed only to the sole properties of the individual neurons but largely to the direct or indirect influence of other neurons in the network [Pol+16; MPF05]. A general theory of brain function that can account for the different behaviours cannot be explained by the study of individual neurons alone. Focus on the prominence of individual neurons is fading in the recent years and, as the new paradigm of computational neuroscience, neural network models are helping us to understand behaviour and cognition that do not easily fit within single-neuron frameworks [Yus15]. The neural network models assume

that the function of neural circuits arises from the joint activity of the network of neurons. Advancements in optical and electrophysiological multineuronal recordings have revealed that networks of neurons, rather than single neurons, make physiological units and give rise to the functional properties of the brain [Yus15]. Three categories of connectivity are used to describe the interactions of neuronal networks: structural, functional and effective. These three categories of neuronal network connectivity are interlinked but offer different perspectives. All three forms of connectivity can be defined between units within a nervous system at multiple spatial scales. The units can correspond to either single neurons, populations of neurons, or anatomically segregated brain regions [BS09].

2.2.1 Structural connectivity

Structural connectivity corresponds to the physical (anatomical) connections between the nodes of a neuronal network. The structural connectivity ranges over multiple spatial scales. On the microscopic scale of neurons, the structural connections refer to the synaptic (chemical and electrical synapses) connections between individual neurons. On the intermediate scale, structural connections refer to the connection bundles or synaptic patches that link neuronal populations within a given brain region. On the large scale of the brain, structural connectivity refers to the white matter tracts connecting different brain areas. Irrespective of the spatial scale, structural connectivity is relatively stable on the shorter timescale of seconds to minutes, but plastic and prone to changes on the longer timescale of hours to days. Learning and plasticity happen by changing the structural

connectivity between neurons and brain areas. Structural connections at all levels of scale are both specific and variable [Spo07]. Specificity is found in the arrangement of synaptic connections between distinct neuronal types, in the branching pattern of axonal arborizations, and in the long-range connectivity between brain regions. Variability is found in the shape of individual neurons, in the size and connection of large-scale structures, and corresponding structures in brains of individuals within the same species. Structural variability is considered to be one of the key sources of functional variability.

Mapping the anatomical networks at different scales has been a long-standing technological challenge [BS09]. On the cellular scale of individual neurons, mapping synapses within the tangle of billions of neurons represent an overwhelming problem. Advances in electron microscopy have made possible mapping the complete connection matrix of the nematode *Caenorhabditis elegans* at cellular resolution. Mapping of neuronal connections in the mammalian cortex has been made possible recently by Brainbow [Liv+07], a new promising neuroimaging technique developed by a team of researchers from Harvard University. Brainbow uses a combination of genetic technologies and cell staining techniques and allows visualising complete neuronal circuits by using distinct colours to label individual neurons. Brainbow is proving to be a powerful tool to neurobiologists to gain a better understanding of the brain's complex tangle of neurons. Histological dissection and staining and axonal tracing techniques have been used to map white matter pathways and hence identify structural connection matrices in macaque visual cortex [FVE91] and the cat thalamocortical systems [Sca+99]. The structural network of the human brain at the scale of brain regions

(also called the human connectome) have been mapped using non-invasive MRI techniques like diffusion tensor imaging (DTI) and diffusion spectrum imaging (DSI) which can measure macroscopic axonal organisation in nervous system tissues. DSI technology has been used to generate 500-4000 region of interest cortical connection matrices [Hag+07].

Studies suggest that structural connectivity in neuronal networks at all scales exhibits features of complex networks (described in the section 2.1). Small-world properties have been demonstrated in the cellular networks of the vertebrate brain stem [HGP06]. Studies support the existence of scale-free network connectivity in primary cortical cultures [EM06b] and developing hippocampal networks [Bon+09]. Network analysis of basal brain grey matter areas constructed using DTI revealed many non-random features of connectivity such as high clustering and presence of hubs [IM+07]. Graph analysis of the cortical connection matrices generated using DSI also identified small-world architecture in the cortical networks [Hag+07].

2.2.2 Functional connectivity

Functional connectivity is a statistical concept. Functional connectivity measures the statistical interdependence between the activity of two nodes of a network without any assumptions about the process which causes the statistical relationship [FBC11]. Two nodes are said to be functionally connected if one can predict the activity of one node based on the activity of the other node. It should be emphasised that functional connections do not imply any underlying structural connections or any causal relations. In

some cases, the statistical interdependence can occur because of underlying structural connections. In other cases, the statistical dependence can be present because of common input from a third neuronal or stimulus sources. For example, the primary visual cortex has been shown to have strong functional links between its left and the right cerebral hemispheres, although underlying white matter connections are lacking between those regions [DLIv+13]. However, if two nodes A and B are functionally connected, it does not imply that activation of one node causes the activation of the other node.

Functional connectivity is usually derived from time series observations obtained from a variety of sources including multielectrode arrays (MEAs), electroencephalography (EEG), magnetoencephalography (MEG), and functional magnetic resonance imaging (fMRI). Deviations from the statistical independence between the neuronal elements of the network are usually captured in a correlation matrix (or a covariance matrix), which is commonly used to represent the functional connectivity of the neuronal network. Other measures such as mutual information, spectral coherence or phase-locking are also used as statistical indicators of functional connectivity [Spo07]. Unlike structural connectivity, functional connectivity is highly time-dependent. Functional connections between the nodes of a neuronal network often fluctuate on multiple time scales [Spo07].

2.2.3 Effective connectivity

Effective connectivity represents a third mode of representing and analysing brain networks. While functional connectivity is the correlation concept,

effect connectivity is the causation concept. The term effective connectivity has been defined by various authors in convergent ways [SF10]. Effective connectivity is defined as the causal influence one neural system exerts over another either directly or indirectly, at the synaptic or the cortical level [Fri94]. While functional connectivity just quantifies the statistical dependence between the nodes, effective connectivity refers to the parameters of a model that tries to explain the observed statistical dependencies [Fri11]. Some authors have defined effective connectivity as the simplest possible circuit diagram that can replicate the timing relationships between the recorded nodes of the networks [AP91]. Effective connectivity represents the effective mechanism generating the observed data, and provide interaction coefficients. Feldt et al [FBC11] suggests that the causal effects can be inferred by perturbing the activity of one node and measuring the change in the activity of the other nodes.

Effective connectivity exists between two nodes could exist if activity in one node modulates activity in the other node. Effective connectivity doesn't imply a direct physical connection - simply a causative influence. For example, the spiking of one neuron can lead to the firing of another neuron through a direct monosynaptic link or a polysynaptic path. Also, an effective connectivity between two nodes does not imply that activation of one node results in the activation of the other node. Different forms of causal modulation such as inhibition, phase modulation, firing rate change, etc. can also be envisaged [FBC11].

As causes must precede effects in time, causal effects (and hence effective connectivity) can be inferred through the application of time series causality measures such as Granger causality. Dynamic causal modelling (DCM)

uses a Bayesian framework to compare causal models and select the best model and its parameters (which are the effective connections) on the basis of observed data.

It should be noted that there are overlapping definitions of the terms functional connectivity and effective connectivity in the scientific studies [TC14]. Scientists in the field of brain connectivity have different views on the classification of connectivity metrics. Friston [Fri11] gives a stringent definition for effective connectivity, and he considers dynamic causal modelling and structural equation modelling as effective connectivity measures and classifies Granger causality and transfer entropy as functional connectivity measures. However, Sporns [Spo07] classifies Granger causality and transfer entropy as model-free effective connectivity measures. A review of the functional connectivity measures by Bastos and Schoffelen [BS16] classifies Granger causality as a model-based functional connectivity method and transfer entropy as a model-free functional connectivity method. Some studies use the terms functional connectivity and effective connectivity interchangeably to denote all non-structural connectivity [TC14; Ste+08; HRT13]; while some studies [Pol+16] use the term functional-effective connectivity to denote the non-structural connectivity. This thesis evaluates Ising couplings, kinetic Ising couplings and partial correlations. Since the key papers [HRT13; EDS03] on the application of these metrics to the analysis of neural data have used the term functional connectivity to denote these measures, this thesis will follow the conventions used in the papers and refer to the metrics of Ising couplings, kinetic Ising couplings, partial correlations and cross-correlations as functional connectivity metrics.

2.2.4 Relation between structural and functional connectivity

Several studies [Wat+09; Bon+09] have explored the relationship between the properties of the individual neurons in the network, the structural connectivity in the network, the dynamics in the observed network activity and the functional connectivity metrics calculated from the observed network activity. The studies observed a strong link between network structure and network dynamics. For example, network activity in developing cerebellum which has a regular structural connectivity occurs as travelling waves [Wat+09] and network activity in developing hippocampus which has a scale-free structural connectivity occurs in synchronous bursts [Bon+09]. If different structural connectivity patterns produce different dynamics, then it can be suggested [FBC11] that functional connectivity which captures those dynamics has a non-trivial relation with the structural connectivity and at least some characteristics of the structural connectivity will be captured in the functional connectivity metrics. The problem of inferring the structural connections from the network dynamics is a major challenge in systems neuroscience [PR13].

One of the long standing issues in reconstructing structural connections from the functional connections is that the latter is subject to the effect of indirect connections. Consider the simple example of three neurons A, B, and C where A drives B via an excitatory connection and B drives C via an excitatory connection. In this situation, there will be strong correlations between the activities of A and C and an ideal functional connectivity metric which is calculated from the activities of the three neurons should be able

to discount the indirect connection between A and C. Similarly, when A drives both A and B via excitatory connections, there will be strong correlations between the activities of B and C and an ideal functional connectivity metric should be able to explain away the indirect connection between B and C.

A variety of functional connectivity metrics have been discussed in the literature to discount the indirect interactions and reconstruct the structural connectivity network: Spike train covariances [PR13], Transfer entropy [Ste+12], Granger causality [Zho+14], partial coherence [DES97], partial covariance density [Pol+16]. Maximum entropy based Ising model couplings have also been suggested to discount the indirect interactions and account only for the direct connections [Sch+06; Yu+08]. The coupling parameters of the kinetic formulation of the Ising model (called kinetic Ising model) have been claimed to reconstruct the structural connectivity with great accuracy [HRT13].

Since no comparative analysis of the ability of the Ising couplings and kinetic Ising couplings in relation to other functional connectivity metrics exist in the literature, this thesis evaluates the performance of the Ising couplings and kinetic Ising couplings against the two common metrics of functional connectivity, namely cross-correlation and partial-correlation. The rest of the literature review chapter discusses the background knowledge and ideas relating to the functional connectivity metrics used in the thesis: cross-correlation, partial correlation, Ising couplings, and kinetic Ising couplings.

2.3 Cross-correlation

Cross-correlation is a widely used method to estimate functional connectivity in neuronal systems [NL09]. It is a measure of the temporal correlations between the spike trains of two neurons [WSB03]. Cross-correlation is always evaluated pairwise, for each pair of neurons in the network. One neuron is designated as the reference neuron. The other neuron is called the target neuron. A suitable time frame for correlation, called the correlation window, must be selected considering the delay in the neural circuits. Usually, a correlation window of around 200 ms is selected for synaptic interactions, as time latencies greater than 200 ms are not of interest for synaptic interactions [NL09]. The correlation window is split into a number of equal time segments called bins.

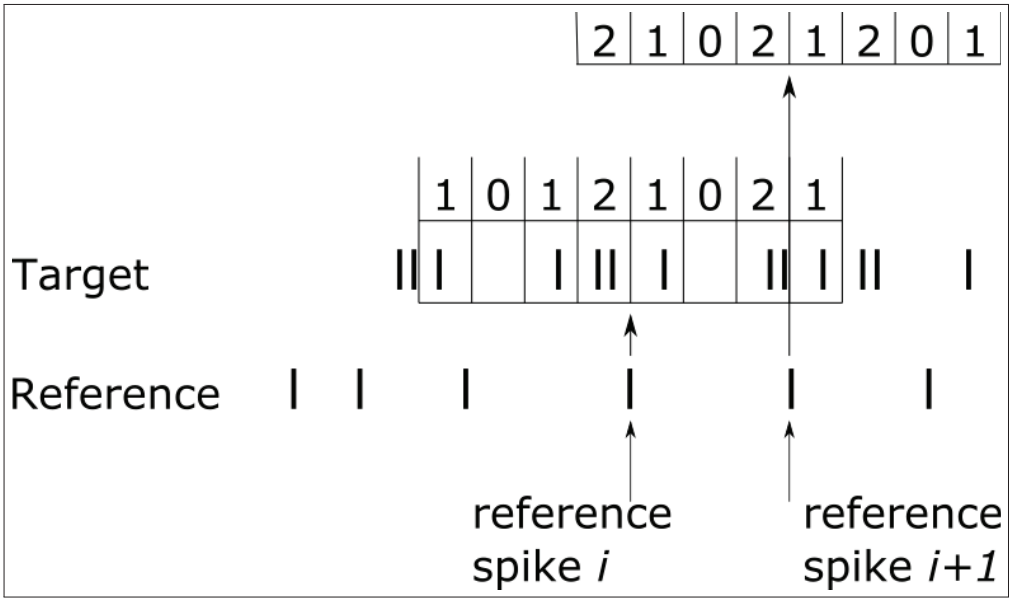

Figure 2.3: Example of a cross-correlation calculation using a eight bin window.

The procedure to perform a cross-correlation between the spike trains of

the two neurons is as follows. The correlation window is centred over the first spike of the reference spike train. The number of spikes of the target spike train that fall into each bin of the correlation window is counted. The above step is repeated for each spike in the reference spike train. The results of each step are accumulated to get the overall cross-correlation. This procedure is schematised in Figure 2.3. The plot of the cross-correlation results is called a cross-correlogram. Thus, the cross-correlogram is a visualisation of the count of the target neuron's spikes at different time delays relative to the spikes of the reference neuron. If the spikes of the target neuron occur at a fixed time relative to spikes of the reference neuron, then a peak in the cross-correlation should occur at a time corresponding to the delay between the reference and the target neuron. It should be noted that bin counts are done for both positive and negative time delays. If the peak of the cross-correlogram occurs for positive time delays, then it implies that the target neuron spikes after the reference neuron. Conversely, if the peak of cross-correlogram occurs for negative time delays, it implies that the target neuron spikes before the reference neuron. Thus, the direction of the connections can be determined from the location of the peak in the cross-correlogram.

Mathematically, cross-correlation is computed as the average value of the product of the spike trains of the reference and the target neurons. Let x and y be the spike trains of the reference and the target neurons, respectively. The cross-correlation function $C_{xy}(\tau)$ is defined as follows [Pol+16]:

$$C_{xy}(\tau) = \frac{1}{\sqrt{N_x N_y}} \sum_{s=1}^{N_x} \sum_{t_i=(\tau-\frac{\triangle\tau}{2})}^{(\tau+\frac{\triangle\tau}{2})} x(t_s) y(t_s - t_i)\,, \tag{2.12}$$

where N_x and N_y are the total number of spikes in the spike trains x and y, respectively, and t_s is the timing of a spike in the spike train x. Equation 2.12 is normalised so that $C_{xy}(\tau)$ takes a value between between 0 and 1.

Cross-correlation can be interpreted as the probability of a neuron (called the target neuron) spiking at a time $(t + \tau)$ conditioned on another reference neuron spiking at a time t where τ is called the time lag [Rie+97; Pol+16]. Thus, the cross-correlation is a good indication of the presence or absence of a linear statistical dependence between the firing of the two neurons. Thus, if two neurons A and B are completely unrelated, then the spike times of A will be totally independent of the spike times of B and the cross-correlogram of the neurons will be flat with no significant peaks. If the target neuron is firing consistently after the reference neuron, then a significant peak should occur in the cross-correlogram of the two neurons. Similarly, if the target neuron's firing decreases consistently with the firing of the reference neuron, then a significant dip will be present in the cross-correlogram. Sometimes, false peaks can occur in a correlogram because of random chance.

The cross-correlation function is symmetric.

$$C_{xy}(\tau) = C_{yx}(-\tau)\,. \tag{2.13}$$

That is, if we compute the cross-correlation function keeping x as the reference and y as the target and then compute cross-correlation function keeping y as the reference and x as the target, we will get the same function but just reversed in time.

Though cross-correlation can discriminate between excitatory and inhibitory connections and can also infer the direction of the connections, cross-correlations cannot distinguish between direct connections and common input connections. A common suggestion to overcome this limitation is to make inferences based on the location of the peak in the cross-correlogram. It was suggested that for common input cases, the peak will occur at a time lag value of zero and for direct connections, the peak will occur at a non-zero delay. However, if the common input to the nodes arrives with different delays, then the above suggestion is not valid rendering cross-correlation unable to discriminate between direct and common-input connections.

2.4 Partial correlation

Frequency domain measures of the association between spike trains have been used to extend the traditional time domain analysis of the spike trains. The Fourier transform of the cross-correlation function called the cross-spectral density (or simply, cross spectrum) is used to calculate the spectral coherence which is defined as the cross-spectral density of 2 spike trains at a frequency ω divided by the square root of the power spectral density of each spike train at a frequency ω. Let $R_{xx}(\tau)$ and $R_{yy}(\tau)$ be the auto-correlation of the spike trains x and y respectively and $R_{xy}(\tau)$ be the cross-correlation between the spike trains x and y. Let $S_{xx}(\omega)$, $S_{yy}(\omega)$, and $S_{xy}(\omega)$ represent the Fourier transform of $R_{xx}(\tau)$, $R_{yy}(\tau)$, and $R_{xy}(\tau)$, respectively. $S_{xx}(\omega)$ and $S_{yy}(\omega)$ are called the power spectral densities of the spike trains x and y, respectively. $S_{xy}(\omega)$ is called the cross-spectral density of x and

y. Spectral coherence SCh_{xy} between two spike trains x and y is given by $|SCh_{xy}(\omega)|^2$ where $SCh_{xy}(\omega)$ calculated as [Pol+16]

$$SCh_{xy}(\omega) = \frac{S_{xy}(\omega)}{\sqrt{S_{xx}(\omega)S_{yy}(\omega)}}\,. \tag{2.14}$$

Coherence is a measure of the phase consistency between the two spike trains at a particular frequency. The coherence ranges between 0 and 1. A coherence of 0 indicates a random phase relationship between the two spike trains at a particular frequency. Similarly, a coherence value of 1 indicates a constant phase relationship between the two spike trains at a particular frequency. Coherence is analogous to the correlation coefficient defined at each frequency. Similar to the correlation coefficient, coherence can describe the linear relationship between two spike trains without any consideration of the rest of the spike trains of the population [Mak+14]. Partial coherences are analogous to the partial correlations of multiple regression analysis. Partial coherence is a frequency domain concept based on the method of linear partialisation and was introduced by Brillenger in 1976 ([BBS76]). Partial coherences describe the relationship between two spike trains after accounting for the linear effects of the other neurons in the population. Let P represent the population of all neurons except x and y. The partialisation process removes the effect of the population P from the cross spectral density S_{xy} of x and y as follows [BBS76; Pas+16]:

$$S_{xy|P}(\omega) = S_{xy}(\omega) - \left(S_{xP}(\omega)\; S_{PP}^{-1}(\omega)\; S_{Py}(\omega)\right), \tag{2.15}$$

where $S_{xy|P}$ is the partial cross-spectral density of the neurons x and y; S_{xP}

corresponds to the cross spectrum between the neuron x and the population P, S_{yP} corresponds to the cross spectrum between the neuron y and the population P; and S_{PP} is the cross spectrum between all the neurons in the population except x and y. The inverse Fourier transform of $S_{xy|P}$ is the partial covariance density,$R_{xy|P}(\tau)$.

Partialisation analysis in the frequency domain recommended the use of the partial spectral coherence $|C_{xy|P}(\omega)|^2$ where

$$C_{xy|P}(\omega) = \frac{S_{xy|P}(\omega)}{\sqrt{S_{xx|P}(\omega)S_{yy|P}(\omega)}} \tag{2.16}$$

Although partial coherence was able to distinguish between direct and indirect connections, it couldn't distinguish between excitatory and inhibitory connections [EDS03]. Based on the partial covariance density $R_{xy|P}(\tau)$, Eichler introduced a partialisation analysis in the time domain called the scaled partial covariance density. This approach combined the advantages of the cross-correlation analysis in the time-domain and the partialisation analysis in the frequency domain. Similar to cross-correlations, scaled partial covariance density can distinguish between excitatory and inhibitory connections with peaks and troughs. Analogous to partial coherence approach, scaled partial covariance density can discriminate between direct and indirect connections [EDS03].

The scaled partial covariance density (SPCD) $S_{xy|P}(\tau)$, is defined as

$$S_{xy|P}(\tau) = \frac{R_{xy|P}(\tau)}{\sqrt{r_x r_y}}\,, \tag{2.17}$$

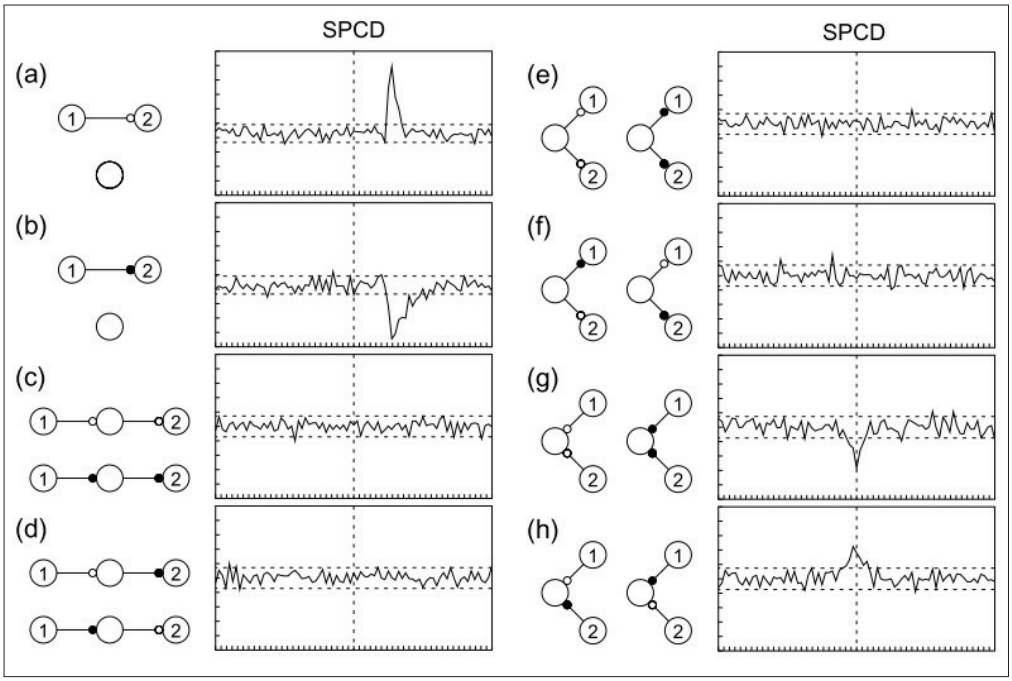

Figure 2.4: SPCD inferring connections in simple three neuron networks [EDS03]. Links with an open dot are excitatory connections. Links with a filled dot are inhibitory connections. In all cases, the scaled partial covariance density $S_{21|3}(\tau)$ between the neurons 1 and 2 is plotted. Except for the converging connections in cases g and h, SPCD is able to discriminate direct connections from indirect connections and common inputs. *Image reproduced with permission of the rights holder,Springer*.

where r_x and r_y are the maximum peak values of the autocorrelation function.

The partial spectral coherence and the partial cross spectral density can be efficiently computed from the inversion of the spectral matrix $S(\omega)$ of the whole set of nodes [EDS03; Ide+07]. If $G(\omega) = S(\omega)^{-1}$, then

$$C_{xy|P}(\omega) = -\frac{G_{xy}(\omega)}{\sqrt{G_{xx}(\omega)G_{yy}(\omega)}}\,, \tag{2.18}$$

$$S_{xy|P}(\omega) = \frac{C_{xy|P}(\omega)}{1 - |C_{xy|P}(\omega)|^2}\,, \tag{2.19}$$

$$S_{xy|P}(\omega) = -\frac{G_{xy}(\omega)}{\sqrt{G_{xx}(\omega)G_{yy}(\omega)}}\frac{1}{1 - |C_{xy|P}(\omega)|^2}\,. \tag{2.20}$$

Figure 2.4 illustrates how effectively SPCD can differentiate between the direct and indirect connections in simple networks of three neurons simulated using integrate and fire model. For each case, the scaled partial covariance density $S_{21|3}(\tau)$ calculated from the simulated data is plotted. Cases a and b correspond to direct excitatory and inhibitory connections respectively. It can be seen that the SPCD features positive peaks and negative troughs for excitatory and inhibitory connections, respectively. Cases c and d correspond, respectively, to indirect excitatory and inhibitory connections via a third neuron. It can be observed that the partialization process has removed the linear effect of the intermediate neuron. Cases e and f illustrate SPCD removing the effect of common input. Cases g and h show that SPCD

is unsuccessful in removing the effect of converging connections. This so-called "marrying-parents effect" [EDS03] results in a peak in the SPCD if the inputs are of the opposite type and a trough if the inputs are of the same type. It should be noted that partialisation can remove the effect of indirect connections and common input connections of the third neuron only if the spike train of the third neuron is recorded. In practice, it is possible that only a subset of the network nodes is recorded. In that case, SPCD cannot remove the linear effect of neurons whose activity are not recorded and can reveal the connectivity only relative to the set of the recorded neurons [EDS03].

2.5 Ising models

This section discusses the Ising model, which is a statistical model of the activity of neurons and is increasingly applied in the field of computational neuroscience.

2.5.1 Maximum entropy models

Building statistical models of the spike trains requires constructing the probability distribution of all the spike patterns. For N number of neurons in the population, the number of possible spike patterns is 2^N (the reason being the firing of each neuron is represented as a binary quantity). This high dimensionality of the space of the possible spike patterns makes collecting enough data to construct the probability distribution a hard task [RNL08]. One approach to building good statistical description of the spike patterns

without having to examine all the possible patterns is to use parametric models [RTH09]. In this approach, one fits the data with the parametric probability distribution with a smaller number of parameters when compared to the number of possible spike patterns. Maximum entropy models have gained a lot of interest in the recent years as parametric models to describe the spike data from neurons following the pioneering studies by Shlens et al [Shl+06] and Schneidman et al [Sch+06].

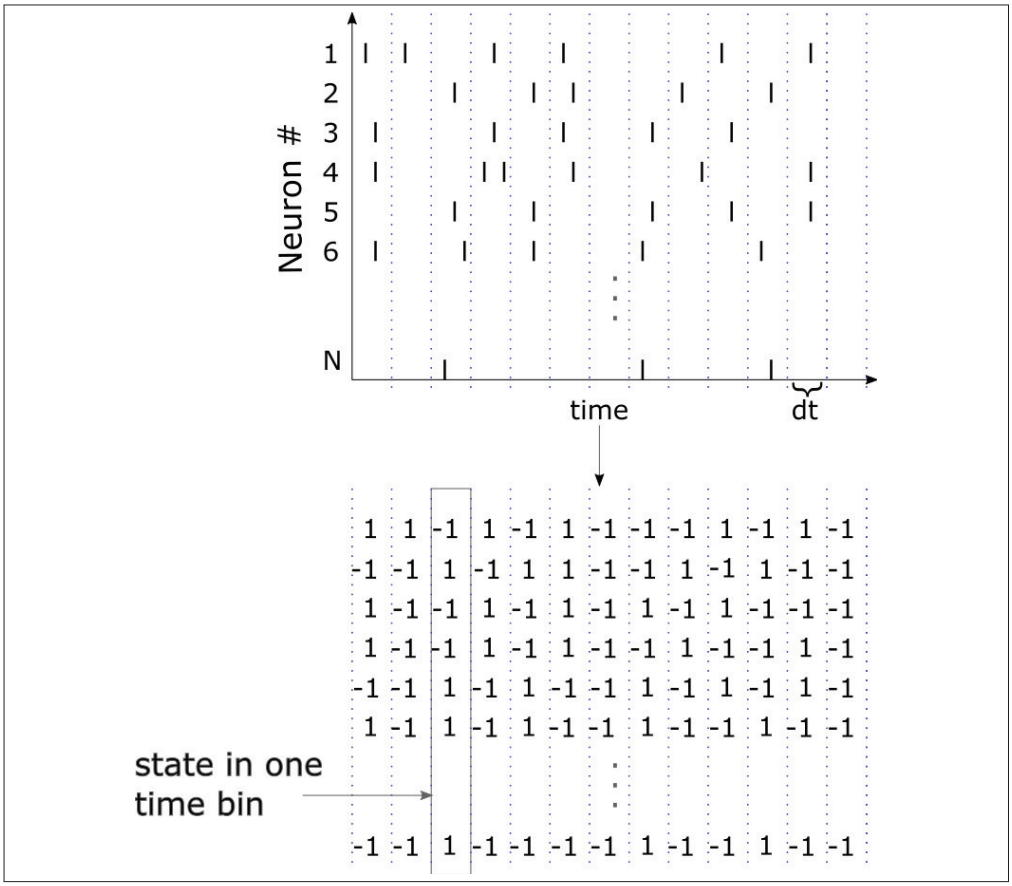

Figure 2.5: Binary representation of neuronal spiking activity

The spike data from a neuron can be represented by either a vector of spike times (a point representation) or a binary vector of 1s and -1s. Maximum entropy models work on the binary representation of spike train data which

can be obtained from the spike times of the neuron by dividing the time into bins of equal width and representing the state of each bin using a binary variable based on the presence of a spike in that time bin. Let the state of a neuron i in a time bin t be represented using the notation σ_i^t, which can take 2 values: +1 for the presence of a spike and -1 for the absence of a spike. This form of binary representation has been used historically to represent neuronal spiking activity [Hop82]. Thus, the time-binned spike train data from a group of neurons can be visualised as a big array, (N x T matrix for N neurons and T time bins), of +1s and -1s as shown in Figure 2.5.

Following this notation, the average firing rate of a neuron i is given by

$$\langle \sigma_i \rangle = \frac{1}{T} \sum_{t=1}^{T} \sigma_i^t \,, \tag{2.21}$$

where T represents the total number of time bins for the duration of the recording, and t is the bin number.

The pairwise correlations for a neuron pair i and j is given by

$$\langle \sigma_i \sigma_j \rangle = \frac{1}{T} \sum_{t=1}^{T} \sigma_i^t \sigma_j^t \,, \tag{2.22}$$

where the angled brackets denote temporal averaging.

In a given time bin, the state vector σ denotes the state of N neurons (out of 2^N possible states) , and is represented as:

$$\sigma = \{\sigma_1, \sigma_2, \sigma_3, \ldots \sigma_N\} \,. \tag{2.23}$$

A first step towards understanding the collective firing activity of these neurons would be to construct a model that accounts for the probability distribution of the states of the ensemble of neurons. The simplest model to characterize the distribution is a first-order model which assumes that the neurons are independent and seeks to fit only the average firing rate of the neurons. However, studies [Nir+01; Mas83] have shown that the first-order model which assumes that the neurons are independent is unable to account for the frequencies for the joint firing event of two or more neurons. Schneidman et al [Sch+06] observed that the true distribution observed from a group of retinal cells was almost exponential and whereas the response distribution generated assuming the cells are independent was a Poisson distribution. Schneidman further observed that even for typical firing patterns in the network, such as a single neuron firing while others are not firing, the independent model made large-scale errors. Additionally, the estimates by the independent model and the actual observations were even highly anti-correlated for some firing patterns in the population.

As the first-order model which seeks to fit only the average firing rate of the neurons is unable to characterize the response distribution of neurons, the next approach is to consider a second-order model which seeks to fit both the average firing rates and all pairwise correlations. There are countless second-order models that will agree with the given average firing rates and pairwise correlations. Hence, the challenge now is to generate a probability distribution that agree only with the measured pairwise correlations and does not make any assumptions about higher-order correlations.

The maximum entropy (also abbreviated as max-ent) approach provides a

way to specify a model that fits the average firing rates and pairwise correlations found in the data and is maximally unconstrained for all higher-order correlations [Yu+08]. Relaxing all other constraints can be accomplished by maximizing the entropy of the model, subject to fitting the chosen correlations. Let P_i denote the probability that event i occurs (with $\Sigma P_i = 1$), then the entropy is given by $H = -\Sigma P_i.logP_i$. "The maximum entropy distribution is the set of probabilities P_i that maximise H, subject to a set of specified constraints" [NV07].The maximum entropy distribution provides null hypotheses for quantities which are not constrained explicitly. Mathematically, maximizing the entropy is equivalent to selecting the maximum likelihood distribution which satisfies the specified constraints [Shl+06].

Maximum entropy distributions occur in several familiar scenarios [NV07]. When the constraint is a specific mean, the exponential distribution gives the maximum entropy distribution. When the constraints are a specific mean and variance, the Gaussian distribution gives the maximum entropy distribution. Similarly, when the constraint is a marginal distribution of the individual variables, the maximum entropy distribution is the product distribution of the variables.

Shlens & co-workers [Shl+06] and Schneidman & co-workers [Sch+06] observed that the probability distribution of the second-order maximum entropy model of spike trains(which was constrained only by the average firing rates and pairwise correlations) was able to explain around 90% of the correlation structure of the multi-neuronal spiking patterns measured in the retina. Shlens et al. [Shl+06] recorded the activity patterns of the cells of a small retinal region using a multi-electrode array and then drew groups of

seven cells. Then for each group of seven cells, the probability of all possible (2^7) activity patterns was calculated from the measurements. They then wanted to understand if the entire set of spiking pattern frequencies can be captured from a smaller number of parameters — the spiking rate of individual neurons (seven parameters) and the pairwise joint firing rates for every pair of neurons (21 parameters). Shlens et al. observed that the computed maximum entropy response distribution was hardly distinguishable when compared to the measured response distribution.

The consequences of the results from Shlens et al. can be well appreciated when they are extrapolated to a network of larger size [NV07]. In an N-neuron network, we need to describe the frequencies of 2^N activity patterns. For a network of 25 neurons, this equates to approximately 32 million; and for a network of size 60, the number of activity patterns is astronomical. In a pairwise max-ent model, N + N(N-1)/2 parameters (the firing rate of individual neurons and their pairwise firing frequencies) could explain the multi-neuronal frequencies. Thus the number of parameters needed to describe a network of N neurons has decreased greatly (325 for N=25 and 1830 for N=60).

Schneidman et al. [Sch+06] also conducted a similar study and observed that the global multi-neuronal activity patterns from a group of retinal ganglion cells could be accounted for by a maximum entropy model which is estimated from pairwise correlations alone. This conclusion has also been later reported by other research groups for both *in vivo* [Yu+08] and *in vitro* [Tan+08] recordings. Marre et al. [Mar+09] observed that a maximum entropy model based on the correlation values and respecting a Markovian assumption was able to describe the spatiotemporal statistics of the activity

on simple network models and recordings in the mammalian parietal cortex *in vivo*. These developments have generated to a lot of interest in the maximum entropy models in the past few years [Yeh+10].

As previously discussed, models of several orders can be used to capture the data. A first-order model takes into account only the firing rates $\langle \sigma_i \rangle$ that are present in the data and it makes the assumption that all higher-order interactions, such as $\langle \sigma_i \sigma_j \rangle$, are independent and, can be calculated from the product of the first-order interactions: $\langle \sigma_i \sigma_j \rangle = \langle \sigma_i \rangle \langle \sigma_j \rangle$. Let P_1 represent the probability distribution generated by a first-order model. A second-order model only accounts for the firing rates and pairwise correlations and assumes that all higher-order interactions can be computed from the first and second-order interactions. Let P_2 represent the probability distribution generated by a second-order model. For N neurons, the probability distribution of a Nth order model (denoted by P_N would be indistinguishable from the probability distribution of the data and would capture interactions of all order (1 to N) found in the data.

The Shannon entropy S of a probability distribution P(σ) is given by:

$$S = -\sum_{k=1}^{2^N} P(\sigma_k).\log(P(\sigma_k))\,. \tag{2.24}$$

As increasing the order of interactions always has the opposite effect on the entropy [CT12; Sch+06], the entropy of higher-order models, $S_2, ...S_N$, is always smaller than the entropy of the first-order model, S_1. Multi-information, I_N is defined as the difference between the entropy of the first-order model and the entropy of the actual data [Sch+06].

$$I_N = S_1 - S_N \,. \tag{2.25}$$

The amount of entropy explained by the second-order maximum entropy model is:

$$I_2 = S_1 - S_2 \,. \tag{2.26}$$

Therefore the second-order maximum entropy model's performance is measured by the fraction of the multi-information I_N that it captures. It is given by the ratio r:

$$r = \frac{I_2}{I_N} \,. \tag{2.27}$$

The ratio r can take a value between 0 and 1, where 1 represents 100% performance. The ratio r is related to the Kullback-Leibler divergence (which is a measure of how difficult it is to distinguish two probability distributions [Shl+06] as follows:

$$r = \frac{D_1 - D_2}{D_1} \,, \tag{2.28}$$

where D_1 is the Kullback-Leibler divergence between P_1 and P_N, given by

$$D_1 = \sum_{i=1}^{2^N} P_N(\sigma_i).\log_2 \left(\frac{P_N(\sigma_i)}{P_1(\sigma_i)} \right) , \tag{2.29}$$

and D_2 is the Kullback-Leibler divergence between P_2 and P_N:

$$D_2 = \sum_{i=1}^{2^N} P_N(\sigma_i).\log_2 \left(\frac{P_N(\sigma_i)}{P_2(\sigma_i)} \right) . \tag{2.30}$$

The r ratio is an intuitive measure of how much better a model would do when compared to a first-order model [Yeh+10]. While applying the second-order model to their data, both Shlens [Shl+06] and Schneidman [Sch+06] found that the r ratio of the second-order model was close to 0.90 on average. This suggests that the second-order maximum entropy model was able to predict the probability of most states correctly and hence could account for approximately 90 % of the spatial correlation in the data. Even with a r ratio of 0.9, it should be noted that the errors in the predictions of few states were very high. This can be attributed to the inaccurate estimates of the entropy of a distribution of states. Very low firing rates of neurons along with a short recording duration will result in data insufficient to sample the probability distribution of all the possible states rendering the entropy estimates inexact. This problem becomes exponentially worse as the number of neurons in the recording increases [RNL08]. Long duration of recordings are necessary to reduce this problem. Both Shlens and Schneidman circumvented this problem by making long recordings to ensure sufficient sampling of all the states.

2.5.2 Relation between maximum entropy models and Ising models

In a physical system, it is known that the maximum entropy distribution consistent with an average energy $\langle E \rangle$ is the Boltzmann distribution, which is given by the following equation

$$P \propto \exp(\frac{-E}{k_B T}) \,, \tag{2.31}$$

where T is the temperature and k_B is the Boltzmann's constant. This can be generalized as follows. If the average values of many variables f_μ describing a system is known, then the maximum entropy distribution is given by

$$P \propto \exp(-\sum_{\mu} \lambda_\mu f_\mu)\,, \tag{2.32}$$

where λ_μ is the Lagrange multiplier for every constraint [Jay57; Sch+06]. In our case, the constraints are the average firing rate $\langle \sigma_i \rangle$ and the average pairwise correlations $\langle \sigma_i \sigma_j \rangle$. The resulting maximum entropy distribution is given by

$$P(\sigma_1, \sigma_2, ..., \sigma_N) = \frac{1}{Z} \exp\left(\sum_i h_i \sigma_i + 0.5 \sum_{i,j} J_{ij} \sigma_i \sigma_j\right)\,, \tag{2.33}$$

where Z is a normalisation factor and h_i, J_{ij} are the Lagrange multipliers chosen such that the averages $\langle \sigma_i \rangle$, $\langle \sigma_i \sigma_j \rangle$ of this probability distribution agree with the average firing rate and average pairwise firings recorded from the observations. The second-order maximum entropy model derived above in equation 2.33 is same as the Ising model, widely used in statistical physics.

The Ising model is a simple theoretical model of ferromagnetism used in statistical physics. The model was invented by the German physicist Wilhelm Lenz in 1920. The model is named after Ernst Ising, a student of Lenz, who chose the model for his doctoral thesis published in 1925. Despite its simplicity, the model can describe a variety of phase transitions including the ferromagnetic-paramagnetic phase transition and the liquid-gas phase

transition. And for this reason, the Ising model has received a lot of attention from both physicists and mathematicians [Gal13].

The Ising model consists of discrete variables which represent the magnetic dipole moments of atomic spins. Consider N atoms arranged in a lattice as shown in Figure 2.6. Each atom has a spin and can either take the value of +1 (upward spin) or -1 (downward spin). The spin of the i^{th} atom is represented by the discrete variable $\sigma_i \in$ {-1, +1}.

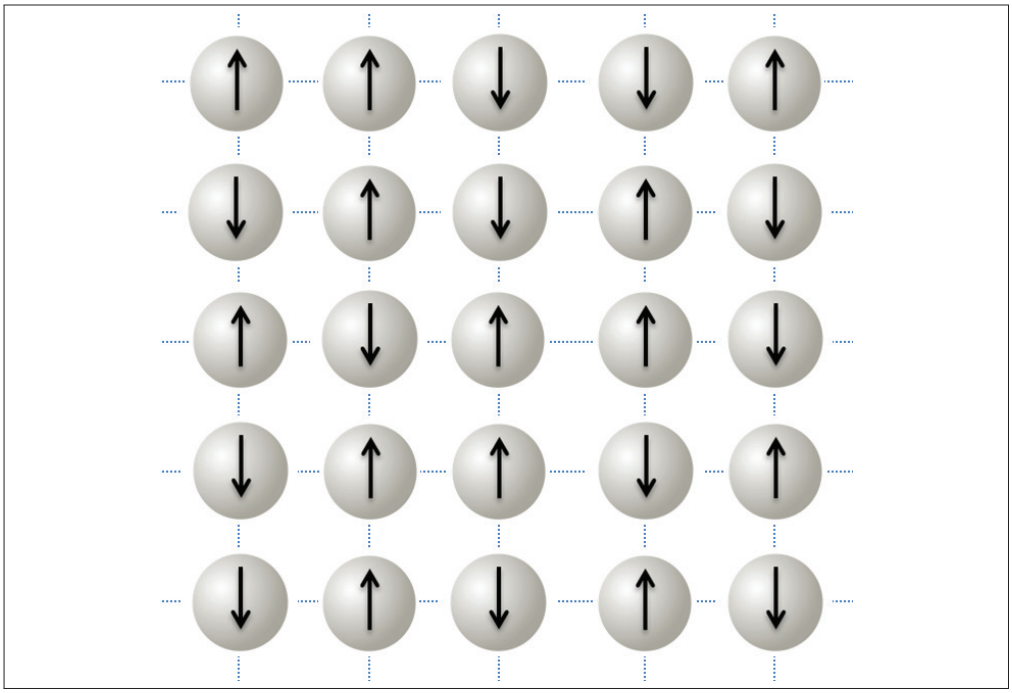

Figure 2.6: Two-dimensional illustration of an Ising model. The up and down arrows represent positive and negative spins respectively.

The spin configuration σ = { σ_1,σ_2,...σ_N } can take one of the possible 2^N configurations. For any two spins $i, j \in$ N, one has an interaction J_{ij}. A positive J_{ij} coupling (ferromagnetic interaction) favours the spin i to align with the spin j. A negative J_{ij} coupling (anti-ferromagnetic interaction) favours the

spin i to spin in a direction opposite to that of the spin j. A zero J_{ij} implies no interaction between the spin i and j. Each spin also has an external magnetic field h_i interacting with it. The field parameter h is an indication of how likely will the spin i be up in the absence of interaction from other spins. A positive field h_i tends to drive the spin i up and a negative field h_i tends to drive the spin i down. The energy of a spin configuration σ is given by the Hamiltonian function

$$E(\sigma) = -\sum_i h_i \sigma_i - 0.5 \sum_{i,j} J_{ij} \sigma_i \sigma_j \,. \tag{2.34}$$

The Ising model is studied at equilibrium. At equilibrium, the probability that the Ising model is in a configuration σ is given by the Gibbs measure P(σ) defined below

$$P(\sigma) = \frac{1}{Z(T)} \exp\left(-\frac{E(\sigma)}{k_B T}\right) , \tag{2.35}$$

where k_B is the Boltzmann constant, T is the temperature and Z is the normalization factor and is called the partition function. Z is defined as

$$Z(T) = \sum_\sigma \exp\left(-\frac{E(\sigma)}{k_B T}\right) . \tag{2.36}$$

It can be seen that the Gibbs equilibrium distribution equation 2.35 for the Ising model is same as the maximum entropy probability distribution equation 2.33 when $k_B T = 1$. Changing the temperature just amounts to rescaling the J_{ij}'s and h_i's by a constant factor. The terms second-order maximum

entropy model and Ising model are hence used interchangeably in this thesis.

2.5.3 Fitting the parameters of the Ising model

Usually, in statistical physics, one has the knowledge of the parameters of the Ising model and is tasked to find the moments of the model which can be measured from the experiments. One faces the inverse Ising problem when one has the knowledge of the data statistics, namely the measured average firing rate and the pairwise correlations, and is tasked with finding the parameters of the Ising model which can reproduce the observed moments.

The average firing rate and the pairwise correlations of the observations ($\langle\sigma_i\rangle_{data}$ and $\langle\sigma_i\sigma_j\rangle_{data}$) can be calculated from the spike train data using the equations 2.21 and 2.22. The expected values of the individual firing rates and the pairwise interactions of the Ising model ($\langle\sigma_i\rangle_{model}$ and $\langle\sigma_i\sigma_j\rangle_{model}$) can be calculated as follows.

As described in subsection 2.5.2, the energy of a configuration of N spins $\sigma = \{\sigma_1, \sigma_2, ..., \sigma_N\}$ of the model is given by

$$E(\sigma) = -\sum_{i=1}^{N} h_i\sigma_i - 0.5\sum_{i=1}^{N}\sum_{j=1}^{N} J_{ij}\sigma_i\sigma_j\,, \tag{2.37}$$

where the summation in the second term is carried out such that $i \neq j$.

The probability of occurrence of each configuration (out of the 2^N possible configurations) can be calculated based on the energy assigned to the

configurations. The probabilities of the energies in an Ising model are distributed exponentially in a manner that maximises entropy [Jay57]. Hence, the probability of the occurrence of a configuration σ_k is given by

$$\begin{aligned} P(\sigma_k) &\propto e^{-E(\sigma_k)} \\ &= \frac{e^{-E(\sigma_k)}}{\sum_{i=1}^{2^N} e^{-E(\sigma_i)}} \,. \end{aligned} \tag{2.38}$$

The denominator term in equation 2.38 is a normalization factor (called the partition function in statistical mechanics) and involves summation over each of the possible 2^N configurations. One can see that the equation 2.38 makes configurations with low energy more probable than configurations with high energy.

The expected values of the individual firing rates $\langle \sigma_i \rangle_{model}$ and the pairwise interactions $\langle \sigma_i \sigma_j \rangle_{model}$ of the Ising model can be calculated from the knowledge of the probability of each configuration as follows:

$$\langle \sigma_i \rangle_{model} = \sum_{k=1}^{2^N} \sigma_i(\sigma_k) P(\sigma_k) \,, \tag{2.39}$$

$$\langle \sigma_i \sigma_j \rangle_{model} = \sum_{k=1}^{2^N} \sigma_i(\sigma_k) \sigma_j(\sigma_k) P(\sigma_k) \,, \tag{2.40}$$

where $\sigma_i(\sigma_k)$ indicates the state (which can be either +1 or -1) of neuron i for the configuration σ_k.

As can be seen from equations 2.39 and 2.40, calculating $\langle \sigma_i \rangle_{model}$ and $\langle \sigma_i \sigma_j \rangle_{model}$

exactly involves summation over 2^N terms and is a computationally intensive task. This exact method of calculating the Ising model averages is possible only for small N. For larger N, one has to resort to either analytical approximation methods like mean-field approximation methods (explained in the subsection A.1) or to numerical techniques like Markov Chain Monte Carlo simulations (explained in the subsection 2.5.3.1).

Boltzmann learning method [RTH09] is a typical method to improve the agreement between $\langle \sigma_i \rangle_{data}$, $\langle \sigma_i \sigma_j \rangle_{data}$ and $\langle \sigma_i \rangle_{model}$, $\langle \sigma_i \sigma_j \rangle_{model}$. The Boltzmann learning method involves iterative updates to the Ising model parameters h_i and j_{ij} as follows:

$$\delta h_i = \alpha.(\langle \sigma_i \rangle_{data} - \langle \sigma_i \rangle_{model}) \,, \tag{2.41}$$

$$\delta J_{ij} = \alpha.(\langle \sigma_i \sigma_j \rangle_{data} - \langle \sigma_i \sigma_j \rangle_{model}) \,, \tag{2.42}$$

where α is the learning rate. It is usually held constant and is generally kept less than 1 to get a smoother convergence.

It can be seen from equations 2.41 and 2.42 that when the model average is less than the average from the data, the last term of the equations 2.41 and 2.41, namely ($\langle \sigma_i \sigma_j \rangle_{data} - \langle \sigma_i \sigma_j \rangle_{model}$), becomes positive leading to an increase in h_i or J_{ij}. Conversely, when the model average exceeds the average from the data, the last term becomes negative leading to a decrease in the value of h_i or J_{ij}. After the adjustment of h_i and J_{ij} in an iteration, new values of $\langle \sigma_i \rangle_{model}$ and $\langle \sigma_i \rangle_{model}$ are computed for the new values of h_i and J_{ij}. The iterations continue till the $\langle \sigma_i \rangle_{model}$ and $\langle \sigma_i \sigma_j \rangle_{model}$ agree with

$\langle \sigma_i \rangle_{data}$ and $\langle \sigma_i \sigma_j \rangle_{data}$) within the desired accuracy. Boltzmann learning is a very slow algorithm as the averages $\langle \sigma_i \rangle_{model}$ and $\langle \sigma_{ij} \rangle_{model}$ have to be computed for each iteration and the direct way of computing the averages $\langle \sigma_i \rangle_{model}$ and $\langle \sigma_{ij} \rangle_{model}$ involves summation over 2^N terms and is computationally expensive. Mean field approximations [RTH09] have been developed to solve the inverse Ising problem. However, such approximations suffer from a limited range of validity. Monte Carlo sampling based on Metropolis-Hastings simulation is another method to compute the model averages and is discussed next.

2.5.3.1 Metropolis-Hastings algorithm

Out of the possible 2^N configurations needed to calculate the partition function, some configurations are more probable and some are less probable. However, the direct summation would waste as much computing effort on a less probable configuration as it does on a more probable configuration. A better alternative would be to use a biased sampling which generates representative samples which constitute an appropriate proportion of different configurations. The Metropolis-Hastings algorithm is the most commonly used Markov Chain Monte Carlo (MCMC) method to compute Ising model estimations [NB99]. In Monte Carlo methods, randomly generated samples are used to approximate a quantity of interest. In Markov Chain Monte Carlo methods, the random samples are generated using a Markov chain. One starts with a random sample and uses it to generate the next sample and so on. Each sample only depends on the previous sample. The transition rule between the samples is constructed such that the states the Markov chain will take also sample from a target probability distribution.

Metropolis-Hastings algorithm is named after Nicholas Metropolis, who was an author along with Arianna W. Rosenbluth, Marshall N. Rosenbluth, Augusta H. Teller, and Edward Teller of the 1953 paper 'Equation of State Calculations by Fast Computing Machines' which first proposed the algorithm for the specific case of the canonical ensemble. W.K. Hastings later extended the algorithm to the more general case in 1970 [NB99].

The basic idea of Metropolis sampling is to generate a collection of samples according to a desired distribution $P(x)$ (Boltzmann distribution in the case of Ising models). To achieve this, Metropolis sampling uses a Markov chain which converges to a stationary distribution π(x) such that π(x) = P(x). A Markov process is defined by its transition probability T(x′ | x) which gives the probability of moving from a state x to another state x′. Detailed balance is a sufficient but not necessary condition for the Markov chain to converge to a stationary distribution. Detailed balance means that the probability of being in state x and moving to state x′ is equal to the probability of being in state x′ and then moving to state x.

$$P(x)T(x'|x) = P(x')T(x|x')\,. \tag{2.43}$$

The transition probability of the Markov chain can be derived from the above condition of detailed balance. The above equation 2.43 can be rewritten as

$$\frac{T(x'|x)}{T(x|x')} = \frac{P(x')}{P(x)}\,. \tag{2.44}$$

The transition probability T(x′ | x) can be split into two components: the

proposal probability and the acceptance probability. The proposal probability g(x′ | x) is the conditional probability of proposing a state x′ given x, and the acceptance probability A(x′ | x) is the conditional probability to accept the proposed state x′. The transition probability can then be written as the product of the proposal probability and the acceptance probability.

$$T(x'|x) = g(x'|x).A(x'|x)\,. \tag{2.45}$$

Inserting the relation of 2.45 in 2.44 gives

$$\frac{A(x'|x)}{A(x|x')} = \frac{P(x')}{P(x)}\frac{g(x|x')}{g(x'|x)}\,. \tag{2.46}$$

The algorithm assumes flipping a single spin as the only way to transition from a state to another state. In that case, the two selection probabilities are equal, g(x | x′)=g(x′ | x). Hence equation 2.46 reduces to

$$\frac{A(x'|x)}{A(x|x')} = \frac{P(x')}{P(x)}\,. \tag{2.47}$$

The probability of occurrence of a state x in an Ising model is proportional to the exponent of the energy of state x. Hence the ratio of the probability of being in state x′ and the probability of being in state x is equal to the exponent of the energy difference between x′ and x, $\Delta E = E(x') - E(x)$.

$$\frac{A(x'|x)}{A(x|x')} = e^{-\Delta E}\,. \tag{2.48}$$

However, this doesn't help to uniquely specify A(x' | x). One common choice is the Metropolis choice:

$$A(x'|x) = \begin{cases} e^{-\Delta E}, & \Delta E > 0 \\ 1, & \text{otherwise} \end{cases} \tag{2.49}$$

The above equation 2.49 which defines the transition probability of the Metropolis-Hastings algorithm for Ising model can be rewritten as

$$A(x'|x) = \min(1, e^{-\Delta E})\,. \tag{2.50}$$

The Metropolis-Hastings algorithm consists of the following steps:

1. Pick an initial configuration at random.
2. Pick a single spin i and flip it. Compute the change in energy Δ E = E(x')-E(x). One may compute Δ E by separately computing E(x) and E(x'). Since the change between both configurations is only at the spin i, one may derive a computationally inexpensive expression for Δ E using equation 2.37. Accept the new configuration with the probability $\min(1, e^{-\Delta E})$. If accepted, the configuration x transits to the new configuration x'. If not accepted, the configuration stays at x. Flipping a single spin and deciding whether to accept the flip constitutes a Metropolis step.
3. Performing a Metropolis step for all the spins (1 to N) constitutes a Metropolis sweep. Observables are usually measured once every sweep.

4. Performing M sweeps is a complete experiment. M should be chosen so that the standard deviation of the measured Ising model average reduces to a desired level of accuracy.

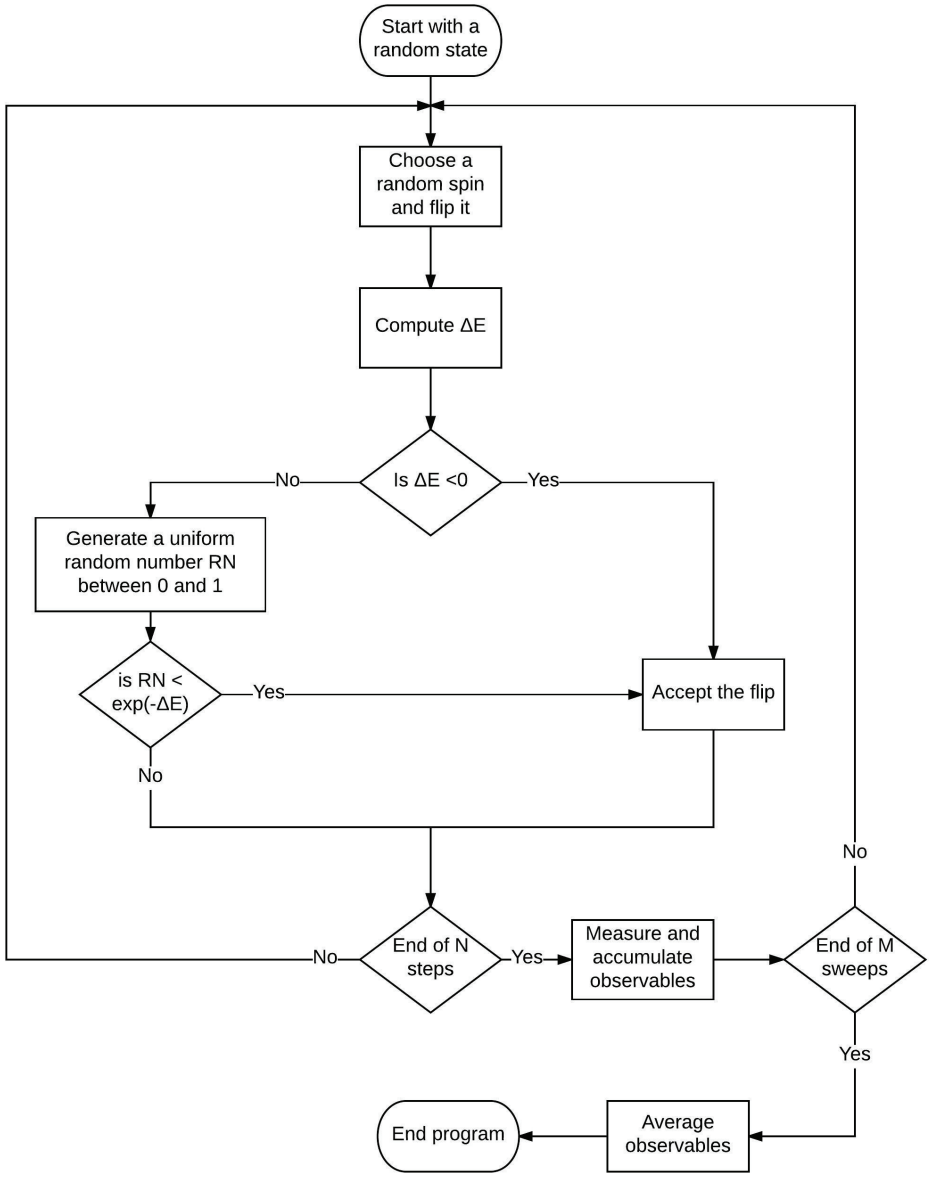

Figure 2.7: Flowchart of Metropolis-Hastings algorithm.

Before running the M metropolis sweeps in which the observables are accumulated and measured, one should first run L Metropolis sweeps to allow for the Markov chain to converge to the equilibrium distribution. The L sweeps are called the burn-in or the thermalisation period. The M sweeps are called the accumulation period. The states generated by the Markov chain during the burn-in period are not used to measure the Ising model observables of interest. A rule of thumb for choosing the number of sweeps for the burn-in period is about 10 to 20% of the total number of sweeps in the simulation.

The steps executed in the Metropolis algorithm are best summarised in the flowchart depicted in Figure 2.7.

2.5.4 Reconstructing structural connectivity using Ising couplings

With the success of the Ising model in characterizing the firing activity of neuronal ensembles, the coupling parameter of the Ising model lends itself as a measure of functional connectivity.

Since Ising parameters are calculated taking all the correlations in the network into account, the Ising coupling parameters are able to correct the indirect effects of the network [BC13; Sch+06; GSS11]. [Tka+09] describes Ising coupling parameter J_{ij} as "the direct mutual interaction between neurons i and j that remains after the contributions from other interactions in the network have been disentangled". Yu et al[Yu+08] suggested that Ising coupling parameters can distinguish between correlations caused by shared inputs and correlations caused by direct mutual interaction. Hence

Yu et al applied Ising models to built the functional interaction network for neuronal recording taken in vivo from visual cortex of cats and observed that the resultant functional networks have small world properties. The ability of Ising coupling parameters to account only for the direct interactions in the network renders them as robust indicators of the underlying structural connectivity in the network.

However, the question of how the Ising couplings compare against the conventional functional connectivity measures under different network conditions has not been answered in a systematic and quantitative manner. Chapter 4 answers this question by systematically studying the relationship between Ising couplings and the underlying structural connections and contrast it to partial and cross-correlations, in *in silico* neuronal networks for different network conditions.

2.6 Kinetic Ising models

The term "Ising model" and the term "equilibrium Ising model" will be used interchangeably in this thesis to refer to the Ising model defined by the equation 2.33 and described in the preceding section 2.5. To resolve ambiguity, kinetic Ising model will be explicitly mentioned. The Ising model is defined solely by the Gibbs equilibrium distribution. It only uses the probability distribution of the spins and ignores the temporal order of the spins as it is based on a stationarity assumption. Even though the Gibbs equilibrium is satisfied in many applications, the equilibrium assumption may not hold for systems driven by time-dependent external fields [RH11]. The condition of detailed balance may not be satisfied in those systems. Also, the

assumption of symmetric connections is not realistic when the Ising models are applied to biological networks such as neuronal networks. Kinetic and non-equilibrium models have a bigger relevance for studying biological systems.

Relaxing the assumptions of equilibrium and symmetric couplings led to the development of inference methods based on a kinetic formulation of the equivalent Ising system that results in maximum likelihood estimations of the transition probabilities between successive states of the system [Cap+15]. The Ising model is referred to as a kinetic Ising model if the state of the spins follow a certain dynamics and are dependent on the time.

Following earlier notations used in this thesis, the state of each neuron in a time bin t is represented by the binary variable $\sigma_i(t) = \pm 1$ depending on neuron i spiking in the time bin t. In a kinetic Ising model, the objective is to infer a statistical model which maximizes the probabilities of the spike histories $\sigma_i(t)_{i=1}^{N}$, $1 \leq t \leq$ T, where N is the total number of neurons in the network and T is the total number of time bins. This is different from the objective of a standard Ising model where one ignores the temporal order of the spike patterns and is interested only in modelling the probability distribution of the spike patterns. Based on Glauber dynamics [Gla63], Hertz and Roudi [HRT13] proposed the following kinetic Ising model for the neuronal spiking data.

At each time step t, the neuron i receive inputs from both the external field h_i and the other presynaptic neurons in the network. The total field on a neuron i in a time bin t, $H_i(t)$ is given by the sum of the external field component and the synaptic component and is calculated as

$$H_i(t) = h_i + \sum_j J_{ij}\sigma_j(t)\,. \tag{2.51}$$

At the next time step (t+1), the neuron i fires with a probability equal to the logistic sigmoidal function of its total field input conditional on the state of the network at time step t:

$$P(\sigma_i(t+1) = 1|\sigma_j(t)) = f(H_i(t))\,, \tag{2.52}$$

where f(x) is the logistic sigmoidal function given by

$$f(x) = \frac{1}{1+e^{-2x}}\,. \tag{2.53}$$

Equation 2.52 can be rewritten as

$$P(\sigma_i(t+1)|\sigma_j(t)) = \frac{\exp[\sigma_i(t+1)H_i(t)]}{2\cosh H_i(t)}\,, \tag{2.54}$$

$$P(\sigma_i(t+1)|\sigma_j(t)) = \frac{1}{2}[1+\sigma_i(t+1)\tanh H_i(t)]\,. \tag{2.55}$$

Since $H_i(t)$ (and hence the state of the system at a time $(t+1)$) is a function of the state of the network at time step t only, the dynamics described in equation 2.55 is Markovian. The external field parameter h_i and the couplings J_{ij} are the parameters of the kinetic Ising model. The field parameter h_i can be generalized to be time dependent. If the field parameter h_i is time dependent, then the network statistics will be non-stationary. This makes it possible to apply kinetic Ising models to describe non-stationary

data, assuming that the couplings J_{ij} do not vary with time. In case of non-stationary data, one needs data from many runs of the system to compute $h_i(t)$ as the different time steps are not statistically equivalent.

The probability $P_t(\sigma)$ that the system is in state σ at time t can be derived from the knowledge of the transition probability equation 2.54 as follows:

$$P_t(\sigma) = \sum_{\sigma'} P(\sigma(t)|\sigma'(t-1))P_{t-1}(\sigma')\,, \tag{2.56}$$

where $P(\sigma(t)|\sigma'(t-1))$ is the transition probability from state σ' at time-bin $(t-1)$ to state σ at time-bin t and is given by

$$P(\sigma(t)|\sigma'(t-1)) = \prod_i \frac{\exp[\sigma_i(t)H_i(t-1)]}{2\cosh H_i(t-1)}\,. \tag{2.57}$$

This kinetic Ising model is the maximum entropy model for each time step, given mean magnetizations and one step separated correlations [RH11]. The neurons/spins in a kinetic Ising model in a time-step can be updated either synchronously or asynchronously. If all the neurons are updated simultaneously in parallel in a time step, the update is called a synchronous update. In an asynchronous update, each time-step is further divided into N smaller time increments. One neuron is randomly selected and updated in a time increment. During the N time increments, each neuron gets selected to be updated once on average. But it is not guaranteed that each neuron will be selected and updated in a time step consisting of N time increments. This mode of update where the neurons are updated sequentially within a time step is called an asynchronous update. If the neurons are updated asynchronously, then the kinetic Ising model reduces to the

Gibbs equilibrium distribution of the standard Ising model if the external field parameter h_i is independent of time and the coupling parameter J_{ij} are symmetric. For the case of synchronous updates, if the field h_i is constant in time, then the network relaxes to a stationary distribution (though not to the same distribution described by the Gibbs equilibrium distribution). Since such a distribution cannot be described by the Gibbs equilibrium distribution, it is called a non-equilibrium distribution though it is stationary [HRT13]. Since the synchronous model will be easier to apply for the time-binned data (like the neuronal spiking trains), this work focuses solely on the synchronously updated kinetic Ising models. A detailed treatment of asynchronously updated kinetic Ising models is available at [Zen+11; Zen+13]. Also, it should be noted that kinetic Ising model can be seen as a special case of generalised linear models (GLM) with a one-step time kernel [HRT13; RDH15].

2.6.1 Inference of parameters of the kinetic Ising models

Let us first consider the case where the field parameter h_i is constant in time and the probability distribution P(σ) is stationary. The log-likelihood that the kinetic Ising model generated the data is given by

$$\begin{aligned}\mathcal{L}[\sigma, J, h] &= \sum_{t=1}^{T-1}\sum_{i=1}^{N} \log(P(\sigma_i(t+1)|\sigma(t)) \\ &= \sum_{t=1}^{T-1}\sum_{i=1}^{N} [\sigma_i(t+1)H_i(t) - \log 2\text{cosh}H_i(t)]\,. \end{aligned} \tag{2.58}$$

The model parameters h_i and J_{ij} can be found by maximizing the log-likelihood of the data under the model. Similar to the Boltzmann learning method of the standard Ising model, the maximization can be performed using a gradient ascent algorithm. One starts with an initial value for the model field parameters and the coupling parameters and adjusts them iteratively using the following rules

$$\delta h_i = \alpha \frac{\partial \mathcal{L}}{\partial h_i}\,, \tag{2.59}$$

$$\delta h_i = \alpha[\langle \sigma_i(t+1)\rangle_t - \langle \tanh H_i(t)\rangle_t]\,, \tag{2.60}$$

$$\delta J_{ij} = \alpha \frac{\partial \mathcal{L}}{\partial J_{ij}}\,, \tag{2.61}$$

$$\delta J_{ij} = \alpha\left[\langle \sigma_i(t+1)\sigma_j(t)\rangle_t - \langle \tanh H_i(t)\sigma_j(t)\rangle_t\right]\,, \tag{2.62}$$

where α is the learning rate.

It can be observed that pair of equations 2.60 and 2.62 are similar in form to the pair of equations 2.41 and 2.42 corresponding to the equilibrium Ising model. The right-hand side of both pairs of equations is the difference between the averages of the data and the averages of the model. Computing the model averages in the case of equilibrium Ising model involves the summation of 2^N terms and is time-consuming. However, in the case of kinetic Ising model, the model averages can be computed directly and quickly from the model parameters and the spike train data. Hence the gradient ascent algorithm for kinetic Ising model runs much faster when

compared to that of equilibrium Ising model. Theoretically, the gradient ascent algorithm defined as in equations 2.60 and 2.62 will recover the exact values of the model parameters h and J after infinite iterations for spike-train data of infinite length [HRT13].

In the non-stationary case, the field parameter h_i is not constant and depends on time. As the time-bins are not statistically equivalent, data from many runs of the experiment is needed in the non-stationary case [HRT13]. Let $\sigma_i(t, r)$ denote the state of the neuron i in the time-bin t during the r^{th} run. It should be noted that since h_i is time-dependant, H_i is also now time-dependent.

Most of the discussions for the stationary case applies to the non-stationary case and hence the gradient ascent learning rules for $h_i(t)$ and J_{ij} can be written in a form analogous to the stationary case as follows [RH11]:

$$\delta h_i(t) = \alpha[\langle \sigma_i(t+1, r)\rangle_r - \langle \tanh H_i(t, r)\rangle_r] \,, \tag{2.63}$$

$$\delta J_{ij} = \alpha \left[\langle \sigma_i(t+1)\sigma_j(t)\rangle_{t,r} - \langle \tanh H_i(t, r)\sigma_j(t, r)\rangle_{t,r}\right] \,, \tag{2.64}$$

where $\langle ...\rangle_{t,r}$ represents averaging over both time and repeats and $\langle ...\rangle_r$ represents averaging over repeats.

2.6.2 Kinetic Ising model with time delays

The kinetic Ising model proposed by Hertz and Roudi [HRT13] did not account for networks with variable spike transmission delays. Capone et al [Cap+15] extended the kinetic Ising model to account for variable spike transmission delays.

To understand the role of the size of the time-bin (time-step) on the inference of the Ising parameters, Capone et al simulated a pure excitatory network of 50 neurons with a spike transmission delay δ of 3ms for all the neuron pairs. The spike trains were then binarised for different choice of time-bins dt and the kinetic Ising coupling inferred for each choice of time-bin were analysed. It was observed that only when the time-bin size was equal to the spike transmission delay, the histogram of the Ising couplings corresponding to connected and unconnected pairs were separated. When the time bin size did not match the spike transmission delay, some J_{ij} couplings corresponding to the neurons which are connected (by an excitatory link) were even inferred as negative and appeared to have been estimated as inhibitory. Capone et al explained their observation based on equation A.21. A spike fired by a presynaptic neuron j reached the neuron i at a time $t + \delta_{ij}$ (where δ_{ij} is the spike transmission delay from presynaptic neuron j to neuron i). Only when the time-bin size dt was equal to the transmission delay δ_{ij}, the conditional probability $P((\sigma_i(t + dt) = 1)|(\sigma_j(t) = 1))$ (the numerator term in equation A.21) and hence the Ising coupling J_{ij} was maximum. Thus, Capone et al established that the choice of time-bin should be based on the spike transmission delay in the network.

As the kinetic Ising model discussed so far cannot cater to networks with

variable spike transmission delays, Capone et al [Cap+15] conceived a two-step method to solve this problem. They suggested to first estimate the spike transmission delay for each neuron pair, and then use the estimated pair dependent delay in the extended kinetic Ising model as follows:

$$H_i(t) = h_i + \sum_j J_{ij}\sigma_j(t - \delta_{ij})\,. \tag{2.65}$$

As the spike transmission delay for each pair of neurons was handled, the inference method was made independent from the choice of the time-bin dt for a network with variable spike transmission delays.

Instead of maximizing the log-likelihood of the model under the data to estimate δ_{ij} used in equation 2.65, Capone et al suggested to infer δ_{ij} as the time when the time-retarded cross-correlation between the neurons i and j reaches a peak/dip. This idea is based on the observation that the cross-correlation peaks or dips (depending on whether the connection is excitatory or inhibitory) at a time close to the spike transmission delay.

Capone et al applied the two-step extended kinetic Ising model to a simulated network of excitatory and inhibitory Izhikevich neurons with variable spike transmission delays and observed that there is a clear separation between the kinetic Ising couplings corresponding to the connected pairs and the unconnected pairs.

2.6.3 Reconstructing structural connectivity using kinetic Ising couplings

The advantages of kinetic Ising couplings over Ising couplings are that they are directional (whereas Ising model couplings are symmetric by construction) and can also account for non-stationary neural data. As kinetic Ising couplings take into account the whole network activity, they have been found to discard the spurious effect of common inputs and indirect connections in the network [RDH15].

As the kinetic Ising couplings can correctly identify the true connections in the network, they are very effective in reconstruction of the structural networks. Hertz et al [Her+10] observed that the coupling parameters of a kinetic formulation of the Ising model were able to reconstruct the structural connections of a model cortical network very reliably. Assuming correct level of sparsity, the average false positive and false negative rates were found to be around 5.6% and 7.2% respectively in their study.

Over the recent years, there has been a growing interest in application of kinetic Ising models for network reconstruction. Mean field approximations of the kinetic Ising model were developed to infer the structural connectivity in networks [RH11; Zen+11]. Capone et al [Cap+15] extended the kinetic Ising model (as described in section 2.6.2) to account for variable spike transmission delays and found that the extended model was successful in distinguishing the connected and unconnected pairs of neurons in the network.

Roudi et al [RDH15] observed that kinetic Ising couplings performed better than cross-correlations in identifying excitatory and inhibitory links in

a simulated network (kinetic Ising couplings identified 94% and 62% of the inhibitory connections and excitatory ones; cross-correlation analysis identified only 68% and 22% of the inhibitory and excitatory connections, respectively). The results from [RDH15] are not surprising as cross-correlation analysis is known to be susceptible to the impact of indirect interactions arising out of poly-synaptic connections and common inputs [EDS03; Ada+12].

A more appropriate benchmark for the inference of structural connections is partial correlation as it is known to be effective in removing indirect interactions [EDS03; Pol+16]. Comparing kinetic Ising couplings against partial correlations will help to make a choice regarding the right functional connectivity tool to reconstruct the structural connectivity. No comparison has yet been carried out between kinetic Ising couplings and partial correlations in assessing their performance in inferring the structural links. Also, the effect of network conditions on the relative performance of kinetic Ising couplings and partial correlation has not be studied previously. Chapter 5 presents the results of the systematic study of the predictability of the underlying structural connections by kinetic Ising couplings, in comparison to partial and cross-correlations, in *in silico* neuronal networks and discuss how the predictability is affected by different network conditions.

2.7 Summary

In summary, this chapter presented the background concepts pertaining to complex networks and the three types of connectivity found in neuronal networks (structural, functional and effective). The conventional functional

connectivity metric of cross-correlation and the limitations of the cross-correlation approach while inferring the structural connections were discussed. Partial-correlation based on scaled partial covariance density which has been shown to outperform cross-correlations in reconstructing structural connections was then presented. The chapter then introduced maximum entropy based Ising models and presented the inference of the parameters of the Ising model. Finally, the kinetic Ising model and an extended kinetic Ising model that can cope with a distribution of spike transmission delays were discussed. Though Ising couplings and kinetic Ising couplings are claimed to be good indicators of the structural connectivity, the chapter highlighted the gap in the existing literature about lack of benchmark on the performance of Ising and kinetic Ising couplings against partial correlations in inferring the structural connections for different network conditions. The results of the comparative study of the performance of Ising couplings against partial correlation is presented in chapter 4. And the results of the comparative study of the performance of kinetic Ising couplings against partial correlation is presented in chapter 5. The methods used in the comparative studies are discussed in the next chapter.

Chapter 3

Methods

Contents

This thesis attempts to reconstruct the structural connections from functional connectivity metrics in *in silico* networks. The functional connectivity metrics are calculated from the spike data recordings of the network activity. The functional connectivity metrics considered in this thesis are

equilibrium Ising couplings, kinetic Ising couplings, cross-correlations, and partial correlations. This chapter will discuss the methods used in this thesis. Firstly, the chapter describes the *in silico* simulation network used to generate the spiking data. Then, the methods used to calculate the functional connectivity metrics are given. Finally, the procedure to evaluate the performance of the functional connectivity metrics in reconstructing the structural connectivity is discussed. As in other chapters of this thesis, the usage of the term "Ising couplings" refers to the equilibrium Ising couplings. Kinetic Ising couplings are mentioned explicitly.

3.1 Simulation network

3.1.1 Neuronal dynamics

The *in silico* simulation network consisted of N Izhikevich spiking model neurons [Izh03]. Izhikevich model was chosen for its computational efficiency and its capability to generate several firing patterns based on four parameters [Izh04]. The Izhikevich model is a two-dimensional (2-D) system of ordinary differential equations:

$$v^{'} = 0.04v^2 + 5v + 140 - u + I\,, \tag{3.1}$$

$$u^{'} = a(bv - u)\,, \tag{3.2}$$

with the auxiliary after-spike resetting

$$\text{if } v \geq 30 \text{ mV, then } v \leftarrow c, u \leftarrow u + d\,. \tag{3.3}$$

Here a, b, c, and d are the parameters of the model, v is the neuron's membrane potential, and u is the membrane recovery variable. The latter variable serves to provide negative feedback to v and simulates deactivating sodium current and activating potassium current. Once the spike reaches a peak value (+30 mV), the value of v and u are reset as per the equation 3.3. The variable I represents the total input current to the neuron. The function $0.04v^2 + 5v + 140$ is chosen such that v has mV scale and the time t has ms scale. The model's resting potential value varies according to the value of b and ranges between -70 and -60 mV. The 30 mV occurring in equation 3.3 is the peak value of the spike and not the threshold of the neuron model. Similar to biological neurons, the model has a dynamic threshold. The threshold potential can vary between a minimum of -55 mV to a maximum of -40 mV depending on value of v before the initiation of the spike.

The parameter a denotes the time scale of the membrane recovery variable u. Smaller value of a corresponds to slower recovery. The parameter b denotes the sensitivity of the membrane recovery variable u to the subthreshold fluctuations of the membrane voltage v. The parameter c denotes the reset value of the membrane voltage v after the spike. The parameter d denotes the reset value of the membrane recovery variable u after the spike. The Izhikevich simple spiking model is able to produce different bursting and spiking behaviours of biological neurons for different values of the parameters (see Figure 3.1). The model is suitable for simulating large number of neurons as it is computationally efficient and requires only 13 FLOPs for simulation of 1 ms duration [Izh04].

To achieve heterogeneity in the spiking dynamics of the neurons, the excitatory neurons in the simulation network were modeled using the parameters

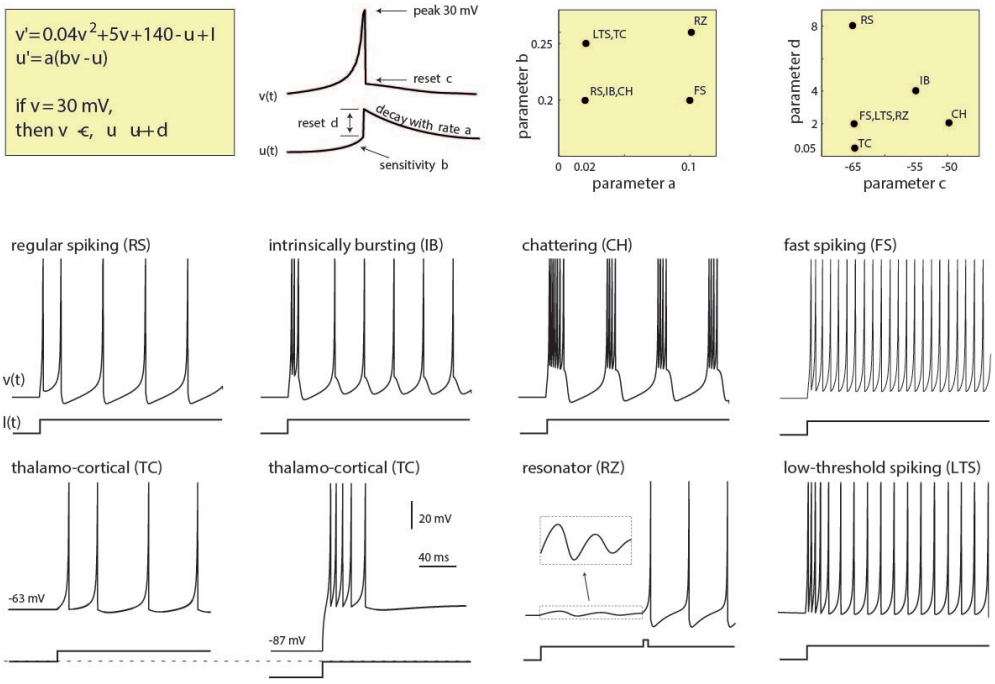

Figure 3.1: Top left : Graphical illustration of the parameters a, b, c and d of the Izhikevich model. Top right: Different parameter values resulting in different firing patterns (bottom) of common neuron types. Excitatory:RS, IB and CH. Inhibitory:FS and LTS. Electronic version of the figure and reproduction permissions are freely available at www.izhikevich.com

(a, b) = (0.02, 0.2) and (c, d) = $(-65, 8) + (15, -6)\mathrm{r}^2$, where r is a uniformly distributed random variable in the interval (0, 1). The case of r=0 corresponds to a regular spiking neuron model and r=1 corresponds to a chattering neuron model. r^2 was used to bias the distribution towards regular spiking neurons. The inhibitory neurons were modeled using the parameters (a, b) = (0.02, 0.25) + (0.08, -0.05)r and (c, d) = (-65, 2). The case of r=0 corresponds to the low threshold spiking class of inhibitory neurons and the case of r=1 corresponds to the fast spiking class of inhibitory neurons. The ratio of excitatory to inhibitory neurons was set to 4:1 in agreement with the experimental studies [MS02].

Inspired by Rocha et al [DLR+07], the total input current, I_i, to each neuron i was modeled using the equation:

$$I_i = I_i^{base} + \left[(1 - CF) * I_i^{thalamic} + CF * I_i^{synaptic}\right]. \tag{3.4}$$

The total input current I_i to each neuron i consisted of 3 components: I_i^{base} was a constant input with an additive Gaussian noise of zero mean and unit variance which influenced the average firing rate of the neuron. $I_i^{thalamic}$ was a noisy random input which was given by a Gaussian variable multiplied by a constant and was uncorrelated for any two neurons. $I_i^{synaptic}$ of a neuron i was the sum of the synaptic inputs from the presynaptic neurons connected to it. CF was a global control factor variable $(0 \leq CF \leq 1)$ which affected the amount of correlation between the firing of the neurons in the networks by controlling the relative contribution of $I_i^{thalamic}$ and $I_i^{synaptic}$. When $CF = 0$, the contribution of $I_i^{synaptic}$ to total input became zero and the input of a neuron was influenced by the noisy $I_i^{thalamic}$ and hence the

firing between the neurons was less correlated. When $CF = 1$, the contribution of the $I_i^{thalamic}$ component became zero. The firing of a neuron increased the $I_i^{synaptic}$ of its postsynaptic neuron and hence the postsynaptic neuron had higher chances of firing together with the presynaptic neuron. Thus, neurons spiked together more when $CF = 1$.

This choice of input allowed the simulation of two modes of functioning of the cortical circuits namely the feedforward mode and the recurrent mode. In the feedforward mode, the cortical circuits respond more to the afferent incoming information from the external pathways rather than the recurrent internal synaptic pathways. The feedforward mode is simulated for low values of CF where the afferent $I_i^{thalamic}$ input component is enhanced and the recurrent $I_i^{synaptic}$ input component is suppressed. In the recurrent mode, the cortical circuits respond more to the recurrent internal synaptic inputs than the external afferent inputs. The recurrent mode is simulated for high values of CF where the $I_i^{synaptic}$ synaptic input component is enhanced and the external $I_i^{thalamic}$ component is suppressed.

The synaptic current $I_i^{synaptic}$ received by a neuron i is described the equations given below [DÖ13]:

$$I_i^{synaptic} = \sum_{j(\neq i)}^{N} g_j(t)(E_{syn} - v_i)\,, \tag{3.5}$$

$$\frac{dg_i}{dt} = \frac{-g_i + g_\infty}{1 - g_\infty}\,, \tag{3.6}$$

$$g_\infty(v_i) = 1/\{1 + \exp(\frac{v^* - v_i}{k})\}\,, \tag{3.7}$$

where g_i is the synaptic gate variable denoting the fraction of open synaptic

ion channels, E_{syn} is the synaptic reversal potential (set to 10 mV), g_∞ is the steady state activation function, k is the synaptic slope factor (set to 2 mV) and the parameter v^* satisfies $g_\infty(v^*) = 0.5$.

The network of Izhikevich neurons was simulated for different values of average firing rates by adjusting the values of I_i^{base}. The different correlation levels were simulated by adjusting the values of the control factor CF, the gain of the noisy random input component $I_i^{thalamic}$ and the gain of the synaptic current $I_i^{synaptic}$. Very weak network correlation condition was simulated using a combination of low value of CF, high gain factor of $I_i^{thalamic}$ and a low gain factor of $I_i^{synaptic}$. This combination results in a high random current component (which is uncorrelated between the neurons) and a low synaptic current component (which is responsible for the correlation between the neurons) and thus yielding a very weak correlated firing condition in the network. Conversely, a high network correlation condition was simulated using a combination of a high value of CF, low gain factor of $I_i^{thalamic}$ and a high gain factor of $I_i^{synaptic}$.

3.1.2 Structural connectivity

The connectivity between the neurons was given by the adjacency matrix A = (w_{ij}). The firing of the jth neuron affected the voltage of the ith neuron by an amount w_{ij} multiplied by CF. The strengths of the links (nonzero w_{ij} in the adjacency matrix) were distributed normally with a mean of 0.6 and a standard deviation of 0.13 and were limited to the interval [0.21,

0.99]. Self-loops were not allowed. The adjacency matrix for each simulated topology (scale-free, small-world, and random networks) was generated using the corresponding topology generation algorithms. Scale-free (SF) topology was generated using directed preferential attachment model for network growth [BA99]. Brain connectivity toolbox [RS10] was used to generate modular small-world (SW) topology with a specified number of fully connected modules connected via randomly distributed inter-module connections. Erdos-Renyi (ER) random networks were generated with a fixed connection probability between all pairs of neurons. For all topologies, the total number of links in the network was fixed at 20% of the total possible links (which is $N * (N - 1)$) as studies [JTR99; MS02; Pol+16] suggest that on an average each neuron is connected to 10% to 30% of the other neurons in *in vitro* cultures. A sample of each network type generated for a network of 30 neurons is presented in Figure 4.5b.

3.1.3 Generation of spike train data

The neuronal network was then simulated for a length of time to capture the spike train data. When the voltage of a neuron reached a threshold (which was a dynamic value, depending on the parameters of the neuron), a spike was initiated. The time of the spike and the number of the neuron which spiked was recorded to generate the spike train data of the simulated neuronal network.

The spike train data was converted to a binary vector by splitting the duration of the simulation into many time bins of equal width. Ising model can only infer the interactions which occur in the same time bin as they are

calculated from equal-time correlations (rather than delayed correlations). Hence, the length of the time bin for Ising couplings should be wider than the spike transmission delay so that the spike of the presynaptic neuron and the spike of the postsynaptic neuron are captured in the same time bin. The spike transmission delay in the simulation network was between 4 ms and 6 ms. Hence, a time bin size of 10 ms was used to bin the firing data for use in Ising models. This choice of bin size also made sure that not more than a single spike from the same neuron fell in the same time bin (for firing rates up to 100 Hz). As kinetic Ising model (and its extended version discussed in section 2.6.2) depend on delayed correlations, the spike train was binned at 1 ms for use with extended version of the kinetic Ising model.

The state of a neuron i in a time bin was represented by σ_i and it took a value of +1 or -1 corresponding to the presence or absence of spikes in that time bin. The average firing rate $\langle \sigma_i \rangle_{data}$ of a neuron i and the average pairwise joint firing rate $\langle \sigma_i \sigma_j \rangle_{data}$ for a pair of neurons i and j were calculated using the following equations [Tan+08]:

$$\langle \sigma_i \rangle_{data} = \frac{1}{T} \sum_{t=1}^{T} \sigma_i^t, \tag{3.8}$$

$$\langle \sigma_i \sigma_j \rangle_{data} = \frac{1}{T} \sum_{t=1}^{T} \sigma_i^t . \sigma_j^t, \tag{3.9}$$

where the angle brackets indicate averaging over time, T was the total number of time bins for the duration of the simulation and σ_i^t was the state of the neuron i in a particular time bin t. The covariance Cov_{ij} between the firing of two neurons i and j was defined as $Cov_{ij} = \langle \sigma_i \sigma_j \rangle_{data} - \langle \sigma_i \rangle_{data} . \langle \sigma_j \rangle_{data}$.

And, the correlation coefficient between the spike trains of the neurons i and j was calculated as $\rho_{ij} = \frac{Cov_{ij}}{s_i s_j}$ where s_i was the standard deviation of firing activity σ_i of the neuron i. The mean network correlation ρ was calculated as the average of the correlation coefficient between all pairs of neurons.

3.2 Calculation of equilibrium Ising parameters

In order to use the Ising model, it is necessary to estimate the parameters h_i and J_{ij} of the model ensuring that the first and second order moments of the model (given by $\langle\sigma_i\rangle_{model}$ and $\langle\sigma_i\sigma_j\rangle_{model}$) match with the observables ($\langle\sigma_i\rangle_{data}$ and $\langle\sigma_i\sigma_j\rangle_{data}$) from the simulation. The direct way to calculate the Ising model parameters h_i and J_{ij} given the averages is Boltzmann learning [RTH09]. A few approximate methods [RTH09] are available to calculate the Ising couplings. The approximate methods make a few assumptions about the network activity. As those assumptions may not be fulfilled in all the cases considered, Ising couplings were calculated exactly using Boltzmann learning in this work. The Boltzmann learning method starts with an initial value for the parameters h_i and J_{ij} and adjusts them iteratively according to equations 3.10 and 3.11 till the first and second order moments of the Ising model ($\langle\sigma_i\rangle_{model}$ and $\langle\sigma_i\sigma_j\rangle_{model}$) agree with the estimates obtained from the simulation data ($\langle\sigma_i\rangle_{data}$ and $\langle\sigma_i\sigma_j\rangle_{data}$) within the desired accuracy.

$$h_i^{new} = h_i^{old} + \alpha.(\langle\sigma_i\rangle_{data} - \langle\sigma_i\rangle_{model}) \,, \tag{3.10}$$

$$J_{ij}^{new} = J_{ij}^{old} + \alpha.(\langle \sigma_i \sigma_j \rangle_{data} - \langle \sigma_i \sigma_j \rangle_{model}) \,, \tag{3.11}$$

where α is the learning rate. It is usually held constant and is generally kept less than 1 to get a smoother convergence.

As can be seen from the above equations, the first and second order moments of the Ising model need to be calculated for each iteration of the gradient descent algorithm. The exact method for computing $\langle \sigma_i \rangle_{model}$ and $\langle \sigma_i \sigma_j \rangle_{model}$ from the Ising parameters h_i and J_{ij} is given by equations 2.39 and 2.40 in section 2.5.3. As can be seen from equations 2.39 and 2.40, the exact method of calculating the first and second order moments of the Ising model has a computational complexity of the order $\mathcal{O}(2^N)$ [Yeh+10] and is a computationally intensive task. This exact method of calculating the Ising model averages was used only for small N ($\leq$ 20). For larger N, Monte Carlo sampling based on standard Metropolis-Hastings simulation (explained in section 2.5.3.1) was used. The Metropolis Hastings has a complexity of $\mathcal{O}(\text{NumberOfIterations})$. A very large number of iterations of the order of 10^7 was used to calculate $\langle \sigma_i \rangle_{model}$ and $\langle \sigma_i \sigma_j \rangle_{model}$ in this work.

3.3 Calculation of kinetic Ising parameters

This thesis uses the extended kinetic Ising model (described in section 2.6.2) introduced by Capone et al in [Cap+15]. The change introduced by Capone et al allowed the kinetic Ising model to account for variable synaptic interaction delays. Using the same notations introduced earlier in section 3.1.3, $\sigma_i(t)$ denotes the state of a neuron i recorded in a time bin t and

$\sigma = \{\sigma_i(t)\}, 1 \leq i \leq N$. The kinetic Ising model is based on a stochastic dynamics where the configuration $\sigma(t+1)$ depends on $\sigma(t)$. At each time-step, $\sigma(t+1)$ is sampled according to the probability distribution:

$$P(\sigma_i(t+1)|\sigma(t)) = \frac{\exp[\sigma_i(t+1)H_i(t)]}{2\cosh H_i(t)}\,, \tag{3.12}$$

$$H_i(t) = h_i + \sum_j [J_{ij}\sigma_j(t-\delta_{ij})]\,, \tag{3.13}$$

where δ_{ij} denotes the synaptic transmission delay from the presynaptic neuron j to the postsynaptic neuron i.

The coupling parameters of the kinetic Ising model J_{ij} are non-symmetric. Hence the model has N(N-1) coupling parameters J_{ij} and N field parameters h_i. The parameters of the model are derived by maximizing the log-likelihood of the data under the model which is given by the equation 2.58 in section 2.6.1. This results in the following learning rules [HRT13]

$$\delta h_i = \alpha[\langle\sigma_i(t+1)\rangle - \langle\tanh H_i(t)\rangle]\,, \tag{3.14}$$

$$\delta J_{ij} = \alpha[\langle\sigma_i(t+1)\sigma_j(t)\rangle - \langle\tanh H_i(t)\sigma_j(t)\rangle]\,. \tag{3.15}$$

Equations 3.14 and 3.15 have a form analogous to the the equations 3.10 and 3.11 of the equilibrium Ising case. The right hand side of both sets of equations are the difference between the averages over the data and the averages of the model. The averages of the kinetic Ising model can be

calculated directly from the data and the model parameters. Whereas in the case of equilibrium Ising model, computation of the averages of the model requires large number of iterations of the Metropolis Hastings simulation or summation 2^N terms. Hence, the gradient descent algorithm in the case of kinetic Ising parameters was much faster than in the case of equilibrium Ising parameters [HRT13]. The synaptic transmission delay δ_{ij} for a given pair ij of neurons were calculated from the cross-correlogram between the neurons. The time lag corresponding to the peak/dip (depending on whether the connection is excitatory or inhibitory) of the cross-correlogram corresponded to the synaptic interaction delay δ_{ij}.

3.4 Calculation of cross-correlations and partial correlations

Cross-correlation can be interpreted as the probability of one neuron (called the target neuron) spiking at time $(t + \tau)$ conditioned on the reference neuron spiking at a time t where Let x and y be the spike trains of the reference and the target neurons respectively. The cross-correlation function $C_{xy}(\tau)$ is defined as

$$C_{xy}(\tau) = \frac{1}{\sqrt{N_x N_y}} \sum_{s=1}^{N_x} \sum_{ti=(\tau-\frac{\triangle\tau}{2})}^{(\tau+\frac{\triangle\tau}{2})} x(t_s) y(t_s - t_i)\,, \tag{3.16}$$

where N_x and N_y are the total number of spikes in the spike trains x and y, respectively, τ is called the time lag, and t_s is the timing of a spike in the spike train x. The cross correlation function is computed for each pair of

neurons. The cross-correlation function is symmetric. That is, if we compute the cross-correlation function keeping x as reference and y as the target and then compute cross-correlation function keeping y as reference and x as the target, we will get the same function but just reversed in time.

$$C_{xy}(\tau) = C_{yx}(-\tau)\,. \tag{3.17}$$

The cross-correlation based functional connectivity matrix(CCM) is an N x N matrix. The (i,j) element of the CCM corresponds to the maximum amplitude of the cross-correlation function for the neuron pair (i,j). Because of equation 3.17, the CCM matrix is symmetric i.e. CCM(i,j) = CCM(j,i) and the symmetric CCM cannot account for the direction of the links.

It is however possible to detect the direction of the links using the cross-correlation function from the location of the peak of the cross-correlation function. If the peak is located to the right side of the center of correlation window, then the reference neuron is pre-synaptic to the target neuron. On the other hand, if the peak is located to the left side of the center of correlation window, then the reference neuron is post synaptic to the target neuron. Thus a directional and asymmetric CCM can also be obtained from the cross-correlation function.

Cross-correlation fails to distinguish between direct and indirect connections as it is calculated pairwise for each pair without any consideration of influence of the other elements of the network on the activity of the pair of neurons. Partial correlation approach attempts to solve this problem by removing the linear contribution of other neurons in the population when calculating the dependence for a pair of neurons. Consider x and y as

two neurons in a population P of neurons. The partialised cross-spectrum $S_{xy|P}$ between neurons x and y can be obtained as follows [BBS76; EDS03; Pas+16]:

$$S_{xy|P} = S_{xy} - (S_{xP}\, S_{PP}^{-1}\, S_{Py})\,, \tag{3.18}$$

where S_{xy} is the full cross spectrum between the neurons x and y, $S_{xP}(S_{yP})$ corresponds to the cross spectrum between the neuron x (y) and the population P and S_{PP} is the cross spectrum between the rest of the neurons in the population P. The partial correlation function is given by a scaled version of the inverse Fourier transform of $S_{xy|P}$. Similar to obtaining the symmetric and directional versions of the CCM matrix, one can obtain a symmetric and a directional version of the partial connectivity based functional connectivity matrix (PCM) as well.

An open-source toolbox based on C#, ToolConnect [Pas+16], was used in this work to compute both the directional and non-directional cross-correlation and partial correlation matrices (CCM and PCM). A time correlation window of 150 ms and a bin size of 1 ms were used to compute the cross-correlation and partial correlation matrices.

3.5 Evaluation of functional connectivity matrices

The structural connectivity matrix (also called the adjacency matrix) is a directional and sparsely connected (i.e. connectivity defined only between

specific pairs of neurons) binary matrix. The functional connectivity matrices are generally all-to-all connected matrices and can be directional or non-directional. Equilibrium Ising couplings are non-directional, while the kinetic Ising couplings are directional. Cross-correlation and partial correlation matrices can be directional or non-directional. For meaningful comparison with the structural connectivity matrix, the functional connectivity matrices should be reduced to a sparse binary form, through thresholding and binarising [RS10]. Thresholding absolute values of the functional connectivity matrices will also take into account negative values, which can occur in these matrices (which are indications of inhibitory links in the structural topology). If the functional connectivity matrix is non-directional, then the structural connectivity matrix should be symmetrised and converted to a non-directional matrix before comparison with the functional connectivity matrix.

In this work, the results of the comparison between the thresholded and binarised functional connectivity matrices (FCM) and the structural connectivity matrix (SCM) were recorded using the metrics of true positives (TP), false positives (FP), true negatives (TN) and false negatives (FN). If a non-zero value in the FCM corresponds to a non-zero value in the SCM, it is recorded as a TP. If a zero value in the FCM corresponds to a zero value in the SCM, it is recorded as a TN. If a zero value in the FCM corresponds to a non-zero value in the SCM, it is called a FN. If a non-zero value in the FCM corresponds to a zero value in the SCM, it is called as a FP.

The performance of the functional connectivity metrics to uncover the underlying structural connectivity was assessed by the amount of match between the SCM and the FCM for different threshold levels. The results of

the comparison were analysed using the standard receiver operating characteristic (ROC) curve analysis. The ROC is a standard method to study the performance of a binary classifier as the classification threshold is varied [Faw06]. The ROC curve is the plot of the relationship between the true positive ratio (TPR) and the false positive ratio (FPR) for different threshold levels. The TPR is defined as the ratio of the number of links in the FCM that match the the existing links in SCM to the total number of links in the SCM. FPR is the defined as the ratio of the links in FCM that do not match the links in SCM to the total number of zeros in the SCM. TPR and FPR are given by the following equations:

$$TPR = \frac{TP}{P} = \frac{TP}{(TP + FN)}\,, \tag{3.19}$$

$$FPR = \frac{FP}{N} = \frac{FP}{(TN + FP)}\,. \tag{3.20}$$

The highest threshold level leads to a zero TPR as well as a zero FPR. At the other extreme, the lowest threshold level leads to a 100% TPR and a 100% FPR. Intermediate levels of thresholds give rise to a curve of TPR vs FPR as a function of the threshold. Thus, the ROC curve shows the trade-off between sensitivity (same as TPR) and specificity (defined as 1-FPR). An increase in sensitivity will always be accompanied by a decrease in specificity. A random classifier will have a ROC curve along the diagonal line joining (0,0) and (1,1). A perfect classifier will have a ROC curve hugging the upper left corner of the plot. The more the ROC curve of a classifier deviates from the diagonal, the better is its performance. An example of the ROC curve is shown in Figure 3.2.

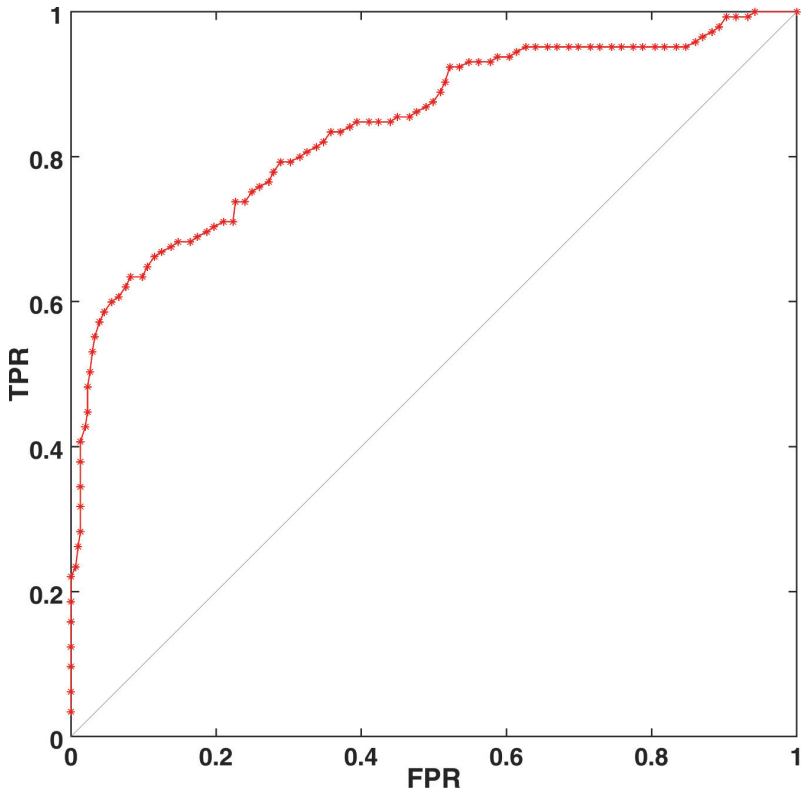

Figure 3.2: Example of a ROC curve.

A common approach to summarize the performance of the ROC curve in a single number is to calculate the area under the ROC curve (abbreviated as AUC) [Faw06]. The value of the AUC will be between 0 and 1 as the ROC curve covers a portion of the area under unit square (both TRP and FPR vary from 0 to 1). A random classifier will have an AUC value of 0.5. A perfect classifier will have an AUC value of 1.0. The closer the value of AUC is to 1, the better is the classifier.

Though, the AUC score is a widely used method to assess the performance of classifiers, it suffers from a few disadvantages as well. One of the main

disadvantages is that it states explicitly nothing about individual parameters such as sensitivity and specificity. It is a global measure and summarizes the performance over the entire ROC space including the regions in which one would rarely operate, e.g. the very high threshold region (which corresponds to a low TPR as well as a low FPR) and a very low threshold region (which corresponds to a high TPR as well as a high FPR). Hence, it is a good idea to use complementary metrics to get a complete picture on the performance of the functional connectivity metrics. Along with the AUC scores, the paired measures of true positive rate and false positive rate for a relevant threshold value and the noise to signal ratio metric are used in this work to evaluate the functional connectivity metrics.

Hertz, Roudi and Tyrcha [HRT13] introduced a noise to signal ratio (NSR) metric to capture the overlap between the functional connectivity couplings corresponding to the presence of an anatomical connection and the couplings corresponding to the absence of an anatomical connection in the structural connectivity matrix. Functional connectivity couplings for which an anatomical connection actually exists will have some spread (given by the standard deviation sd_1) around a mean value (given by μ_1). Similarly, functional connectivity couplings for which there are no anatomical connections will also be spread (with a standard deviation sd_2) around a mean value μ_2 (Please refer to Figure 3.3). When the spread of these two distributions is small when compared to the difference between their mean values, the overlap between the two distributions reduces and it is easier to identify the functional couplings for which anatomical connections exists. The noise to signal ratio is given by

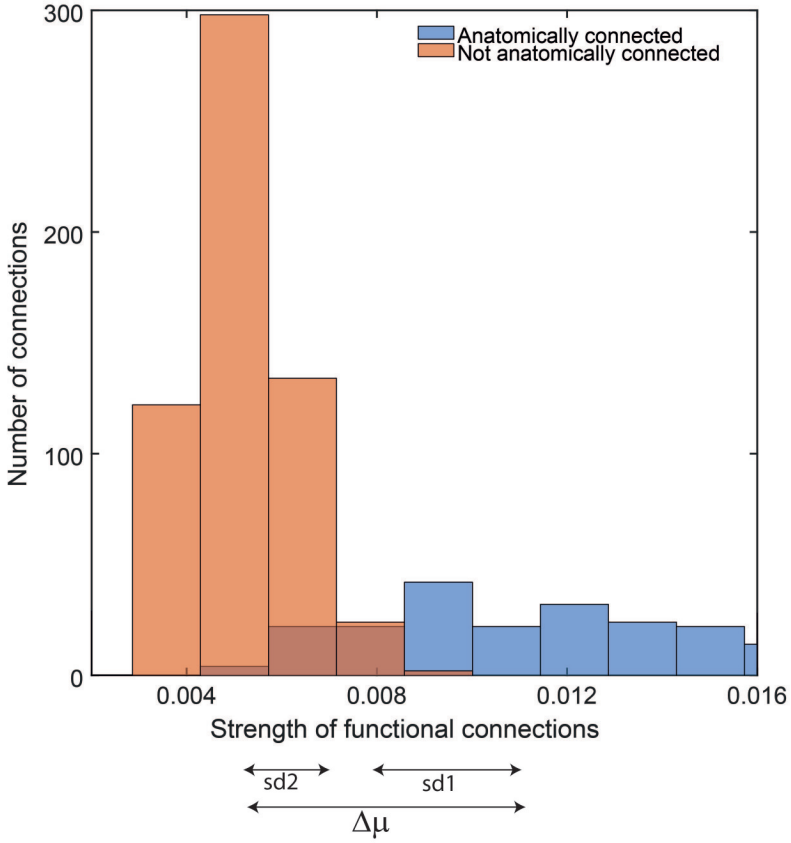

Figure 3.3: Illustration of noise to signal ratio calculation.

$$NSR = \frac{sd_1 + sd_2}{|\mu_1 - \mu_2|} = \frac{sd_1 + sd_2}{\Delta\mu}\,. \tag{3.21}$$

The noise to signal ratio is a measure of the error in the reconstruction of the structural network connections. The smaller the noise to signal ratio, the higher is the discrimination between the functional connections which are anatomically connected and those which are not anatomically connected.

3.6 Summary

To sum up, an *in silico* network of Izhikevich neurons with a known structural connectivity was simulated to generate the spike train data. Gradient descent algorithm was used to obtain the Ising model parameters that model the first order and second order averages from the spike train data binned at 10 ms. Parameters of the kinetic Ising model extended to account for variable spike transmission delays were computed using a two-step approach. First, the spike transmission delay for each pair of neurons was inferred from the cross-correlograms. Then gradient descent algorithm was used to obtain the parameters of the kinetic Ising model that match the delayed correlations from the spike train data binned at 1 ms. Both the directional and non-directional versions of the cross-correlation based connectivity matrix (CCM) and partial correlation based connectivity matrix (PCM) were then computed for a time correlation window of 150 ms and a bin size of 1 ms. Ising coupling matrix and the non-directional version of the cross-correlations and partial correlations matrix were compared against the symmetrized structural connectivity matrix for different threshold levels. Similarly, kinetic Ising coupling matrix and the directional version of the cross-correlations and partial correlations matrix were compared against the structural connectivity matrix for different threshold levels. Results of the comparison for Ising couplings are presented in chapter 4 and the results for kinetic Ising couplings are presented in chapter 5.

Chapter 4

Inferring structural connectivity using Ising couplings

Contents

This chapter presents the results of investigations of the equilibrium Ising model's ability to infer the structural connections and contrast it to that of partial correlations and cross-correlations in *in silico* networks for different network conditions. As the Ising couplings are non-directional, they were compared with the non-directional versions of the cross-correlation

and partial correlation matrices. The primary criterion used for the comparison was the AUC metric discussed in the section 3.5. For brevity, equilibrium Ising models will be referred to as Ising models henceforth in this chapter.

This study used *in silico* networks as the structural connections are known and different network conditions can be controlled easily by construction. In contrast, it is difficult to evaluate the performance of a functional connectivity tool to infer the underlying synaptic connectivity in *in vivo* or *in vitro* neuronal networks as the real anatomical connectivity in those networks is not known fully [Ste+12].

This thesis evaluated Ising couplings against partial and cross-correlations in scale-free, modular small-world and random network topologies of *in silico* networks, as studies [MPM15] suggest that the structural connectivity in neuronal networks exhibits features of complex networks. Studies support the existence of scale-free network connectivity in primary cortical cultures [EM06a] and developing hippocampal networks [Bon+09]. The activity of cultured neurons during maturation suggest an evolution of the network structure from a random topology to a small-world topology [Dow+12]. Also, this work studied the performance of the three functional connectivity metrics for different firing rates and correlation levels in networks of different sizes as literature [Cha+15; IS10] indicate that the activity of neuronal network is characterized by such factors.

4.1 Effect of mean network correlation

The performance of the three functional connectivity measures to uncover the underlying synaptic connectivity for different levels of network correlation for fixed firing rates in scale-free networks was initially studied. The results from the the study on scale-free networks of 30 nodes for a fixed mean firing rate of 20 Hz is shown in Figure 4.1b. For very weak levels of correlation ($\rho = 0.001$ and $\rho = 0.003$), partial correlations and cross-correlations performed no better than a random classifier and their AUC values were close to 0.5. In contrast, the AUC value of Ising couplings was significantly higher when compared to partial correlations and cross-correlations ($p < 0.01$, two-sample t-tests). When the network correlation level increased, the AUC of Ising couplings increased and then gradually decreased. This can be explained as follows. When the network correlation was very small, the synaptic connectivity in the network had a very weak effect on the spike trains of the the neurons in the network and the neurons with the weakest synaptic connections were indistinguishable from the unconnected neurons. As the correlation level increased, the effect of synaptic connectivity on the spike trains became stronger, and the gap between the correlation in the spike trains of the connected neurons and the unconnected neurons increased. As a direct result, the detectability of the links also increased. However, after a particular point, the effect of the indirect connections became stronger and it became difficult for Ising couplings to distinguish between the direct connections and the indirect connections and the AUC dropped as a result.

The AUC curve of partial correlations followed a similar pattern. However,

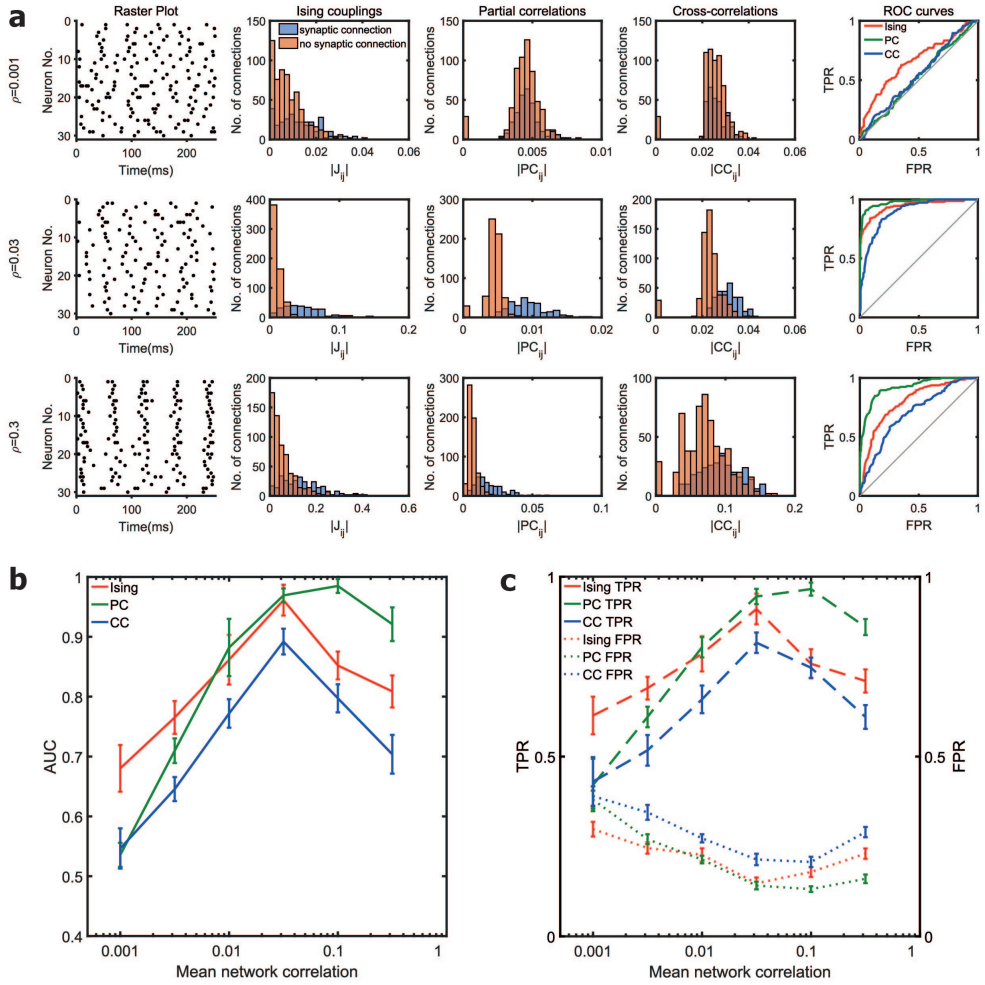

Figure 4.1: **Effect of mean network correlation: (a)** The first column in each row shows the raster plot of the spiking activity from a simulated neuronal network for a firing rate of 20 Hz and different network correlation levels. The first, second and third rows correspond to mean network correlation levels (ρ) of 0.001, 0.03 and 0.3 respectively. Histogram of the Ising couplings, partial correlations and cross-correlations for the pairs of neurons that are synaptically connected and not connected are shown respectively in the second, third and fourth columns. The corresponding ROC curves are shown in the last column. **(b)** Plot of the AUC values for different mean network correlation levels and a fixed firing rate of 20 Hz in scale-free networks of 30 neurons. Mean value was calculated from 10 simulated networks. **(c)** True positive rate (TPR) and false positive rate (FPR) for the reconstruction of the structural connections by the three functional connectivity metrics thresholded at a sparsity threshold value of 20%.

the performance of partial correlation increased at a much faster rate with increase in the correlation levels, and soon it equalled and eventually surpassed Ising couplings for strong levels of correlation ($\rho = 0.1$ and $\rho = 0.3$). The AUC of partial correlations was significantly higher than that of Ising couplings for strong levels of correlation ($p < 0.01$, two-sample t-tests). For intermediate levels of network correlation ($\rho = 0.01$ and $\rho = 0.03$), there was no difference between the AUC values of Ising couplings and partial correlations. The superior performance of the partial correlations at stronger levels of network correlations can be explained as follows. When the network correlation is strong, a spike in the presynaptic neuron evokes a spike in the postsynaptic neuron with high probability, and a linear dependency emerges between the spike train of the presynaptic and the post synaptic neurons. Though indirect interactions emerge in the case of strong network correlations, the relationship between the spike trains of the indirectly connected neurons is still linear. As partial correlation can remove the linear effects of the population, partial correlations were able to discount the effect of spurious indirect interactions introduced at stronger levels of network correlation. The study tested for the range of correlation levels for different fixed firing rates and different network sizes and found that the same trend persisted for all cases.

The AUC score gives a good summary of the performance of the functional connectivity metrics for every possible threshold value. However, in practice, one has to use a single threshold value typically. This work tested the quality of reconstruction of the structural links for a sparsity threshold value of 20% (the strongest 20% of the functional connectivity links are considered to represent the structural links) assuming that other methods are

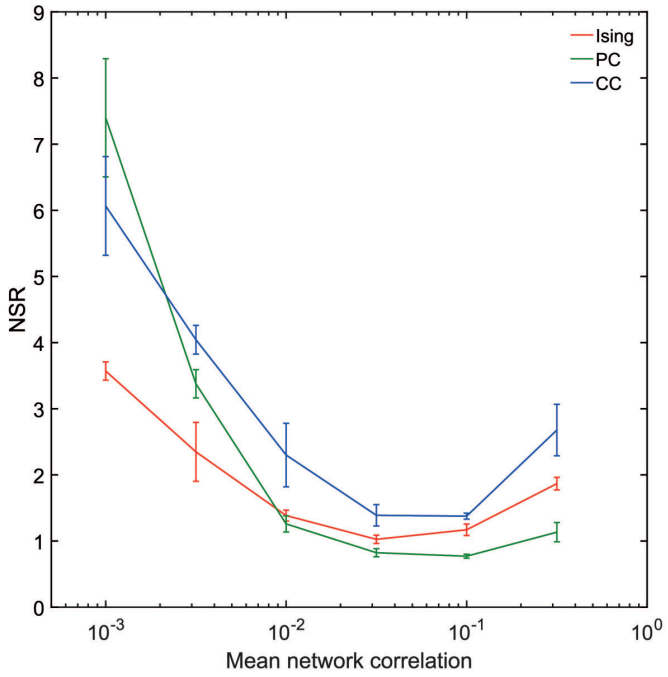

Figure 4.2: **Effect of mean network correlation on the noise to signal ratio:** Plot of the NSR values for different mean network correlation levels and a fixed firing rate of 20 Hz in scale-free networks of 30 neurons. Data was averaged over 10 simulated networks. Lower the NSR value, better is the performance. For weaker correlation levels (0.001 and 0.003), NSR value of Ising couplings was significantly lower compared to partial and cross-correlations. For stronger correlation levels (0.1 and 0.3), partial correlations had a significantly lower NSR value compared to Ising couplings and cross-correlations ($p < 0.01$, two-sample t-tests).

used to arrive at the true sparsity threshold value of 20% and the results are presented in Figure 4.1c. The results are in general agreement with the results obtained earlier using the AUC scores. One can see that a higher AUC score in Figure 4.1b corresponds to a higher true positive rate (TPR) and a lower false positive rate (FPR) in Figure 4.1c.

The noise to signal ratio (NSR) metric (discussed in the section 3.5) was also used to evaluate the performance of the three functional connectivity metrics for the range of correlation values and the results of the evaluation are plotted in Figure 4.2. The results obtained using NSR metric confirms the results obtained using the AUC scores. At lower values of correlation, Ising couplings delivered a significantly superior performance with a relatively low NSR score. However, at higher values of correlation, partial correlation delivered a significantly better performance ($p < 0.01$, two-sample t-tests).

4.2 Effect of mean firing rate

This section reports an instigation of the effect of mean firing rate on the quality of recovery of the structural connections. Figure 4.3b and 4.3c present the effect of firing rate on the AUC of Ising couplings, partial and cross-correlations for fixed network correlation levels of 0.001 and 0.3 respectively. At a weak correlation level of 0.001, the AUC values of partial and cross-correlations remained low at around 0.5 and the AUC of Ising couplings was significantly higher than those of partial and cross-correlations for all firing rates ($p < 0.01$, two-sample t-tests). At a strong value of correlation of 0.3, all the three functional connectivity metrics show an increase

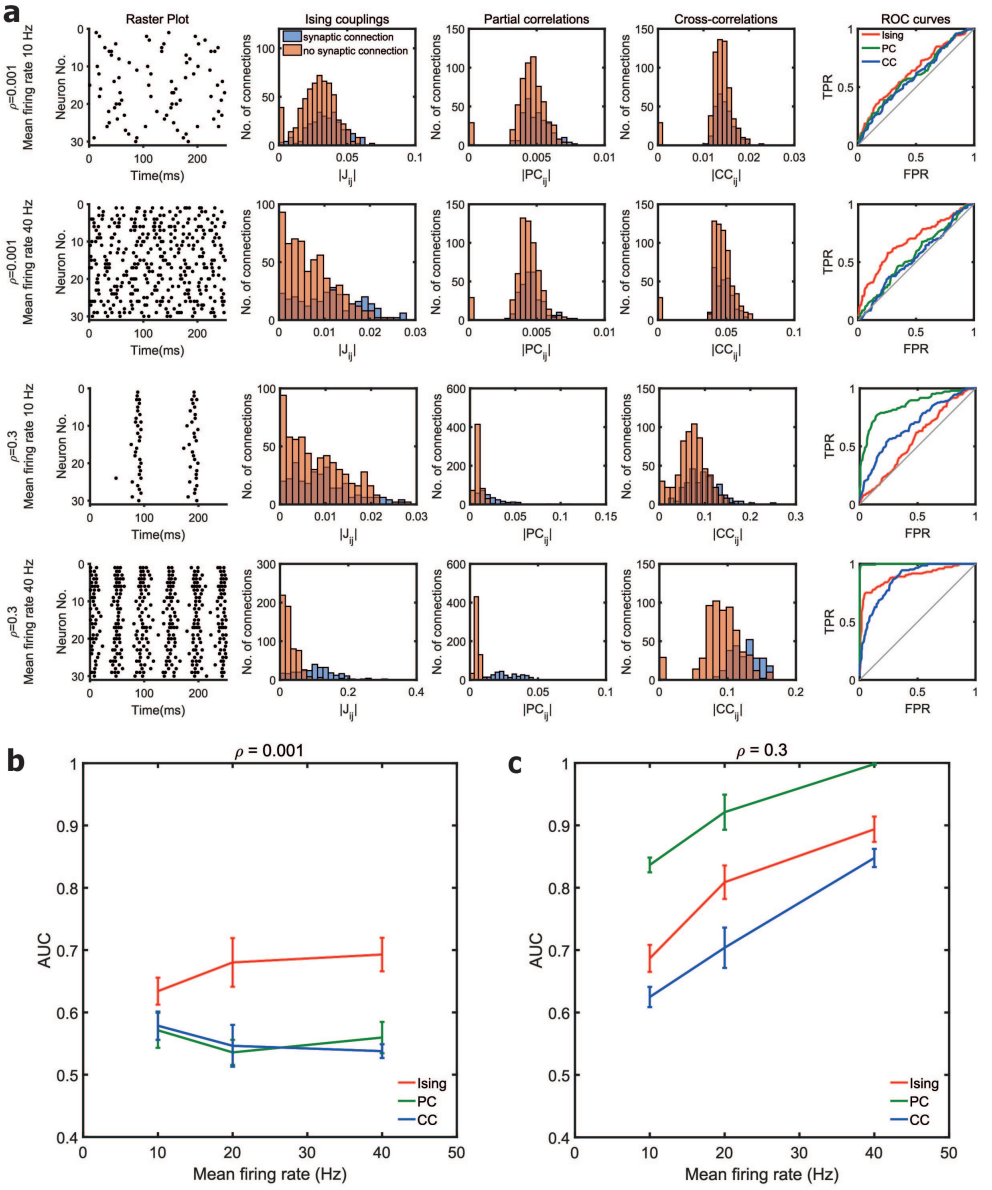

Figure 4.3: **Effect of mean network firing rate: (a)** The first and second rows correspond to firing rates of 10 Hz and 40 Hz respectively for a fixed correlation level (ρ) of 0.001. The third and fourth rows correspond to firing rates of 10 Hz and 40 Hz respectively for a fixed correlation level of 0.3. Raster plot of the spiking activity is shown in the first column. Histogram of the Ising couplings, partial correlations and cross-correlations for the pairs of neurons that are synaptically connected and not connected are shown respectively in the second, third and fourth columns. The corresponding ROC curves are shown in the last column. **(b)** and **(c)** Plot of the AUC values for different firing rates and fixed mean network correlation levels of 0.001 and 0.3 respectively in scale-free networks of 30 neurons. Mean value was calculated from 10 simulated networks.

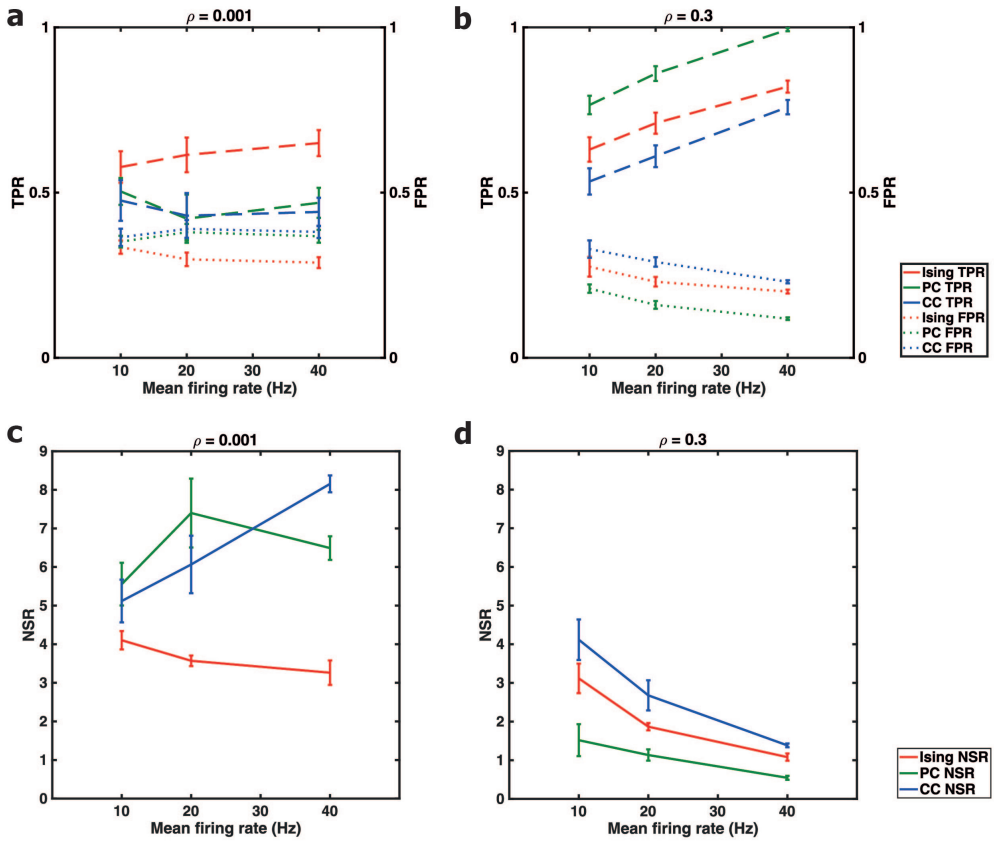

Figure 4.4: **Effect of mean network firing rate: (a)** and **(b)** Plot of the True positive rate (TPR) and false positive rate (FPR) for the reconstruction of the structural connections by the three functional connectivity metrics thresholded at a sparsity threshold value of 20% for different firing rates and fixed mean network correlation levels of 0.001 and 0.3 respectively in scale-free networks of 30 neurons. **(c)** and **(d)** Plot of the NSR values for different firing rates and fixed mean network correlation levels of 0.001 and 0.3 respectively in scale-free networks of 30 neurons. Mean value was calculated from 10 simulated networks.

in performance with an increase in firing rates. The relative difference between the AUC scores of partial correlations and Ising couplings persisted, and partial correlation detected significantly ($p < 0.01$, two-sample t-tests) more links when the correlation was strong for all the firing rates considered. Our observation that the AUC of partial correlations and cross-correlations increases with firing rates is consistent with the similar observations of Eichler [EDS03].

Along with the AUC scores, the paired measures of true positive rate and false positive rate for a sparsity threshold value of 20 % and the noise to signal ratio metrics were also calculated and plotted (Figure 4.4). The TPR and FPR plots and the NSR plot confirm the trend seen with the AUC scores.

4.3 Effect of network topology

Apart from networks with scale-free connectivity, the study assessed the performance of Ising couplings, cross-correlations and partial correlations in networks of neurons with modular small-world connectivity and random connectivity. The link density was maintained the same across the three topologies. The results of the assessment for networks of 30 nodes for a mean firing rate of 20 Hz are plotted in Figure 4.5. The trend of how the AUC scores of the three functional connectivity metrics vary with the network correlation levels did not change across topologies. The AUC scores of Ising couplings, partial and cross-correlations in scale-free topology were not considerably different from their corresponding scores in random topology. However, the AUC scores of the three metrics in the small-world networks were considerably higher than their corresponding scores

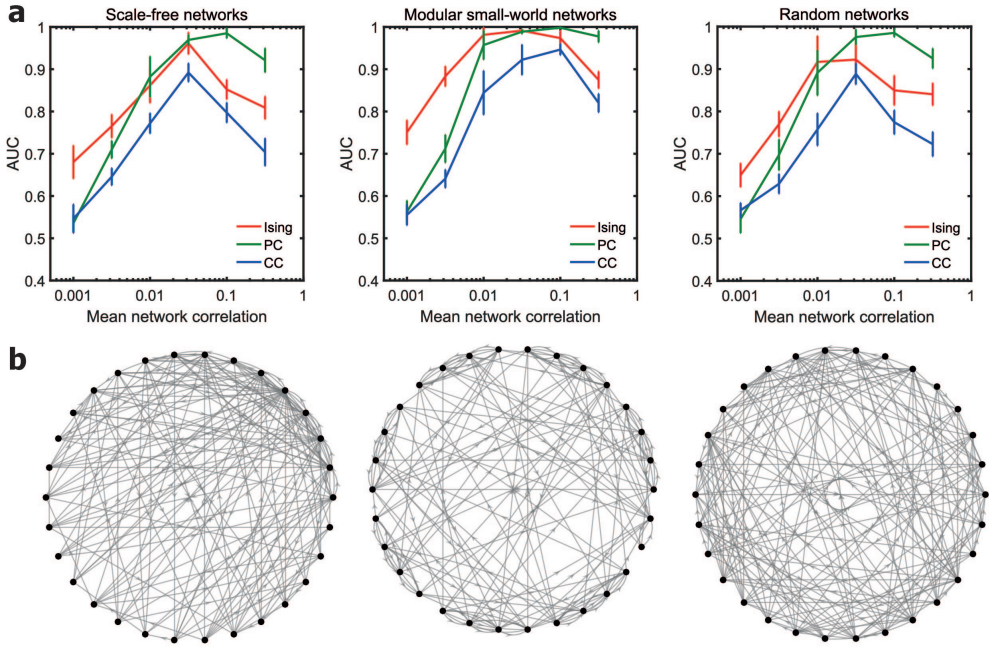

Figure 4.5: **Effect of network topology: (a)** Plot of the AUC values for networks of 30 neurons with scale-free (SF), small-world (SW) and Erdos-Renyi(ER) random network topologies. Data was averaged over 10 simulated networks for each network condition. Firing rate was fixed at 20 Hz in all cases. All the three topologies had the same link density of 0.2. **(b)** Example of the structural connectivity network for each topology. Scale-free networks form a few highly connected hub nodes. Modular small-world networks present a balance of segregation and integration via dense intra-module connections and sparse inter-module connections. Most nodes in random networks have similar degree distribution.

in scale-free networks. The high relative performance of the metrics in the case of small-world networks when compared to scale-free networks or randomly connected networks can be explained as a direct effect of the topology construction. The modular small-world networks were constructed by linking together fully connected modules with randomly distributed inter-module connections [RS10]. The number of inter-module connections was fewer when compared to intra-module connections. Hence each node was influenced more strongly by the direct interactions from the other nodes in the same module (there were no indirect interactions within a module as each node was connected to every other node in the module) when compared to the indirect interactions from nodes in the other modules. So, the effect of indirect interactions was weaker in the case of small-world networks when compared to scale-free and random networks. And as a result, all the three functional connectivity metrics performed better at disentangling direct interactions from indirect interactions in the modular small-world topology when compared to the other two topologies. To sum up, Ising couplings performed better at weaker levels of correlations and partial correlations performed better at stronger levels of correlation irrespective of the underlying structural connectivity topology.

4.4 Effect of network size

To study how the number of nodes in the network affected the reconstruction of the structural connections, the three functional connectivity metrics for networks of different sizes (11, 20, 30, 60 and 120 nodes) were computed

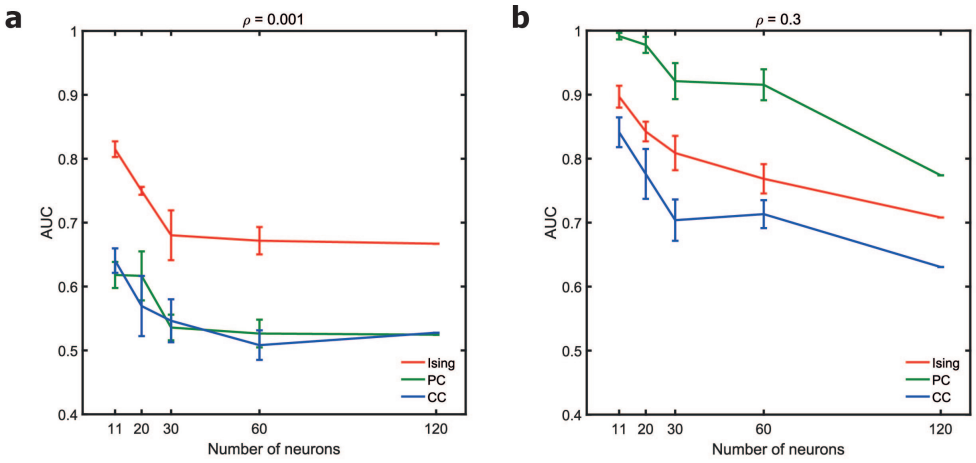

Figure 4.6: **Effect of network size:** Plot of the AUC values for networks of various sizes for a fixed firing rate of 20 Hz and correlation levels of 0.001 and 0.3 are displayed in the left panel **(a)** and the right panel **(b)** respectively. The mean value was calculated from 10 networks for all cases except for networks of 120 nodes in which case the data is from the simulation of a single network.

and analysed. For both weak (Figure 4.6a) and strong (Figure 4.6b) correlation cases, all the three functional connectivity metrics displayed a reduced performance with an increase in the number of nodes. Partial correlation is known to have a reduction in performance with increased network size because of the marrying-parents effect [EDS03] (When two neurons A and B share a post synaptic neuron C, then the two input neurons A and B can become correlated as an artifact). The current results show that Ising model also suffers a reduction in detectability of the structural links for larger networks. Though the performance of all the three metrics decreased with increase in network size, the relative performance difference between Ising and partial correlation remained. As a result, Ising couplings had the highest AUC in weaker correlation levels in networks of all sizes and partial correlations was the winner at stronger correlation levels in networks of all sizes.

4.5 Effect of network density

The structural networks considered so far had a network density of 0.2. To study the impact of the network density, structural networks were constructed with a network density of 0.5. The new structural networks were simulated to generate activity patterns and the resulting functional connectivity metrics were computed. Figure 4.7 shows the plot of the AUC scores for Ising couplings and partial correlations for networks with the network density 0.2 and 0.5. It can be observed that even for networks with a higher network density of 0.5, the pattern of Ising couplings performing better at lower values of correlation and partial correlations performing

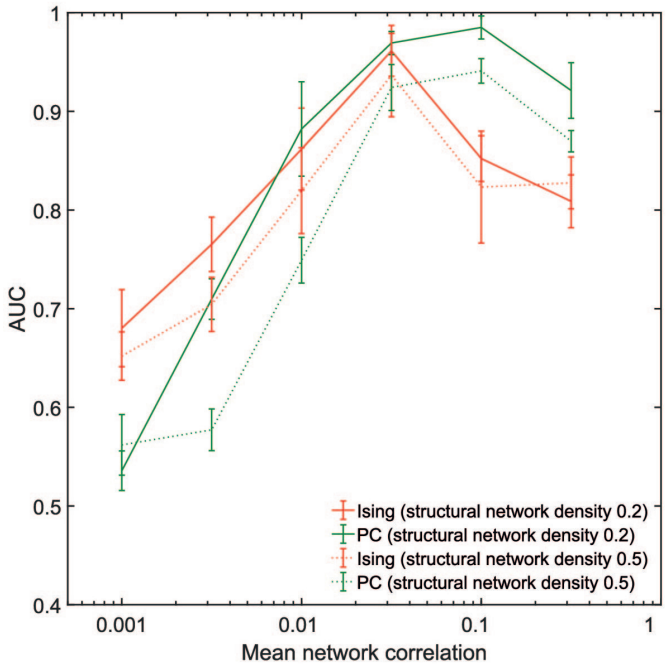

Figure 4.7: **Effect of network density:** Plot of the AUC values of Ising couplings and partial correlations of networks with two different network densities for a fixed firing rate of 20 Hz and varying correlation levels. Data was averaged over 10 scale-free networks of 30 nodes.

better at higher values of correlation was preserved. Another interesting observation is that the AUC score of partial correlations in networks with higher network density are significantly smaller when compared to the corresponding scores in networks with a network density of 0.2 ($p < 0.01$, two-sample t-tests). This observation is consistent with the similar observations of Poli et al ([Pol+16]). The reduced performance of the partial couplings with increasing network density can again be attributed to the marrying-parents effect. Ising couplings also showed a reduced performance when the network density increased. However, the study did not find any significant statistical difference between the AUC scores of Ising couplings corresponding to the networks with two different network densities ($p < 0.01$, two-sample t-tests).

4.6 Impact of the fit of Ising parameters

Ising parameters were computed using the gradient descent method. The cost function of the gradient descent algorithm was defined as the maximum difference between the $< \sigma_i >$ or $< \sigma_i \sigma_j >$ of the Ising model and that of the data from the simulation. The cost function quantified the error in the fit of the Ising model parameters. Greater the difference between the averages of the model and the data, greater is the error in the fit of the model parameters. The gradient descent algorithm was run for different values of the cost function to study how the fit of the Ising model parameters affected the reconstruction of the structural connectivity. Figure 4.8 shows the plot of the AUC values for different values of the error in the fit of the

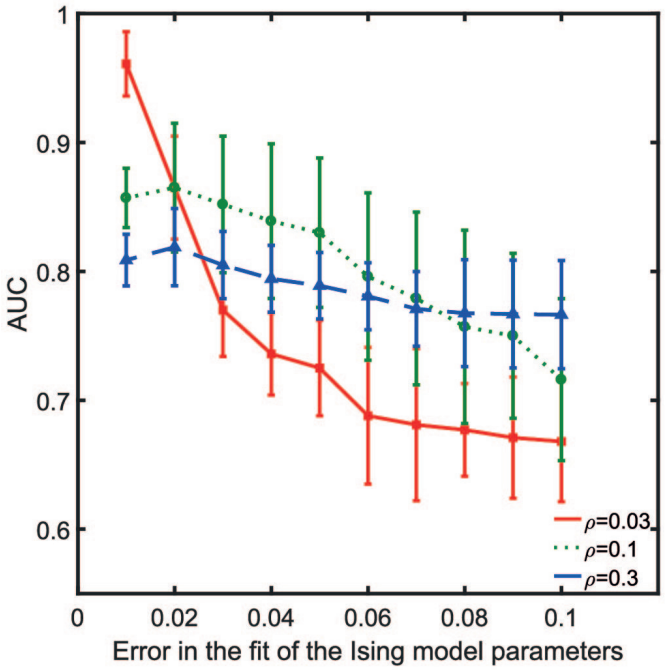

Figure 4.8: **Effect of fit of the Ising model parameters on the inference of structural links:** The error in the fit of the Ising model parameters is plotted against the AUC values obtained for the corresponding error levels for three mean network correlation levels (ρ) and a fixed firing rate for scale-free networks of 30 neurons. In all cases, lower the error in the fit of the Ising model parameters, higher was the detection of links in the structural connectivity matrix.

Ising model parameters. It can be seen that the capability of the Ising parameters to reconstruct the structural connectivity (given by the AUC score) increased with the decrease in the error in the fit of model parameters. It is to be noted that the gradient descent algorithm takes more time to compute more accurate model parameters. Thus, the number of the structural links correctly detected by the Ising parameters depends on the accuracy of the estimation of the model parameters, which, in turn, depends on the time the gradient descent algorithm is run for. In comparison, partial and cross-correlations can be computed using analytical solutions and also the time required to compute partial correlations is a fraction of the time required to compute Ising parameters, especially for larger systems.

4.7 Discussions

Functional connectivity metrics have been widely used to infer the underlying structural connectivity of the neuronal circuits [Yat+15; MPM15; Orl+14]. However, the conventional functional connectivity metric of cross-correlation is susceptible to the impact of indirect interactions arising out of poly-synaptic connections and common inputs. Maximum entropy based Ising models have been suggested to discount the effect of indirect interactions and account for only the direct interactions [Sch+06; GSS11; BC13]. Similarly, partial correlation approach has also been reported to remove the linear contribution of other neurons in the population and measure the direct interaction strength [BBS76; EDS03]. Which of the above two functional connectivity approaches provides the best measure of the underlying structural connectivity remains an open question, which has been addressed in

this work.

Poli et al [Pol+16] reported that partial correlation outperformed cross-correlation and transfer entropy in inferring the synaptic connectivity in simulated networks of neuronal assemblies. At the same time, the study by Watanabe et al [Wat+13] showed that the Ising couplings obtained from a resting state fMRI data represented the anatomical connections of the brain more accurately than partial correlation and other common functional connectivity measures. No comparison has yet been carried out between Ising couplings and partial correlations in the microscopic scale of neuronal networks for a wide set of network conditions and network topologies. This work systematically studied the predictability of the underlying structural connections by Ising couplings, in comparison to partial and cross-correlations, in *in silico* neuronal networks and how the predictability is affected by different network conditions. As it is possible to fully control the underlying topology and the different network conditions in the case of *in silico* networks, *in silico* networks of Izhikevich neurons [Izh03] were used in the study.

The main observation was that the relative performance of the three functional connectivity tools was determined primarily by the network correlation levels (Figure 4.1). Partial and cross-correlations performed only as well as a random classifier at very weak levels of network correlation ($\rho = 0.001$). In contrast, Ising couplings had a considerably higher AUC score when compared to partial correlations when the correlation levels were very weak ($\rho = 0.001$ and $\rho = 0.003$). However, partial correlation gained the advantage when the network correlation increased. Partial correlation performed better than Ising couplings at higher correlation levels

($\rho = 0.1$ and $\rho = 0.3$). At higher network correlation levels, whenever a presynaptic neuron spikes, there is a high chance that the postsynaptic neuron will spike as well and the relation between the spike trains of the neurons in the network tend to become linear. As partial correlations can remove the linear effects of the activity of all other neurons while assessing the relationship between two spike trains [BBS76], partial correlations outperform Ising couplings at higher network correlation levels. The trend was found to be consistent across different firing rates, network sizes and network topologies (Figure 4.1).

Also, when the network correlation levels are very high, synchronization of more than two neurons and higher order correlations become more relevant. Ising model is a second order log-linear model and the Ising coupling parameters J_{ij} correspond to the second order coefficients of the generalized log-linear model of order n [Mar+00]. The second order coefficients of a log-linear model can represent only the second order (pairwise) interactions and cannot account for the higher order interactions in a network. As a direct consequence, when higher-order correlations become more relevant at higher values of network correlation, Ising couplings fail in comparison to the partial correlations to represent the actual structure and interactions in the network.

Studies on networks of vertebrate retina [Tka+14; AB10] have reported that the correlation between the activity of pairs of neurons is usually very weak (correlation coefficients in the range 0.001 to 0.1). Ising couplings performing better than partial correlation in very weak regimes of correlation encourages further studies in applying Ising couplings to assess structure-function relationship for *in vivo* and *in vitro* networks of neurons at low

correlations. At the same time, partial correlations are a better choice in networks with high levels of correlation such as bursting neuronal cultures.

With technological advances [Mat+13; Ber+09], the number of electrodes on the MEA are increasing and the performance of the functional connectivity metrics for larger network size becomes important. It is known that the AUC of partial correlations will deteriorate when the number of neurons in the network increases because of the marrying-parents effect [EDS03]. The study observed that the AUC of Ising couplings also decreased when the number of neurons increased. Though all the three functional connectivity metrics suffered a reduction in AUC with an increase in the number of neurons in the network for all tested correlation levels and firing rates (Figure 4.6), network size did not affect the relative performance amongst the tools. Ising couplings had the highest AUC at weaker correlation levels, and partial correlations had the highest AUC at stronger correlation levels for all network sizes.

Along with the performance, the time required to compute the functional connectivity metrics also needs to be considered, especially for larger networks. The Boltzmann learning method used to calculate the Ising parameters is a very slow gradient descent algorithm [RTH09]. For a larger number of nodes, one also has to run long Monte Carlo sampling steps per iteration as exact estimate of the moments of the Ising model are computationally expensive [Yeh+10]. In comparison, analytical solutions exist to compute partial and cross-correlations in a much shorter span of time. For example, computation of partial and cross-correlations for a network of 60 neurons took in the order of minutes using the ToolConnect toolbox [Pas+16] whereas the computation of Ising couplings using the Boltzmann

learning method took in the order of hours. Faster approximation methods [RTH09; CM11] exist to compute Ising couplings quickly. Each approximation method makes a few assumptions about the structure of the underlying network and firing conditions. One has to take care to ensure that the assumptions are met before applying the approximations. This study also observed that the reconstruction of the underlying structural connectivity matrix by Ising couplings depended on the accuracy of the fit of the model parameters (Figure 4.8). The smaller the error in the fit of the model parameters, the higher was the detection of the links in the structural connectivity matrix. This has to be taken into account when opting between a time consuming exact solution vs a quick approximate solution to compute Ising parameters.

Roudi et al [RTH09] calculated equilibrium Ising coupling parameters for a simulated model of cortical network and found no significant relation between the Ising couplings and the synaptic connectivity of the network. The poor performance of the equilibrium Ising model in their work could be attributed to the symmetry of its undirectional couplings, which were nevertheless used to estimate the asymmetric directional connections of the simulated network. For meaningful comparison and analysis between the structural and functional connectivity matrices, both matrices should be reduced to a sparse binary undirected form, through thresholding, binarising, and symmetrising [RS10]. The significantly improved results obtained for Ising couplings in this study corroborate this approach for comparison between the structural and functional connectivity matrices.

Hertz [Her+10] et al observed that the couplings of a kinetic Ising model are successful in recovering the synaptic connectivity of a simulated cortical

network when compared to a standard Ising model. Hertz's results might be taken to indicate that neural system's state transitions are described by the temporal dynamics of the stochastic process. However, in spite of the fact that neural systems might indeed be non-equilibrium, the results of this chapter may indicate that the systems investigated in this study were to a large extent governed by equilibrium states, which can be described by equilibrium Ising models. It is worth noting that Ising model itself will not apply to systems far from equilibrium. A similar study of the capabilities of kinetic Ising model couplings in comparison to partial and cross-correlations for networks involving both excitatory and inhibitory neurons under different network conditions was performed and the results of that study are discussed in the next chapter.

Chapter 5

Inferring structural connectivity using kinetic Ising couplings

Contents

This chapter presents the results of the study on the ability of kinetic Ising models to infer the underlying structural connections when compared to

that of partial correlations and cross-correlations in *in silico* networks under different network conditions. As the kinetic Ising couplings are directional, they were compared with the directional version of the cross-correlation and partial correlation matrices. The terms partial and cross-correlations in the chapter refer to their directional versions. As in chapter 4, AUC metric is the primary criterion used for comparing the performance of the kinetic Ising couplings against partial and cross-correlations. All the functional connectivity metrics in this chapter were computed from 10 minute duration of the spike trains obtained from simulations of scale-free networks with all excitatory links, except in cases where it is explicitly mentioned otherwise.

5.1 Effect of mean network correlation

How the mean network correlation affects the ability of the three functional connectivity metrics was studied on scale-free networks of 30 nodes. Figure 5.1 shows the results of the study for a fixed firing rate of 20Hz. It can be seen from the figure that mean network correlation level plays a critical role in deciding the relative performance of the kinetic Ising couplings compared to partial and cross correlations.

The effect of mean network correlation on the performance of partial correlations is illustrated in Figure 5.2. The figure shows the plot of partial correlograms of three pairs of neurons (the first pair is not synaptically connected, the second pair is weakly connected and the third pair is strongly connected) for different network correlation levels. At weaker levels of correlation, the effect of synaptic connections are weak and the post synaptic

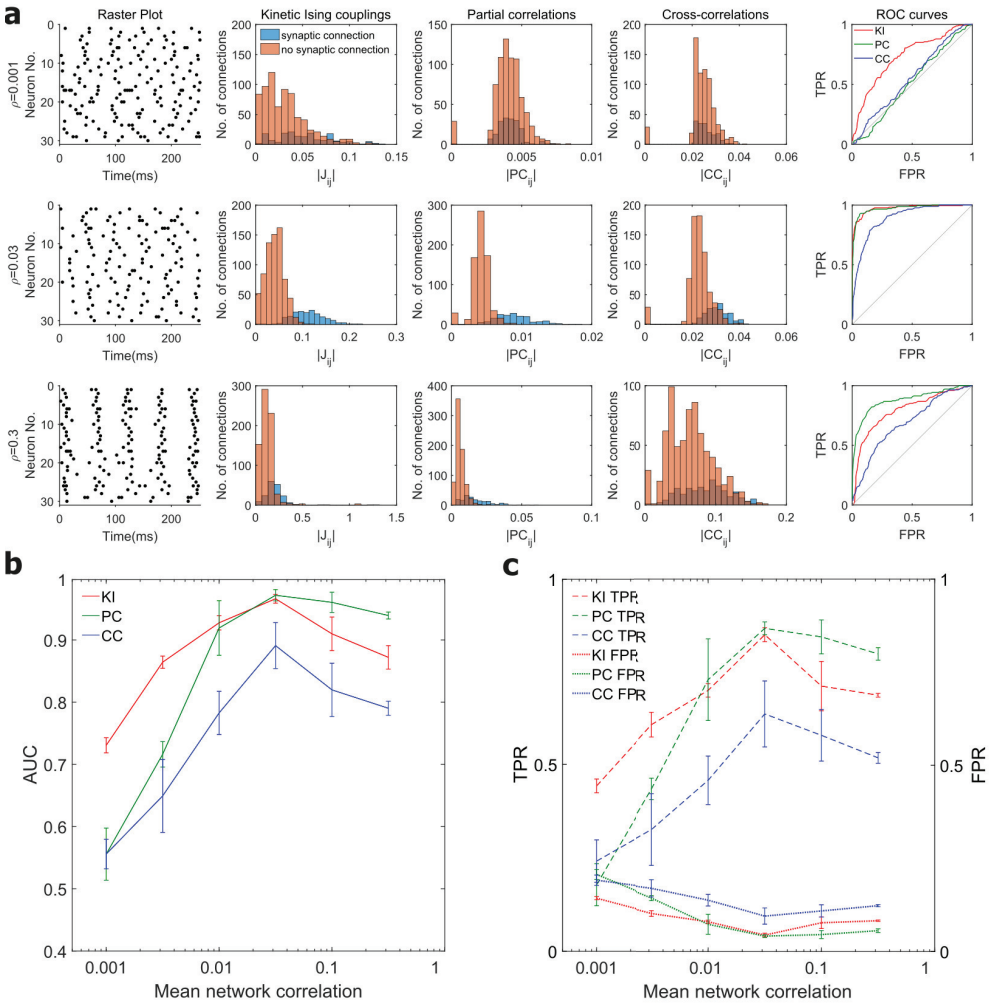

Figure 5.1: **Effect of mean network correlation: (a)** The first column in each row shows the raster plot of the spiking activity from a simulated neuronal network for a firing rate of 20 Hz and different network correlation levels. Histogram of the kinetic Ising couplings, partial correlations and cross-correlations for the pairs of neurons that are synaptically connected and not connected are shown respectively in the second, third and fourth columns. The corresponding ROC curves are shown in the last column. The first, second and third rows correspond to mean network correlation levels (ρ) of 0.001, 0.03 and 0.3 respectively. **(b)** Plot of the AUC values for different mean network correlation levels in scale-free networks of 30 neurons for a fixed firing rate of 20 Hz. Mean value was calculated from ten simulated networks. **(c)** True positive rate (TPR) and false positive rate (FPR) for the reconstruction of the structural connections by the three functional connectivity metrics thresholded at a sparsity threshold value of 20%.

neuron does not fire every time when its presynaptic neuron fires and the relation between the firing of neurons is not linear. As partial correlations can discount only the linear effects of the activity of the network, partial correlations does not discriminate between connected and unconnected pairs of neurons in this case of very weak correlations. This is evident in the top panel of Figure 5.2. The value of the partial correlation (given by the maximum value of the partial correlogram and is indicated by the red vertical line in the plot) for the unconnected pair of neurons is similar to the value of the partial correlation between the weakly and strongly connected pairs of neurons. However, when the correlation levels in the network increase, neurons in the network fire together and the relation between the firing of the neurons becomes linear. As partial correlations can discount the linear effects of the activity of the network, partial correlations can distinguish between connected and unconnected pairs of neurons in this case. This can be seen in the middle panel of Figure 5.2. The maximum value of the partial correlogram of the strongly connected neurons is greater than that of the weakly connected neurons, which in turn is greater than that of the unconnected neurons. As the mean network correlation in the network increases even further, the neurons in the network fire together even more often and the effect of indirect interactions increases to an extent so that the partialisation approach is unable to differentiate between the weakly connected neurons and the unconnected neurons (which may be connected indirectly). This is noticeable in the bottom panel of Figure 5.2. The maximum value of the partial correlogram of the unconnected pair is greater than the maximum value of the partial correlogram of the weakly connected pairs.

Kinetic Ising couplings follow a similar trend to that of partial correlations.

However, kinetic Ising couplings are able to differentiate better between the connected and unconnected pairs at very weak levels of correlations (ρ=0.001 and 0.003) and the AUC values of kinetic Ising couplings are significantly greater ($p < 0.01$, two-sample t-tests) than the AUC values of partial and cross-correlations (Figure 5.1b). For medium levels of correlations (ρ=0.01 and 0.03), kinetic Ising couplings have high AUC's (in the range of 0.9) similar to that of partial correlations. However, for stronger levels of network correlation (ρ=0.1 and 0.3), kinetic Ising couplings are not as good as partial correlations in discriminating direct and indirect connected pairs of neurons and the AUC of kinetic Ising couplings are significantly smaller ($p < 0.01$, two-sample t-tests) than the AUC values of partial correlations (Figure 5.1b). Cross-correlations attain the lowest AUC score for all cases of network correlation (except for 0.001 where both partial and cross-correlations has a AUC score of around 0.5).

The AUC score measures the performance for every threshold value (which includes both practical and impractical threshold values) and may not be an accurate indicator of performance for practical threshold values. Hence the performance of the kinetic Ising couplings and the partial and cross-correlations were also studied using the metrics of true positive rate (TPR) and false positive rate (FPR) for a sparsity threshold value of 20% (assuming that other methods are used to arrive at the correct sparsity threshold value). The performance is graphed in Figure 5.1c. The TPR/FPR metrics display a similar trend to that of the AUC plot in Figure 5.1b. At weaker levels of correlations, kinetic Ising couplings have a higher TPR and a smaller

FPR compared to partial correlations. However, at stronger levels of correlations, partial correlations display a higher TPR and smaller FPR, suggesting better performance. Additionally, the noise to signal (NSR) metric was also used to understand the amount of overlap of the functional connectivity couplings corresponding to synaptically connected and unconnected pairs of neurons in the network. Better performance of the functional connectivity metrics is marked by smaller overlap, and a smaller value of NSR metric indicates a higher performance. The plot of NSR metrics (Figure 5.3) reveal the same performance trend displayed earlier by AUC scores. At weaker correlations, kinetic Ising couplings have a smaller NSR metric whereas at stronger correlations, partial correlations have a smaller NSR score. For intermediate value of correlations, there is no significant difference ($p < 0.01$, two-sample t-tests) between the NSR scores of partial correlations and kinetic Ising couplings.

The effect of correlation was tested on networks of different sizes and topologies and it was observed that the trend seen in Figure 5.1b was consistent.

5.2 Effect of mean network firing rate

The results of the study of how network firing rate affects the performance of kinetic Ising couplings, partial and cross-correlations for a fixed mean network correlation level is shown in Figure 5.4. For a weak correlation levels of 0.001 (Figure 5.4b), there is no strictly increasing or decreasing trend seen for all three functional connectivity measures. However, a clear pattern arises for a stronger correlation level of 0.3 (Figure 5.4c). The AUC score of kinetic Ising couplings, partial and cross-correlations increased

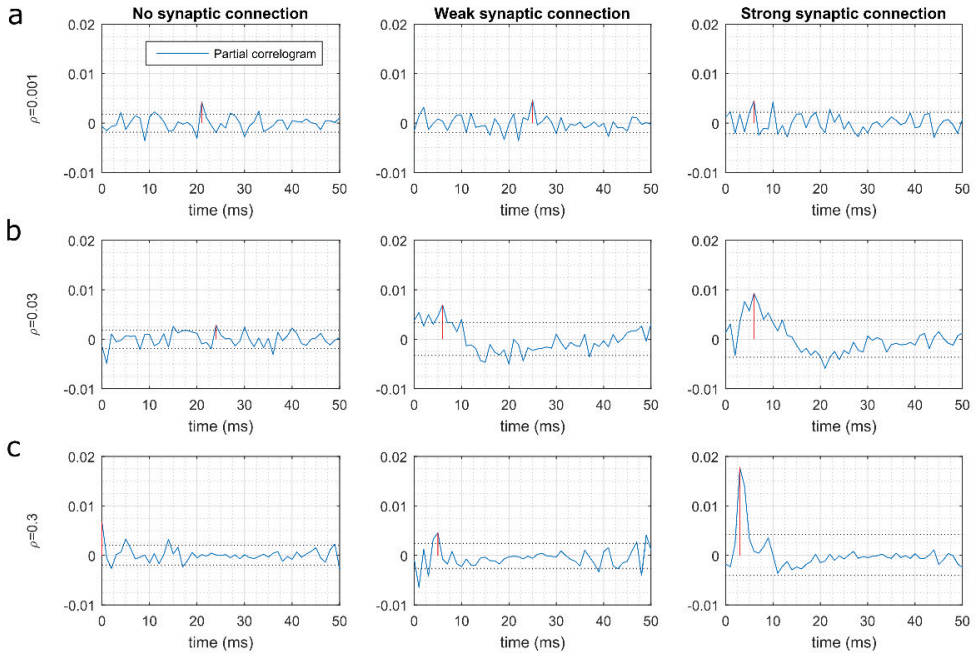

Figure 5.2: **Effect of mean network correlation on the partial correlations:** Partial correlogram corresponding to not connected, weakly connected and strongly connected pair of neurons are shown respectively in the first, second and third columns. The first, second and third rows correspond to mean network correlation levels (ρ) of 0.001, 0.03 and 0.3 respectively. The red marker corresponds to the time where the maximum value of the partial correlogram occurs.

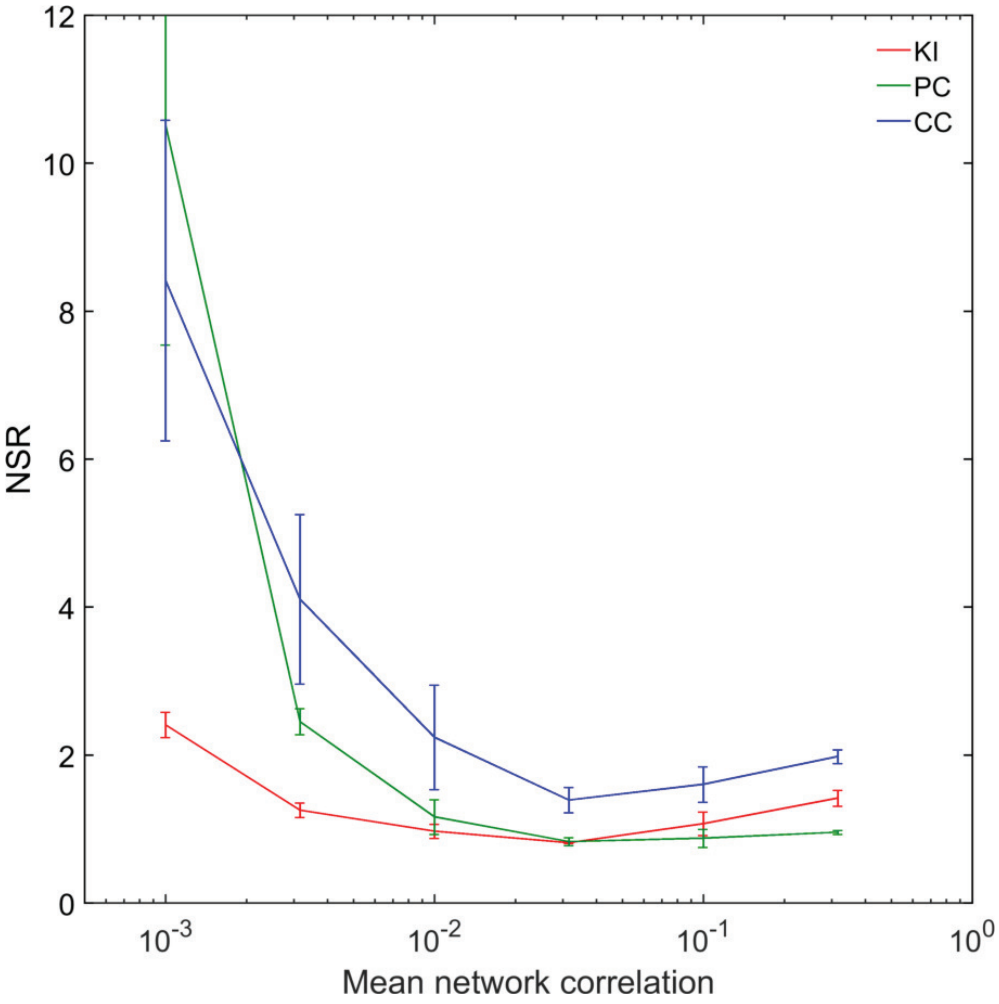

Figure 5.3: **Effect of mean network correlation on the noise to signal ratio:** Plot of the NSR values for different mean network correlation levels and a fixed firing rate of 20 Hz in scale-free networks of 30 neurons. Data was averaged over 10 simulated networks. Lower the NSR value, better is the performance. For weaker correlation levels (0.001 and 0.003), NSR value of kinetic Ising couplings was significantly smaller compared to partial and cross-correlations. For stronger correlation level of 0.3, partial correlations had a significantly smaller NSR value compared to kinetic Ising couplings and cross-correlations ($p < 0.01$, two-sample t-tests).

with an increase in firing rate. The observation that the AUC of partial correlations increases with firing rate is consistent with similar observations by Eichler [EDS03]. Along with the AUC score, the NSR of the functional connectivity metrics for different firing rates was also studied and the results are presented in Figure 5.5. The same trend seen with the AUC scores is reflected in the plot of NSR metrics and the TPR & FPR metrics.

5.3 Effect of network topology

The results discussed so far in this chapter are from scale-free networks. The work primarily focussed on scale-free topology, as scale-free network connectivity has been reported in primary cortical cultures [EM06a] and developing hippocampal networks [Bon+09]. The work also tested the performance of functional connectivity metrics in reconstructing the structural connections in small-world and random topologies, as studies suggest the presence of random topology and small-world topologies in cultured neurons [Dow+12]. Comparison of the AUC scores of kinetic Ising couplings, partial and cross-correlations for the three topologies is presented in Figure 5.6. The results suggested that topology didn't affect the relative performance of the three functional connectivity metrics. The results for the ER random topology and the small-world topology were in line with the performance for scale-free networks. It can be seen that the relative performance in all the three topologies was determined primarily by the mean network correlation levels.

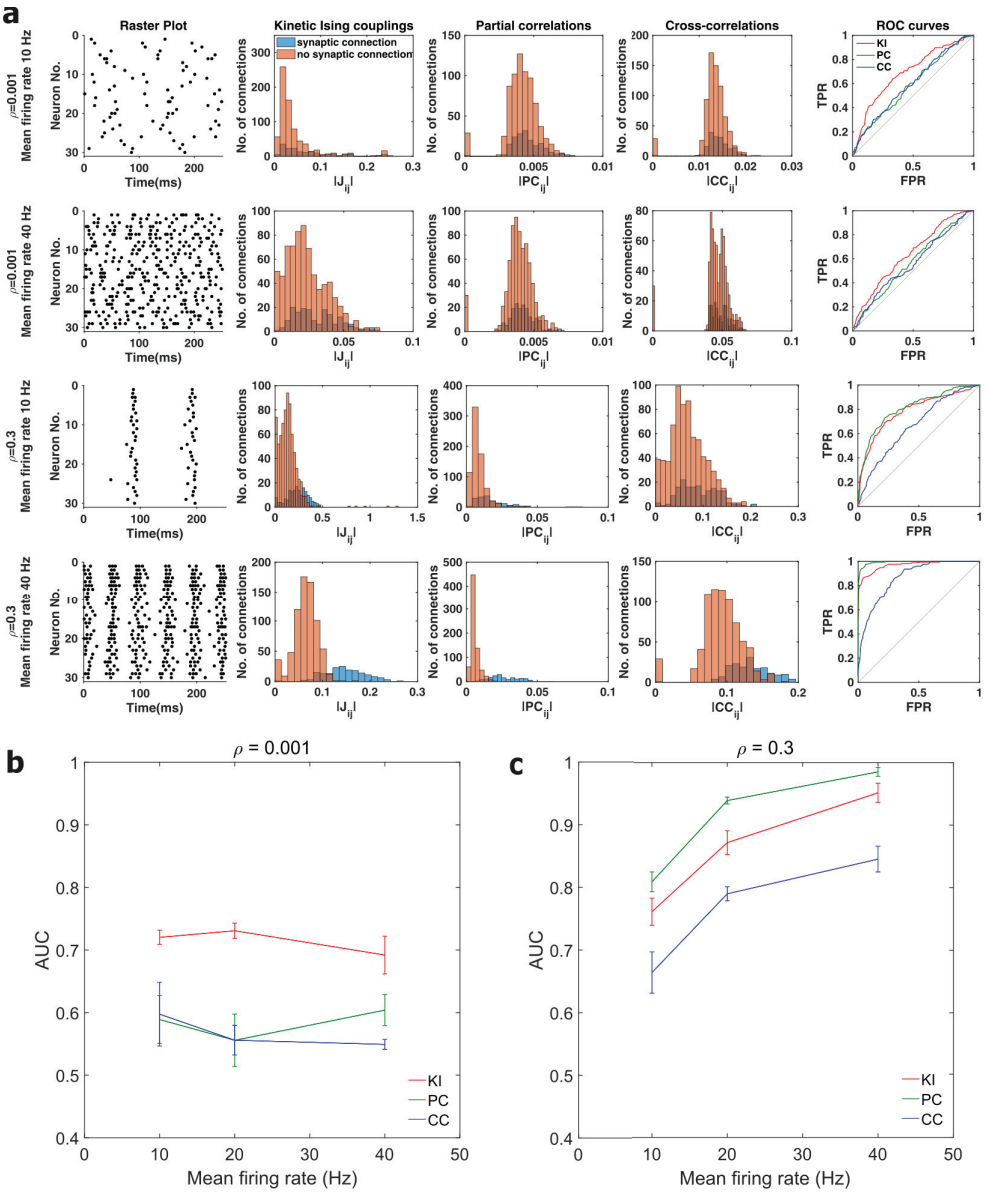

Figure 5.4: **Effect of mean network firing rate: (a)** The first and second rows correspond to firing rates of 10 Hz and 40 Hz respectively for a fixed correlation level (ρ) of 0.001. The third and fourth rows correspond to firing rates of 10 Hz and 40 Hz respectively for a fixed correlation level of 0.3. Raster plot of the spiking activity is shown in the first column. Histogram of the kinetic Ising couplings, partial correlations and cross-correlations for the pairs of neurons that are synaptically connected and not connected are shown respectively in the second, third and fourth columns. The corresponding ROC curves are shown in the last column. **(b)** and **(c)** Plot of the AUC values for different firing rates and fixed mean network correlation levels of 0.001 and 0.3 respectively in scale-free networks of 30 neurons. Mean value was calculated from 10 simulated networks.

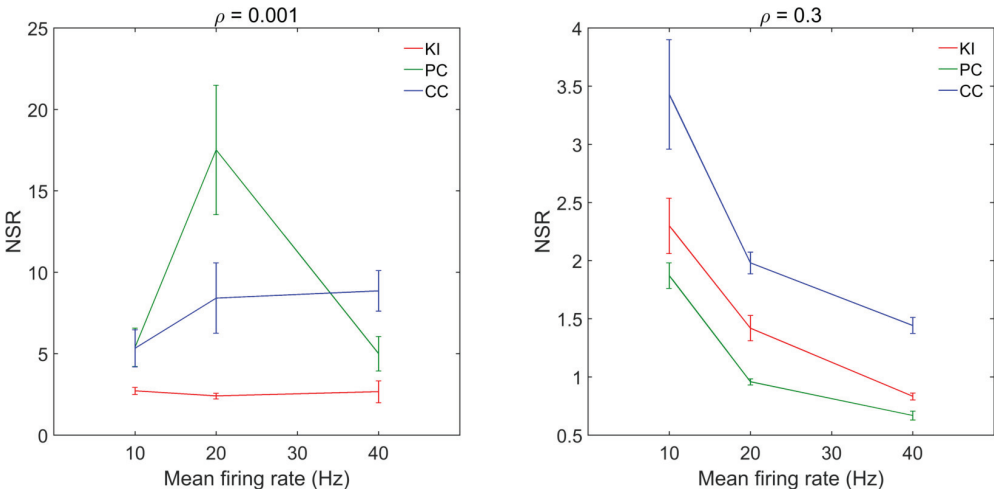

Figure 5.5: **Effect of mean firing rate on the noise to signal ratio:** NSR values for different firing rates and fixed mean network correlation levels of 0.001 and 0.3 are plotted in the left and right panels respectively in scale-free networks of 30 neurons. Data was averaged over 10 simulated networks. Lower the NSR value, better is the performance.

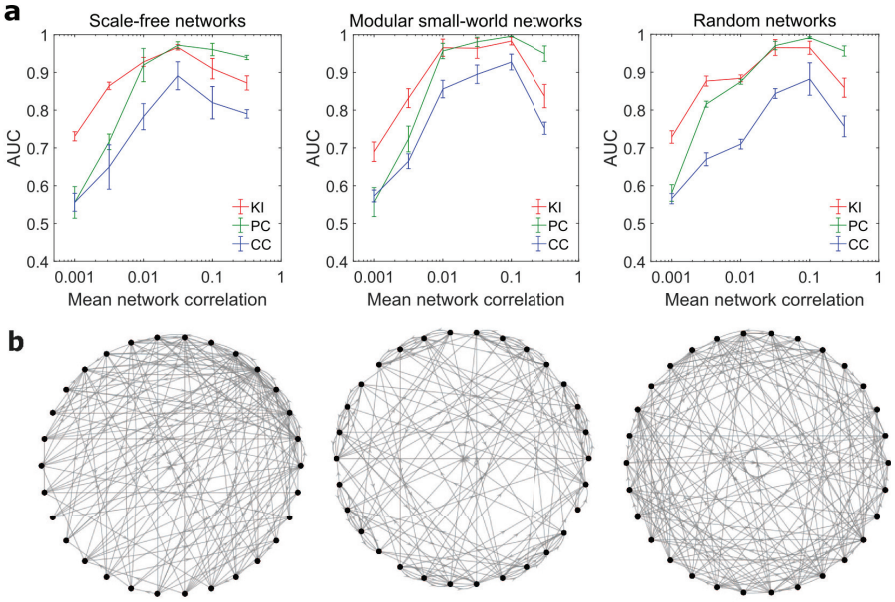

Figure 5.6: **Effect of network topology: (a)** Plot of the AUC values for networks of 30 neurons with scale-free (SF), small-world (SW) and Erdos-Renyi(ER) random network topologies. Data was averaged over 10 simulated networks for each network condition. Firing rate was fixed at 20 Hz in all cases. All the three topologies had the same link density of 0.2. **(b)** Example of the structural connectivity network for each topology. Scale-free networks form a few highly connected hub nodes. Modular small-world networks present a balance of segregation and integration via dense intra-module connections and sparse inter-module connections. Most nodes in random networks have similar degree distribution.

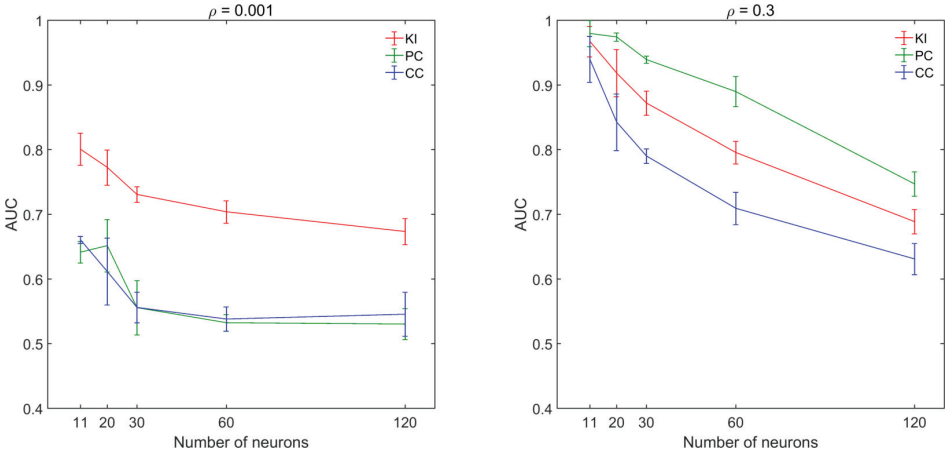

Figure 5.7: **Effect of network size:** Plot of the AUC values for networks of various sizes for a fixed firing rate of 20 Hz and correlation levels of 0.001 and 0.3 are displayed in the left panel and the right panel respectively. The mean value was calculated from 10 networks for all cases.

5.4 Effect of network density

In order to study the effect of link density on the kinetic Ising couplings, partial and cross-correlations, functional connectivity metrics were also computed for networks with a higher link density of 0.5. The results are presented in Figure 5.8. Partial and kinetic Ising couplings for networks with a link density of 0.5 displayed a trend similar to that in networks with a lower link density. However, the AUC values of kinetic Ising couplings and partial correlations in networks with a link density of 0.5 are smaller than the corresponding AUC values in networks with a lower link density of 0.2. This can be explained by the higher link density resulting in increased number of indirect interactions and thereby making the task of distinguishing the direct interactions from indirect interactions more difficult. The decreased performance of partial correlations observed in this study is consistent with similar observations by Poli et al [Pol+16]. The reduced performance of the partial couplings with increasing network density can again be attributed to the marrying-parents effect.

5.5 Effect of network size

The dependence of the performance of the functional connectivity metric on the number of nodes in the network is an important factor to understand as the increasing electrode density of MEAs are making it possible to record from increasing number of nodes. Functional connectivity from networks of varying number of nodes(11, 20, 30, 60 and 120 nodes) were compared and the results are presented in Figure 5.7. It can be seen that

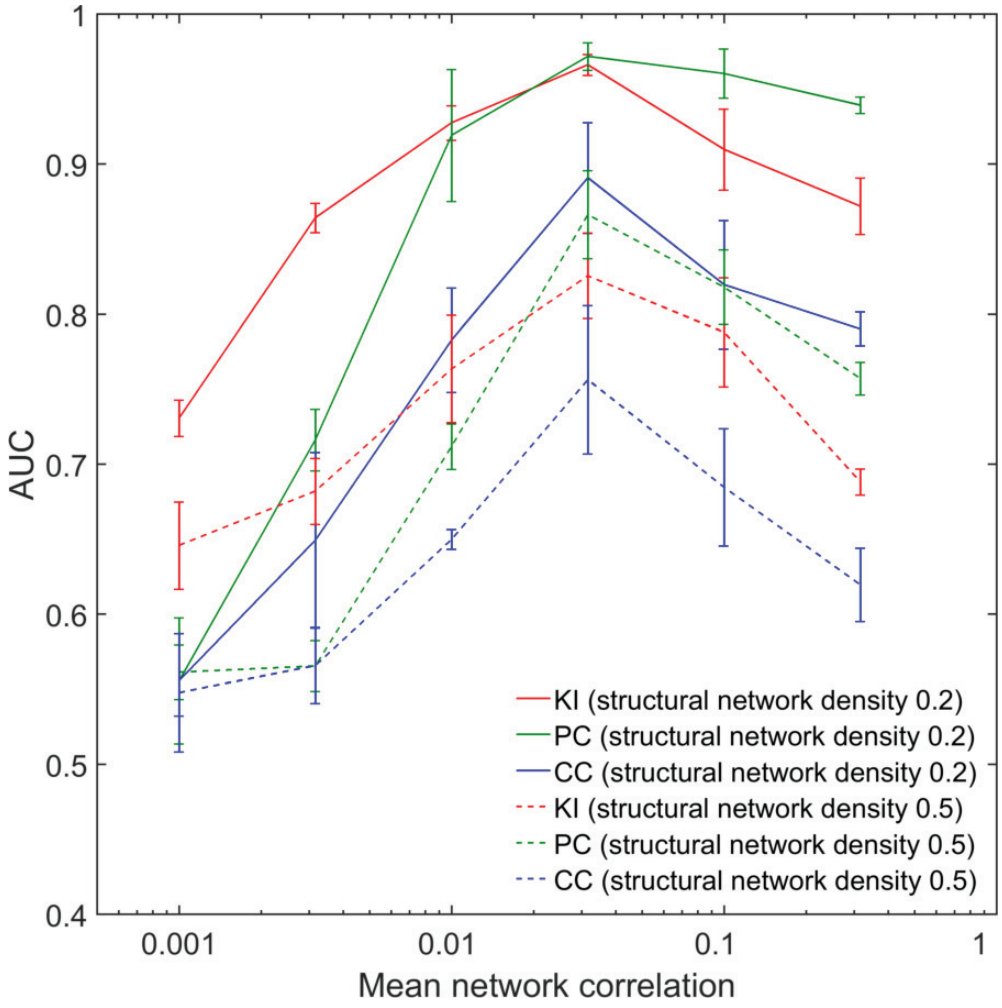

Figure 5.8: **Effect of network density:** Plot of the AUC values of kinetic Ising couplings, partial and cross-correlations of networks with two different network densities for a fixed firing rate of 20 Hz and varying correlation levels. Data was averaged over 10 scale-free networks of 30 nodes.

for both weak and strong levels of correlations, the performance of kinetic Ising couplings, partial and cross-correlations decrease with the increase in number of nodes. However, the relative performance difference between the kinetic Ising couplings and partial correlations persisted. As a result, for strong correlation levels (ρ=0.1 and 0.3), partial correlations had the highest AUC score and for weak correlation levels (ρ=0.001 and 0.003), kinetic Ising couplings had the highest AUC score for all network sizes.

5.6 Effect of inhibitory connections

The networks studied so far had only excitatory synaptic links. To understand how the inhibitory links affect the ability of the functional connectivity matrices to reconstruct the structural connectivity matrix, structural connectivity networks with a mix of 80% excitatory and 20% inhibitory links were generated in agreement with the experimental studies [MS02]. The new structural networks were simulated to generate activity patterns and functional connectivity metrics were computed from the activity patterns. Figure 5.9 shows the plot of the AUC scores for kinetic Ising couplings and partial correlations for networks with excitatory links only and for networks with a mix of excitatory and inhibitory links. It can be observed that there is no significant difference in the AUC scores of both kinetic Ising and partial correlations corresponding to pure excitatory networks and mixed excitatory-inhibitory networks. It should be noted that inhibitory connections will be represented by negative numbers in the functional connectivity matrices.

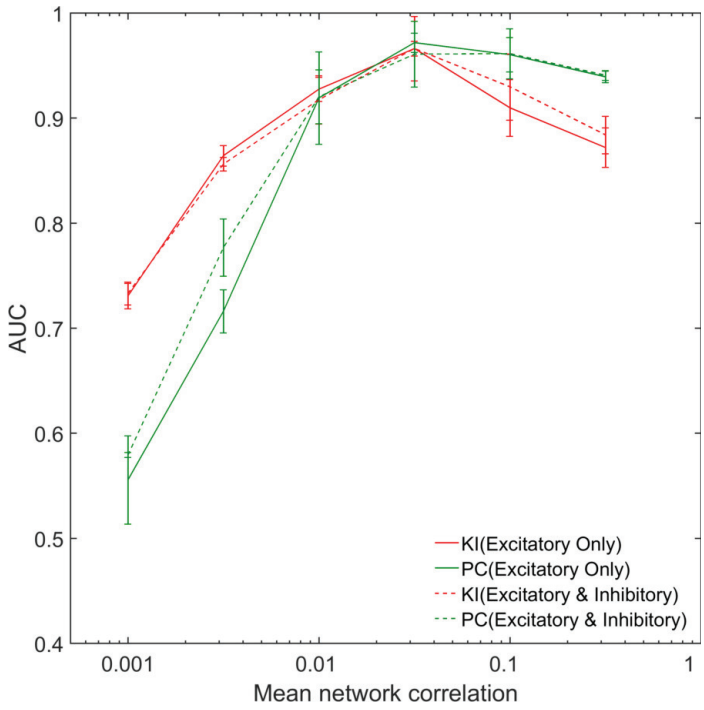

Figure 5.9: **Effect of inhibitory connections:** Plot of the AUC values of kinetic Ising couplings and partial correlations of networks with purely excitatory connections and a mix of excitatory and inhibitory connections for a fixed firing rate of 20 Hz and varying correlation levels. Data was averaged over 10 scale-free networks of 30 nodes.

5.7 Impact of the fit of the kinetic Ising model parameters

This thesis evaluates kinetic Ising parameters over a range of network conditions. As approximation methods to compute the kinetic Ising parameters have a limited range of validity and the assumptions of the approximation methods may not be valid for all the network conditions tested in this thesis, kinetic Ising parameters were computed using the gradient descent method in this work. To study how the fit of the kinetic Ising model parameters affected the reconstruction of the structural connectivity, the gradient descent algorithm was run for different values of the cost function which quantified the error in the fit of the kinetic Ising model parameters. The smaller the difference between the averages of the model and the data, the smaller is the error in the fit of the model parameters. Figure 5.10 shows the plot of the AUC values for different values of the error in the fit of the kinetic Ising model parameters. It can be observed that the a decreased error in the fit of the model parameters implies a higher AUC score. The implication of this result should be considered when choosing between an approximate but faster method against the slower but exact gradient descent method to compute the kinetic Ising model parameters.

5.8 Comparison with equilibrium Ising couplings

To understand how kinetic Ising couplings compare against equilibrium Ising couplings, their AUC scores obtained from the same set of spike train recordings were compared. Figure 5.11 presents the plot of the comparison.

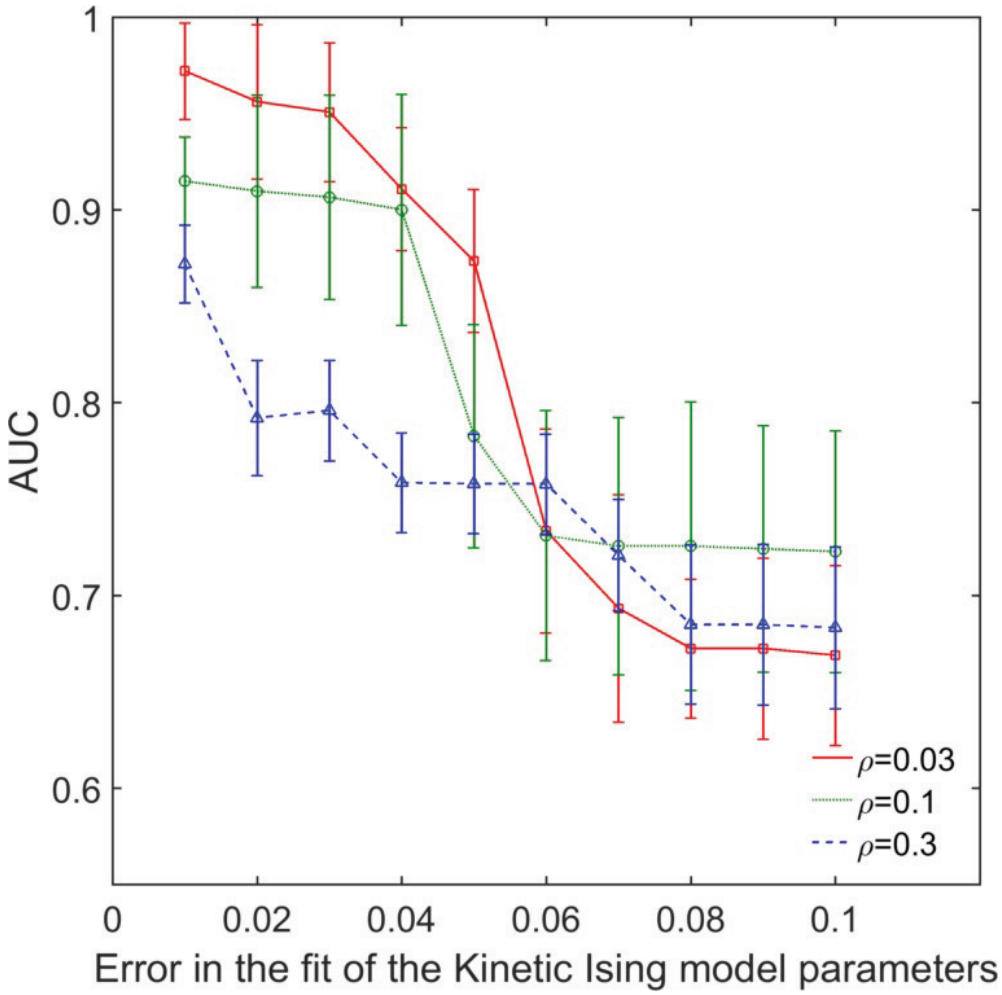

Figure 5.10: **Effect of fit of the kinetic Ising model parameters on the inference of structural links:** The error in the fit of the kinetic Ising model parameters is plotted against the AUC values obtained for the corresponding error levels for three mean network correlation levels (ρ) and a fixed firing rate for scale-free networks of 30 neurons. In all cases, lower the error in the fit of the kinetic Ising model parameters, higher was the detection of links in the structural connectivity matrix.

It should be noted that kinetic Ising couplings are directional (asymmetric) whereas the equilibrium Ising couplings are non-directional (symmetric). Hence the AUC calculated for kinetic Ising couplings is based on the actual structural connectivity matrix (which is asymmetric) and the AUC calculated for the equilibrium Ising couplings is based on the symmetrised structural connectivity matrix (which accounts only for the presence of links and does not account for the direction of the links). To make fair comparisons between the AUC scores of the kinetic Ising couplings and the equilibrium Ising couplings, the kinetic Ising coupling matrix was symmetrised and compared with the symmetrised structural connectivity matrix and the AUC scores obtained was also added to the Figure 5.11. It can be seen that in all cases, the kinetic Ising couplings and the symmetrised kinetic Ising couplings had either the same or a significantly larger AUC score when compared to equilibrium Ising couplings. This suggests that even if one is not interested in the directionality of the inferred structural links, kinetic Ising couplings will give a better or at least a similar performance when compared to the equilibrium Ising couplings.

5.9 Discussions

Since the relation between the actual synaptic connections in a neuronal network and the functional connections inferred from the recording of the neuronal activity is non-trivial [RDH15], inferring the underlying structural connectivity from functional connectivity measures is a useful strategy. As it is now possible to record the activity of closely spaced neurons

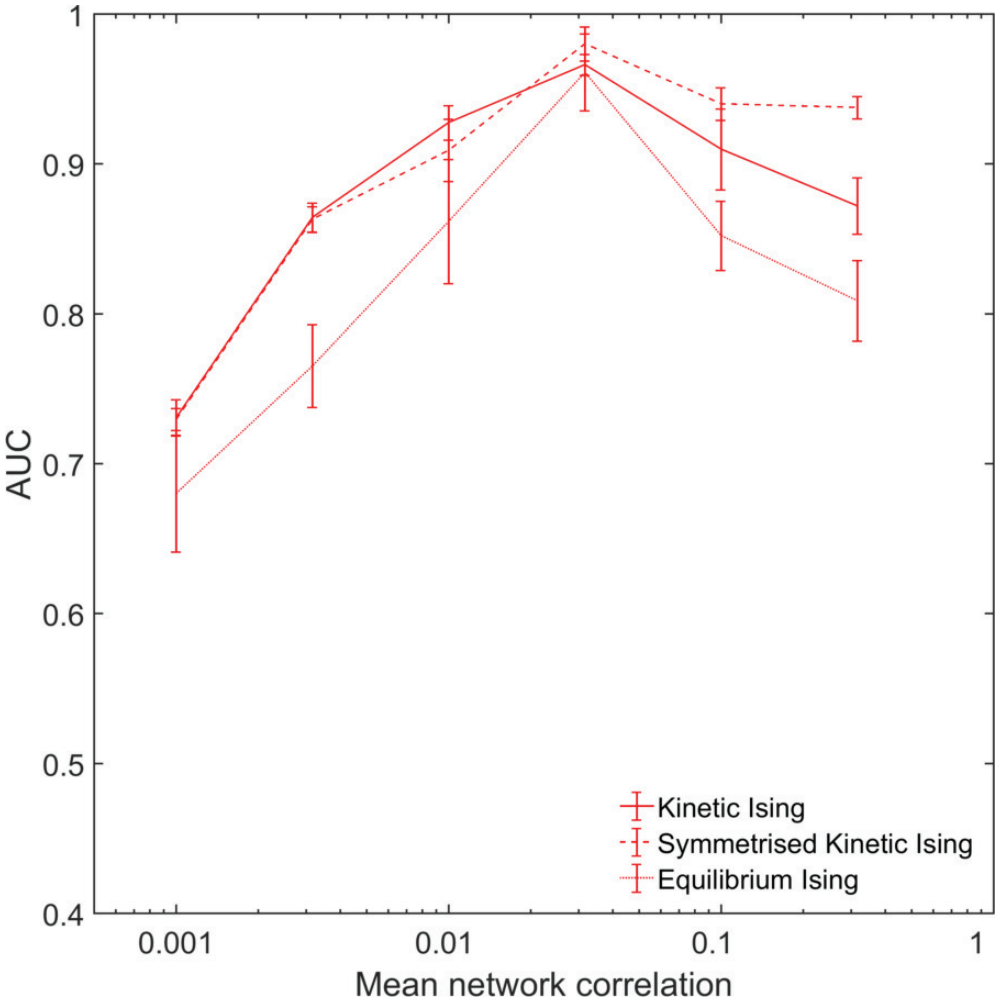

Figure 5.11: **Comparison between equilibrium Ising couplings and kinetic Ising couplings:** Plot of the AUC scores of the kinetic Ising couplings, symmetrised kinetic Ising couplings and equilibrium Ising couplings for different mean network correlation levels and a fixed firing rate of 20 Hz in scale-free networks of 30 neurons. Data was averaged over 10 simulated networks.

at high temporal resolution over long periods of time [Mac+10], having reliable functional connectivity measures that can reconstruct the structural connections is becoming increasingly important. Hertz et al [HRT13] observed that the coupling parameters of a kinetic Ising model were able to reconstruct the structural connections of a model cortical network very reliably. This success generated an interest in the application of kinetic Ising models to infer synaptic connectivity in simulated models of cortical networks ([Cap+15; RH11] and to understand functional connectivity in *in vivo* recordings of hippocampal grid cells in rats [DMR15].

Meanwhile, partial correlations based on scaled partial covariance density were also reported to be effective in inferring structural connection in *in silico* networks [Pol+16]. However, the performance of the kinetic Ising couplings in comparison to partial correlations in inferring the structural connections has not been studied previously. This chapter addresses this question and evaluates the performance of the kinetic Ising couplings in comparison with the partial and cross-correlations under different network conditions and topologies.

The key finding of this chapter is that the mean network correlation level played a significant role in determining the relative performance of kinetic Ising couplings, partial and cross-correlations. At weak network correlation levels ($\rho = 0.001$ and $\rho = 0.003$), kinetic Ising couplings outperformed partial and cross-correlations in inferring the structural links and at strong network correlation levels ($\rho = 0.1$ and $\rho = 0.3$), partial correlations were superior to kinetic Ising couplings in reconstructing the structural connectivity . Both kinetic Ising couplings and partial correlations outperformed

cross-correlations in all cases. This observation is similar to the earlier observation made in the section 4.1 regarding the equilibrium Ising couplings. This confirms that the partialisation approach is very effective in removing the linear effects of the other spike trains in the population while assessing the relationship between two spike trains [BBS76] while kinetic Ising models excel in cases of weak correlations. Also, the topology of the network had no impact on this observation and the same effect of network correlation was observed in scale-free, small-world and ER random network topologies (Figure 5.6).

The study also tested whether the addition of inhibitory links to the network affected the performance of the functional connectivity metrics. Inhibitory connections in the functional connectivity metrics are distinguishable from the excitatory connections by the negative values in the corresponding functional connectivity matrices. Therefore it was observed that there was no difference in the AUC scores of kinetic Ising couplings and partial correlations between neuronal networks with purely excitatory links and networks with a mix of excitatory and inhibitory synaptic connections (Figure 5.9) suggesting both kinetic Ising model and partial correlation can infer inhibitory connections as good as the excitatory connections.

Poli et al [Pol+16] observed that high network density decreases the performance of the partial correlations because of married-nodes effect. The results observed in Figure 5.8 confirm the observations of Poli et al about partial correlations. It can be observed from the results in this thesis (Figure 5.8) that kinetic Ising couplings also suffer a reduction in performance in case of networks with high connection density. Similarly, the performance

of all the three functional connectivity metrics reduced with increased network size (Figure 5.7). However, the relative performance difference between kinetic Ising couplings and partial correlations for the case of weak and strong network correlations did not change with the changes in network density and number of nodes in the network. In all cases, kinetic Ising coupling outperformed partial and cross-correlations in case of very weak correlation and partial correlation outperformed the other two methods in case of strong network correlation.

The decreased performance of all three functional connectivity metrics with increase in number of nodes can be explained as follows. Though marrying-parents effect [EDS03] is suggested as a cause for the decreased performance of partial correlations with increasing number of nodes in the network, it should be remembered that the length of the spike train data was kept the same for all network sizes (11,20,30,60, and 120 nodes). This could have resulted in a relatively smaller amount of statistical information of the correlation structure of the neurons for networks with large number of nodes when compared with networks with smaller number of nodes. A preliminary test done with the longer recordings for larger number of nodes suggests that a longer recording does help to improve the reconstruction for all functional connectivity metrics. However, the relative performance difference between the kinetic Ising couplings and the partial correlations for different correlation levels persisted. A more systematic study on the effect of length of the recording on the relative performance of the functional connectivity metrics has to be followed up in a future study. The study kept the length of the recording at a fixed length of 10 minutes as functional connections are known to fluctuate in time and also neural activity in real

neuronal networks are rarely stationary for longer periods of time [Ste+12].

Similar to the case of equilibrium Ising couplings, increased accuracy of the kinetic model parameters resulted in increased performance (Figure 5.10). This result needs to be taken into consideration when applying approximations such as mean-field methods ([RH11; Cap+15]) proposed for the faster (but less accurate) estimation of kinetic Ising couplings.

Results obtained in this chapter also indicate that kinetic Ising couplings deliver a better performance when compared to the equilibrium Ising couplings. With the added advantage of directionality, applicability in case of non stationary data, a better performance at reconstructing the structural connections along with a faster computation time, kinetic Ising couplings can be considered as a better choice of functional connectivity tool in comparison with the equilibrium Ising couplings.

True and false positive rate calculations to evaluate the performance of the functional connectivity metrics in *in silico* networks considered in this chapter were possible as the ground truth about the structural connectivity is known in *in silico networks*. One of the challenges of extending the application of functional connectivity metrics from *in silico networks* to living networks is that the physical connectivity matrix is unknown in living neuronal networks and a thresholding procedure to differentiate the connected links from the unconnected links becomes critical. An advanced thresholding approach such as cluster-span threshold [Smi+15] or multi-threshold permutation correction [Dra+15] may prove effective in establishing a threshold. Future research in inferring structural connections from

functional connectivity studies should also explore the impact of thresholding approaches so that the functional connectivity studies can be applied to living neuronal networks successfully.

Chapter 6

Conclusions

6.1 Discussions and conclusions

Identification of the structural connectivity of neuronal circuits is a critical step in understanding how neuronal systems behave [HTS10]. Despite the massive technological advancements, mapping the structural connectivity directly through electrophysiological techniques is challenging even for small networks of neurons [Zho+14]. However, it is becoming relatively easy to record the activity of the individual neurons and neuronal populations at high spatial and temporal resolutions [SK11]. Functional connectivity metrics which are obtained by the statistical analysis of the recorded neuronal activity have been suggested to have interdependence with the underlying anatomical connectivity [Wat+09; Bon+09]. Understanding how the structural connectivity in neuronal circuits can be reconstructed by the functional connectivity metrics remains one of the challenges in neuroscience [Ste+12; Orl+14].

The ability of a functional connectivity metric to discount the effect of indirect interactions determines how well it can reconstruct the network structure [Ste+08]. Several studies [Sch+06; GSS11; BC13] have suggested that maximum entropy based Ising models can distinguish the direct interactions from the indirect interactions in a network. Studies by Hertz et al [HRT13; RH11] have shown that parameters of kinetic Ising model were successful in removing the indirect interactions and inferring the true structural connectivity in a simulated model of neurons. Following this, active research is being pursued on kinetic Ising models [RDH15; Cap+15]. However, the performance of Ising couplings and kinetic Ising couplings have not yet been rigorously evaluated against other functional connectivity measures across a broad set of network conditions. This thesis does a methodical assessment of the performance of Ising couplings and kinetic Ising couplings against partial and cross-correlations in *in silico* networks and thereby contributes informed recommendations regarding selection of an appropriate functional connectivity tool.

A number of contributions have been made by this research. Chapter 4 evaluated the performance of Ising couplings against the non-directional version of partial and cross-correlations. It also addressed the question of how firing rate, network correlation, network size, and topology affect the performance of the functional connectivity metrics to unravel the true anatomical structure of neuronal networks. The main finding of the chapter is that, amongst the various tested network conditions, the key factor that influenced the relative performance of Ising couplings, partial and cross-correlations was the mean network correlation level. Compared to partial correlations and cross-correlations, Ising couplings reconstructed the most

structural links, when the correlation levels were weak. The AUC scores of partial and cross correlations were close to that of a random classifier at very weak levels of network correlation. As the correlation levels in the network became stronger, the AUC of partial correlations exceeded that of Ising couplings and cross-correlations. The relative performance of the functional connectivity metrics were insensitive to changes in firing rate, network topologies and sizes of the *in silico* networks under test.

Chapter 5 evaluated the performance of kinetic Ising couplings against the directional version of partial and cross-correlations for different network conditions. Similar to the observations in chapter 4, the mean network correlation level played a significant role in determining the relative performance of kinetic Ising couplings, partial and cross-correlations. Analogous to the behaviour of the equilibrium Ising couplings, kinetic Ising couplings exhibited considerably higher performance in detecting structural links at weaker correlation levels when compared to partial and cross correlations. Partial correlations displayed superior performance over kinetic Ising and cross correlations at strong correlation levels. In all cases, cross correlations consistently scored the lowest AUC among the compared metrics. The topology, network density and addition of inhibitory links to the network did not affect the relative performance of kinetic Ising couplings and partial correlations.

Results obtained in chapter 5 also indicate that kinetic Ising couplings deliver a better performance when compared to the equilibrium Ising couplings. Therefore kinetic Ising coupling presents itself as a more favourable choice over equilibrium Ising coupling as it is a directional measure and is applicable to the case of non-stationary neural data as well. This suggests

that even if one is not interested in the directionality of the inferred structural links, kinetic Ising couplings should be considered over Ising couplings when inferring structural links. As Ising models have been used in the past to explore the structure-function relationship in human brain using neuroimaging techniques [Wat+13], results of this thesis suggest that application of kinetic Ising models couplings in fMRI studies might reveal additional insights.

Vertebrate retina have been reported to be networks with very low correlated levels of activity [Tka+14; AB10]. Results in this thesis which demonstrate the superior performance of the kinetic Ising couplings at very weak correlation levels motivates further application of kinetic Ising model couplings in studying the structure-function relationship in such *in vivo* and *in vitro* networks of neurons with low network correlation levels. On the other hand, partial correlations are a better choice in networks with high levels of correlated activity like neuronal cultures with burst activity [Sur+16].

Kinetic Ising models can be seen as a special case of generalized linear models which has found applications outside computational neuroscience. For example, it has been used to model financial markets [ZLA14]. Results from this thesis are directly applicable to other areas where kinetic Ising models are employed. Caution should be exercised when inferring functional connections based on kinetic Ising couplings in cases of high correlation between the nodes of the network and alternate functional connectivity methods based on partialization approach should be considered.

Understanding the strengths and weaknesses of the individual functional connectivity metrics, the network conditions in which they are applied and

the computational time demands should be considered when selecting a functional connectivity tool and the findings of this thesis guide the process of choosing the right functional connectivity tool to reconstruct the structural connectivity.

6.2 Future work

Structural connectivity was the source of correlations seen in the spike trains of the *in silico* networks simulations in this work. However, the synaptic structure need not be the only source of correlations. Another source of correlation in the spike data is the correlated external inputs which are seen in many neuronal systems, especially sensory systems. It is important to understand how the reconstruction of the structural connectivity is affected by correlation in the inputs. Theoretically, kinetic Ising models with its h parameters which can vary with time has a better chance of separating the correlations caused by external inputs and recovering the synaptic structure. Preliminary investigation [Tyr+13] in this area also confirms the theoretical predictions. An important issue that remains to be elucidated is how the relative performance of the functional connectivity metrics vary with the correlations in the input.

Functional connectivity metrics in this work were computed assuming that the data from every node of the network is available. However, current technologies make it possible to record only from a sample of the population of neurons. Hertz et al [HRT13] were able to reconstruct reliably the structural connections in an under-sampled model cortical network using kinetic Ising couplings. It is suggested that partial correlations are unable to

discount the effect of spike trains from common input nodes which are not recorded [EDS03]. This suggests the need for further evaluation of the impact of sub-sampling on the performance of partial correlations and kinetic Ising models in future works.

This thesis has furthered progress in the application of functional connectivity measures to reconstruct the structural connectivity. Further research in this direction will enable functional connectivity tools working hand in hand with advanced structural connectivity techniques like optogenetics to reconstruct living neuronal networks in the future.

Appendix A

Mean field approximations

A.1 Mean field approximations for equilibrium Ising model

The inverse Ising problem of inferring the model parameters to fit the data from observations is a challenging problem with no simple solution [BC13]. A typical solution to the inverse Ising problem is the Boltzmann learning method, which involves long Monte Carlo simulations followed by small updates to the model parameters. Though exact, the Boltmann learning method is a very slow algorithm. Therefore, one has to resort to approximations. Mean field approximation is a simple approximation method used to solve the inference of Ising parameters. There are many mean field approximation solutions, but they all share a common idea.

The basic idea of a mean field approach is to replace the effect of all other individuals on a given individual by a single average or effective effect. This reduces a multi-body problem into a one-body problem and makes

the problem less complex to solve. The mean field approximation approach assumes that every spin is interacting not with its real neighbours, but with "mean-neighbours" or with a field generated by the mean orientation of the spins. This section presents a simple mean field approximation theory known as Weiss mean field theory. This section uses the notation $m_i = \langle \sigma_i \rangle$ and $C_{ij} = \langle \sigma_i \sigma_j \rangle - m_i m_j$. It should be noted that statisticians would call C_{ij} as covariances but statistical physicists would refer to C_{ij} as correlations [HRT13]. This chapter sticks to the convention used by statistical physicists and refers to C_{ij} as correlations.

It can be recalled that the energy of a configuration in an Ising model is given by

$$E(\sigma) = -\sum_{i=1}^{N} h_i \sigma_i - \sum_i \sum_j J_{ij} \sigma_i \sigma_j \,, \tag{A.1}$$

where the second sum is over each pair of spins when each pair is counted only once.

All contributions to the energy by the spin i is given by

$$\epsilon(\sigma_i) = -h_i \sigma_i - \sum_j J_{ij} \sigma_i \sigma_j \,. \tag{A.2}$$

Mean field theory approximates equation A.2 by replacing σ_j by their mean value m_j = $\langle \sigma_j \rangle$

$$\begin{aligned}\epsilon_{mf}(\sigma_i) &= -h_i\sigma_i - \sum_j J_{ij}\sigma_i \langle\sigma_j\rangle \\ &= -h_i\sigma_i - \sum_j J_{ij}\sigma_i m_j \,. \end{aligned} \tag{A.3}$$

The single-spin Boltzmann distribution can be written as

$$\begin{aligned}P(\sigma_i) &= \frac{e^{-\epsilon_{mf}(\sigma_i)}}{\sum\limits_{\sigma_i=\pm1} e^{-\epsilon_{mf}(\sigma_i)}} \\ &= \frac{e^{-\epsilon_{mf}(\sigma_i)}}{e^{-\epsilon_{mf}} + e^{\epsilon_{mf}}} \,. \end{aligned} \tag{A.4}$$

The average value of σ_i given by m_i can be written as a sum of the Boltzmann probabilities as follows:

$$\begin{aligned}m_i &= \sum_{\sigma_i=\pm1} P(\sigma_i)\sigma_i \\ &= \frac{e^{h_i+\sum_j J_{ij}m_j} - e^{-h_i-\sum_j J_{ij}m_j}}{e^{h_i+\sum_j J_{ij}m_j} + e^{-h_i-\sum_j J_{ij}m_j}} \\ &= \tanh(h_i + \sum_j J_{ij}m_j) \,. \end{aligned} \tag{A.5}$$

From equation A.5, the expression for h_i can be derived as

$$h_i = \tanh^{-1} m_i - \sum_j J_{ij} m_j \,. \tag{A.6}$$

Considering h_i as the external magnetic field and m_i as the average magnetization, the inverse magnetic susceptibilty matrix χ^{-1} is defined as

$$\begin{aligned} \chi_{ij}^{-1} &= \frac{\partial h_i}{\partial m_j} \\ &= \frac{\delta_{ij}}{1 - m_i^2} - J_{ij} \,. \end{aligned} \tag{A.7}$$

In equilibrium statistical physics, there is a theorem that the correlation matrix is equal to the susceptibility matrix (up to a factor of the temperature, which in our case is set to 1) [HRT13]. This leads to

$$(C^{-1})_{ij} = \frac{\delta_{ij}}{1 - m_i^2} - J_{ij} \,, \tag{A.8}$$

where δ_{ij} is the Kronecker delta function and is defined as

$$\delta_{ij} = \begin{cases} 0 & \text{if } i \neq j \\ 1 & \text{if } i = j \end{cases} \tag{A.9}$$

Equivalently, one can write the mean field expression for the Ising coupling matrix J as

$$J_{MF} = P^{-1} - C^{-1} \,, \tag{A.10}$$

where $P_{ij} = (1 - m_i^2)\delta_{ij}$.

Using equations A.6 and A.10, one can obtain the Ising field matrix h_i and the Ising coupling matrix J_{ij} from the knowledge of the average firing rates m_i and the average pairwise correlations C_{ij}.

This mean field solution is a good approximation when the sum over j has many terms (an informal kind of a central-limit argument) [HRT13]. This solution becomes exact in the limits of dense connections for large number of spins. Other approximation methods based on small-correlation expansions [SM09], minimum probability flow [SDBD11], and selective cluster expansion [BC13] have been developed to solve the Inverse Ising problem. Even in cases where the approximation solutions are not used directly, they can serve as initial conditions for Boltzmann learning.

A.2 Mean field approximations for kinetic Ising model

As in the case of equilibrium Ising model, mean-field algorithms, which provide faster approximations when compared to the exact gradient ascent rules, can be derived for kinetic Ising model as well. The stationary case is considered in this section. $\sigma_i(t)$ in the equation 2.62 can be written as

$$\sigma_i(t) = m_i + \delta\sigma_i(t)\,, \tag{A.11}$$

where $m_i = \langle \sigma_i(t) \rangle$. Similar to the equilibrium mean field equation A.5, the value of m_i can be approximated as

$$m_i = \tanh(h_i + \sum_j J_{ij} m_j) \,. \tag{A.12}$$

Hence equation A.11 can be rewritten as

$$\sigma_i(t) = \tanh(h_i + \sum_j J_{ij} m_j) + \delta\sigma_i(t) \,. \tag{A.13}$$

For the exact value of h_i and J_{ij}, δJ_{ij} in the equation 2.62 should be zero. Setting the term J_{ij} in equation 2.62 to zero, substituting the term $\sigma_i(t)$ with equation A.13, and expanding tanh to the first-order results in the following equation [RH11; HRT13]:

$$\langle \delta\sigma_i(t+1)\delta\sigma_j(t) \rangle = (1 - m_i^2) \sum_k J_{ik} \langle \sigma_k(t)\delta\sigma_j(t) \rangle \,. \tag{A.14}$$

The above expression can be written as a simple matrix equation

$$D = AJC \,, \tag{A.15}$$

where

$$D = \langle \delta\sigma_i(t+1)\delta\sigma_j(t) \rangle \ , \tag{A.16}$$

$$C = \langle \delta\sigma_i(t)\delta\sigma_j(t) \rangle \ , \tag{A.17}$$

$$A = (1 - m_i^2)\delta_{ij} \, . \tag{A.18}$$

D is the one-step-delayed correlation matrix, C is the equal time correlation matrix and δ_{ij} is the Kronecker delta function.

From equation A.15, the Ising couplings J_{ij} matrix can be determined as

$$J = A^{-1}DC^{-1} \, . \tag{A.19}$$

After determining J_{ij}, Ising field parameters h_i can be determined from equation A.12 as

$$h_i = \tanh^{-1} m_i - \sum_j J_{ij} m_j \, . \tag{A.20}$$

The above mean field solution is excellent in the limit of weak couplings and for densely connected networks when the standard deviation of the couplings is not large relative to the mean [Tyr+13]. If the standard deviation is large then the fluctuations around the mean field becomes important and the above approximate solution is not valid. Another mean-field based approximation for Ising coupling J_{ij} was derived by Capone et al [Cap+15] as follows:

$$J_{ij} \simeq \frac{P((\sigma_i(t+1)=1)|(\sigma_j(t)=1) - m_i}{m_i(1-m_i)(1-m_j)}\,, \tag{A.21}$$

where $P((\sigma_i(t+dt)=1)|(\sigma_j(t)=1)$ is the probability that the neuron i spikes in the time bin $t+1$ conditional on the pre-synaptic neuron j spiking in the time bin t.

References

[AB10] Feraz Azhar and William Bialek. "When are correlations strong?" *arXiv preprint arXiv:1012.5987* (2010).

[Ada+12] Yusuke Adachi et al. "Functional Connectivity between Anatomically Unconnected Areas Is Shaped by Collective Network-Level Effects in the Macaque Cortex". *Cerebral Cortex* 22.7 (2012), pp. 1586–1592.

[AG85] Ad Aertsen and George L. Gerstein. "Evaluation of neuronal connectivity: Sensitivity of cross-correlation". *Brain Research* 340.2 (1985), pp. 341 –354.

[AP91] Ad Aertsen and Hubert Preissl. "Dynamics of activity and connectivity in physiological neuronal networks". *Nonlinear dynamics and neuronal networks* (1991), pp. 281–301.

[Aze+09] Frederico AC Azevedo et al. "Equal numbers of neuronal and nonneuronal cells make the human brain an isometrically scaled-up primate brain". *Journal of Comparative Neurology* 513.5 (2009), pp. 532–541.

[BA99] Albert-László Barabási and Réka Albert. "Emergence of Scaling in Random Networks". *Science* 286.5439 (1999), pp. 509–512.

[Bar14] Albert-László Barabási. *Network Science*. Cambridge University Press, 2014.

[BBS76] David R. Brillinger, Hugh L. Bryant, and José P. Segundo. "Identification of synaptic interactions". *Biological Cybernetics* 22.4 (1976), pp. 213–228.

[BC13] John Barton and Simona Cocco. "Ising models for neural activity inferred via selective cluster expansion: structural and coding properties". *Journal of Statistical Mechanics: Theory and Experiment* 2013.03 (2013), P03002.

[Ber+09] Luca Berdondini et al. "Active pixel sensor array for high spatio-temporal resolution electrophysiological recordings from single cell to large scale neuronal networks". *Lab on a Chip* 9.18 (2009), pp. 2644–2651.

[Bon+09] Paolo Bonifazi et al. "GABAergic hub neurons orchestrate synchrony in developing hippocampal networks". *Science* 326.5958 (2009), pp. 1419–1424.

[BS09] Ed Bullmore and Olaf Sporns. "Complex brain networks: graph theoretical analysis of structural and functional systems". *Nature Reviews Neuroscience* 10.3 (2009), pp. 186–198.

[BS16] André M. Bastos and Jan-Mathijs Schoffelen. "A Tutorial Review of Functional Connectivity Analysis Methods and Their Interpretational Pitfalls". *Frontiers in Systems Neuroscience* 9.January (2016), pp. 1–23.

[Cap+15] Cristiano Capone et al. "Inferring synaptic structure in presence of neural interaction time scales". *PLoS One* 10.3 (2015), e0118412.

[Cha+15] Paul Charlesworth et al. "Quantitative differences in developmental profiles of spontaneous activity in cortical and hippocampal cultures". *Neural Development* 10.1 (2015), pp. 1–10.

[CM11] Simona Cocco and Rémi Monasson. "Adaptive cluster expansion for inferring Boltzmann machines with noisy data". *Physical review letters* 106.9 (2011), p. 090601.

[CT12] Thomas M Cover and Joy A Thomas. *Elements of information theory*. John Wiley & Sons, 2012.

[Dei11] Karl Deisseroth. "Optogenetics". *Nature methods* 8.1 (2011), pp. 26–29.

[DES97] Rainer Dahlhaus, Michael Eichler, and Jürgen Sandkühler. "Identification of synaptic connections in neural ensembles by graphical models". *Journal of Neuroscience Methods* 77.1 (1997), pp. 93–107.

[DLIv+13] Maria De La Iglesia-vaya et al. "Brain Connections–Resting State fMRI Functional Connectivity". *Novel Frontiers of Advanced Neuroimaging*. InTech, 2013.

[DLR+07] Jaime De La Rocha et al. "Correlation between neural spike trains increases with firing rate". *Nature* 448.7155 (2007), pp. 802–806.

[DMR15] Benjamin Dunn, Maria Mørreaunet, and Yasser Roudi. "Correlations and functional connections in a population of grid cells". *PLoS Computational Biology* 11.2 (2015), e1004052.

[Dow+12] Julia H Downes et al. "Emergence of a small-world functional network in cultured neurons". *PLoS Computational Biology* 8.5 (2012), e1002522.

[Dra+15] Mark Drakesmith et al. "Overcoming the effects of false positives and threshold bias in graph theoretical analyses of neuroimaging data". *NeuroImage* 118 (2015), pp. 313–333.

[DÖ13] Ahmet Şamil Demirkol and Serdar Özoğuz. "A low power real time izhikevich neuron with synchronous network behavior". *İstanbul Ticaret Üniversitesi Fen Bilimleri Dergisi* 12.24 (2013), p. 39.

[EDS03] Michael Eichler, Rainer Dahlhaus, and Jürgen Sandkühler. "Partial correlation analysis for the identification of synaptic connections". *Biological Cybernetics* 89.4 (2003), pp. 289–302.

[EM06a] Danny Eytan and Shimon Marom. "Dynamics and Effective Topology Underlying Synchronization in Networks of Cortical Neurons". *Journal of Neuroscience* 26.33 (2006), pp. 8465–8476.

[EM06b] Danny Eytan and Shimon Marom. "Dynamics and effective topology underlying synchronization in networks of cortical neurons". *Journal of Neuroscience* 26.33 (2006), pp. 8465–8476.

[Faw06] Tom Fawcett. "An introduction to ROC analysis". *Pattern recognition letters* 27.8 (2006), pp. 861–874.

[FBC11] Sarah Feldt, Paolo Bonifazi, and Rosa Cossart. "Dissecting functional connectivity of neuronal microcircuits: experimental and theoretical insights". *Trends in neurosciences* 34.5 (2011), pp. 225–236.

[Fri11] Karl J Friston. "Functional and effective connectivity: a review". *Brain connectivity* 1.1 (2011), pp. 13–36.

[Fri94] Karl J Friston. "Functional and effective connectivity in neuroimaging: a synthesis". *Human brain mapping* 2.1-2 (1994), pp. 56–78.

[FVE91] Daniel J Felleman and David C Van Essen. "Distributed hierarchical processing in the primate cerebral cortex". *Cerebral cortex* 1.1 (1991), pp. 1–47.

[Gal13] Giovanni Gallavotti. *Statistical mechanics: A short treatise*. Springer Science & Business Media, 2013.

[Gla63] Roy J Glauber. "Time-dependent statistics of the Ising model". *Journal of mathematical physics* 4.2 (1963), pp. 294–307.

[GSS11] Elad Ganmor, Ronen Segev, and Elad Schneidman. "The architecture of functional interaction networks in the retina". *Journal of Neuroscience* 31.8 (2011), pp. 3044–3054.

[Hag+07] Patric Hagmann et al. "Mapping human whole-brain structural networks with diffusion MRI". *PLoS One* 2.7 (2007), e597.

[Her+10] John A Hertz et al. "Inferring network connectivity using kinetic Ising models". *BMC Neuroscience* 11.Suppl 1 (2010), P51.

[HG08] Mark D Humphries and Kevin Gurney. "Network 'small-worldness': a quantitative method for determining canonical network equivalence". *PLoS One* 3.4 (2008), e0002051.

[HGP06] Mark D Humphries, Kevin Gurney, and Tony J Prescott. "The brainstem reticular formation is a small-world, not scale-free, network". *Proceedings of the Royal Society of London B: Biological Sciences* 273.1585 (2006), pp. 503–511.

[Hop82] John J Hopfield. "Neural networks and physical systems with emergent collective computational abilities". *Proceedings of the national academy of sciences* 79.8 (1982), pp. 2554–2558.

[HRT13] JohnA Hertz, Yasser Roudi, and Joanna Tyrcha. "Ising models for inferring network structure from spike data". *Principles of Neural Coding*. CRC Press, 2013, pp. 527–546.

[HS13] Martijn P van den Heuvel and Olaf Sporns. "Network hubs in the human brain". *Trends in cognitive sciences* 17.12 (2013), pp. 683–696.

[HTS10] Christopher J Honey, Jean-Philippe Thivierge, and Olaf Sporns. "Can structure predict function in the human brain?" *Neuroimage* 52.3 (2010), pp. 766–776.

[Ide+07] Alessandro Ide et al. "Cross-correlation based methods for estimating the functional connectivity in cortical networks". *BMC Neuroscience* 8.S2 (2007), p. 63.

[IM+07] Y Iturria-Medina et al. "Characterizing brain anatomical connections using diffusion weighted MRI and graph theory". *Neuroimage* 36.3 (2007), pp. 645–660.

[IS10] Miriam Ivenshitz and Menahem Segal. "Neuronal Density Determines Network Connectivity and Spontaneous Activity in Cultured Hippocampus". *Journal of Neurophysiology* 104.2 (2010), pp. 1052–1060.

[Izh03] Eugene M Izhikevich. "Simple model of spiking neurons". *IEEE Transactions on neural networks* 14.6 (2003), pp. 1569–1572.

[Izh04] Eugene M Izhikevich. "Which model to use for cortical spiking neurons?" *IEEE transactions on neural networks* 15.5 (2004), pp. 1063–1070.

[Jay57] Edwin T Jaynes. "Information theory and statistical mechanics". *Physical review* 106.4 (1957), p. 620.

[JTR99] Y Jimbo, T Tateno, and HPC Robinson. "Simultaneous induction of pathway-specific potentiation and depression in networks of cortical neurons". *Biophysical Journal* 76.2 (1999), pp. 670–678.

[Liv+07] Jean Livet et al. "Transgenic strategies for combinatorial expression of fluorescent proteins in the nervous system". *Nature* 450.7166 (2007), pp. 56–62.

[Mac+10] Alessandro Maccione et al. "Experimental Investigation on Spontaneously Active Hippocampal Cultures Recorded by Means of High-Density MEAs: Analysis of the Spatial Resolution Effects". *Frontiers in Neuroengineering* 3 (2010), p. 4.

[Mak+14] Siti N Makhtar et al. "Multivariate partial coherence analysis for identification of neuronal connectivity from multiple electrode array recordings" (2014), pp. 77–82.

[Mar+00] Laura Martignon et al. "Neural coding: higher-order temporal patterns in the neurostatistics of cell assemblies". *Neural Computation* 12.11 (2000), pp. 2621–2653.

[Mar+09] Olivier Marre et al. "Prediction of spatiotemporal patterns of neural activity from pairwise correlations". *Physical review letters* 102.13 (2009), p. 138101.

[Mas83] David N Mastronarde. "Correlated firing of cat retinal ganglion cells. I. Spontaneously active inputs to X-and Y-cells". *Journal of Neurophysiology* 49.2 (1983), pp. 303–324.

[Mat+13] Eiko Matsuda et al. "Analysis of neuronal cells of dissociated primary culture on high-density CMOS electrode array". *Engineering in Medicine and Biology Society (EMBC), 2013 35th Annual International Conference of the IEEE*. IEEE. 2013, pp. 1045–1048.

[MLB10] David Meunier, Renaud Lambiotte, and Edward T Bullmore. "Modular and hierarchically modular organization of brain networks". *Frontiers in neuroscience* 4 (2010).

[MPF05] Valeri A Makarov, Fivos Panetsos, and Oscar de Feo. "A method for determining neural connectivity and inferring the underlying network dynamics using extracellular spike recordings". *Journal of neuroscience methods* 144.2 (2005), pp. 265–279.

[MPM15] Paolo Massobrio, Valentina Pasquale, and Sergio Martinoia. "Self-organized criticality in cortical assemblies occurs in concurrent scale-free and small-world networks". *Scientific reports* 5 (2015).

[MS02] Shimon Marom and Goded Shahaf. "Development, learning and memory in large random networks of cortical neurons: lessons beyond anatomy". *Quarterly Reviews of Biophysics* 35.1 (Feb. 2002), pp. 63–87.

[NB99] MEJ Newman and GT Barkema. *Monte Carlo Methods in Statistical Physics chapter 1-4*. Oxford University Press: New York, USA, 1999.

[Nic07] Miguel AL Nicolelis. *Methods for neural ensemble recordings*. CRC press, 2007.

[Nir+01] Sheila Nirenberg et al. "Retinal ganglion cells act largely as independent encoders". *Nature* 411.6838 (2001), pp. 698–701.

[NL09] Nandakumar S Narayanan and Mark Laubach. "Methods for studying functional interactions among neuronal populations". *Methods in molecular biology* 489 (2009), pp. 135 –65.

[NV07] Sheila H Nirenberg and Jonathan D Victor. "Analyzing the activity of large populations of neurons: how tractable is the problem?" *Current opinion in neurobiology* 17.4 (2007), pp. 397–400.

[Orl+14] Javier G. Orlandi et al. "Transfer entropy reconstruction and labeling of neuronal connections from simulated calcium imaging". *PLoS One* 9.6 (2014), pp. 1–24.

[Pas+16] Vito Paolo Pastore et al. "ToolConnect: A Functional Connectivity Toolbox for In vitro Networks". *Frontiers in Neuroinformatics* 10 (Mar. 2016), p. 13.

[Pol+16] Daniele Poli et al. "From functional to structural connectivity using partial correlation in neuronal assemblies". *Journal of Neural Engineering* 13.2 (2016), p. 026023.

[PR13] Volker Pernice and Stefan Rotter. "Reconstruction of sparse connectivity in neural networks from spike train covariances". *Journal of Statistical Mechanics: Theory and Experiment* 2013.03 (2013), P03008.

[RDH15] Yasser Roudi, Benjamin Dunn, and John Hertz. "Multi-neuronal activity and functional connectivity in cell assemblies." *Current opinion in neurobiology* 32 (2015), pp. 38–44.

[RH11] Yasser Roudi and John Hertz. "Mean field theory for nonequilibrium network reconstruction". *Physical review letters* 106.4 (2011), p. 048702.

[Rie+97] Fred Rieke et al. *Spikes: Exploring the Neural Code*. Cambridge, MA: The MIT Press, 1997.

[RNL08] Yasser Roudi, Sheila Nirenberg, and Peter Latham. "Pairwise maximum entropy models for studying large biological systems: when they can and when they can't work". *PLoS Computational Biology* 5.5 (2008), e1000380.

[RS10] Mikail Rubinov and Olaf Sporns. "Complex network measures of brain connectivity: uses and interpretations". *Neuroimage* 52.3 (2010), pp. 1059–1069.

[RTH09] Yasser Roudi, Joanna Tyrcha, and John Hertz. "Ising model for neural data: model quality and approximate methods for extracting functional connectivity". *Physical Review E* 79.5 (2009), p. 051915.

[Sca+99] JW Scannell et al. "The connectional organization of the cortico-thalamic system of the cat". *Cerebral Cortex* 9.3 (1999), pp. 277–299.

[Sch+06] Elad Schneidman et al. "Weak pairwise correlations imply strongly correlated network states in a neural population". *Nature* 440.7087 (2006), pp. 1007–1012.

[SDBD11] Jascha Sohl-Dickstein, Peter B Battaglino, and Michael R DeWeese. "New method for parameter estimation in probabilistic models: minimum probability flow". *Physical review letters* 107.22 (2011), p. 220601.

[SF10] Klaas Enno Stephan and Karl J Friston. "Analyzing effective connectivity with fMRI". *Wiley interdisciplinary reviews. Cognitive science* 1.3 (2010), pp. 446–459.

[SHK07] Olaf Sporns, Christopher J Honey, and Rolf Kötter. "Identification and classification of hubs in brain networks". *PLoS One* 2.10 (2007), e1049.

[Shl+06] Jonathon Shlens et al. "The structure of multi-neuron firing patterns in primate retina". *Journal of Neuroscience* 26.32 (2006), pp. 8254–8266.

[SK11] Ian H Stevenson and Konrad P Kording. "How advances in neural recording affect data analysis". *Nature neuroscience* 14.2 (2011), pp. 139–142.

[SM09] Vitor Sessak and Rémi Monasson. "Small-correlation expansions for the inverse Ising problem". *Journal of Physics A: Mathematical and Theoretical* 42.5 (2009), p. 055001.

[Smi+15] Keith Smith et al. "Cluster-Span Threshold: An unbiased threshold for binarising weighted complete networks in functional connectivity analysis" (2015), pp. 2840–2843.

[Spo07] Olaf Sporns. "Brain connectivity". *Scholarpedia* 2.10 (2007). revision #91083, p. 4695.

[Spo13] Olaf Sporns. "Structure and function of complex brain networks". *Dialogues in clinical neuroscience* 15.3 (2013), p. 247.

[Ste+08] Ian H. Stevenson et al. "Inferring functional connections between neurons". *Current Opinion in Neurobiology* 18.6 (2008), pp. 582–588.

[Ste+12] Olav Stetter et al. "Model-free reconstruction of excitatory neuronal connectivity from calcium imaging signals". *PLoS Computational Biology* 8.8 (2012), e1002653.

[Sur+16] Jyothsna Suresh et al. "Network burst activity in hippocampal neuronal cultures: the role of synaptic and intrinsic currents". *Journal of Neurophysiology* 115.6 (2016), pp. 3073–3089.

[Tan+08] Aonan Tang et al. "A maximum entropy model applied to spatial and temporal correlations from cortical networks in vitro". *Journal of Neuroscience* 28.2 (2008), pp. 505–518.

[TC14] Marc Timme and Jose Casadiego. "Revealing networks from dynamics: an introduction". *Journal of Physics A: Mathematical and Theoretical* 47.34 (2014), p. 343001.

[Tka+09] Gasper Tkacik et al. "Spin glass models for a network of real neurons". *arXiv preprint arXiv:0912.5409* (2009).

[Tka+14] Gašper Tkačik et al. "Searching for collective behavior in a large network of sensory neurons". *PLoS Computational Biology* 10.1 (2014), e1003408.

[Tyr+13] Joanna Tyrcha et al. "The effect of nonstationarity on models inferred from neural data". *Journal of Statistical Mechanics: Theory and Experiment* 2013.03 (2013), P03005.

[Wat+09] Alanna J Watt et al. "Traveling waves in developing cerebellar cortex mediated by asymmetrical Purkinje cell connectivity." *Nature neuroscience* 12.4 (2009), pp. 463–73.

[Wat+13] Takamitsu Watanabe et al. "A pairwise maximum entropy model accurately describes resting-state human brain networks". *Nature Communications* 4.May 2012 (2013), p. 1370.

[WS98] Duncan J Watts and Steven H Strogatz. "Collective dynamics of 'small-world'networks". *Nature* 393.6684 (1998), pp. 440–442.

[WSB03] Martin A Walter, Liz J Stuart, and Roman Borisyuk. "Spike train correlation visualization" (2003), pp. 555–560.

[Yat+15] Dimitri Yatsenko et al. "Improved estimation and interpretation of correlations in neural circuits". *PLoS Computational Biology* 11.3 (2015), e1004083.

[Yeh+10] Fang-Chin Yeh et al. "Maximum entropy approaches to living neural networks". *Entropy* 12.1 (2010), pp. 89–106.

[Yu+08] Shan Yu et al. "A small world of neuronal synchrony". *Cerebral cortex* 18.12 (2008), pp. 2891–2901.

[Yus15] Rafael Yuste. "From the neuron doctrine to neural networks". *Nature Reviews Neuroscience* 16.8 (2015), pp. 487–497.

[Zen+11] Hong-Li Zeng et al. "Network inference using asynchronously updated kinetic Ising model". *Physical Review E* 83.4 (2011), p. 041135.

[Zen+13] Hong-Li Zeng et al. "Maximum likelihood reconstruction for Ising models with asynchronous updates". *Physical review letters* 110.21 (2013), p. 210601.

[Zho+14] Douglas Zhou et al. "Granger causality network reconstruction of conductance-based integrate-and-fire neuronal systems". *PLoS One* 9.2 (2014), e87636.

[ZLA14] Hong-Li Zeng, Rémi Lemoy, and Mikko Alava. "Financial interaction networks inferred from traded volumes". *Journal of Statistical Mechanics: Theory and Experiment* 2014.7 (2014), P07008.